Optimal control of offshore wind farm collector systems during outages

Harvesting the full potential of inter-array cabling

M.J. Ubbens

Master of Science Thesis

TU Delft Delft University of Technology

Delft Center for Systems and Control

Optimal control of offshore wind farm collector systems during outages

Harvesting the full potential of inter-array cabling

Master of Science Thesis

For the degree of Master of Science in Systems and Control at Delft University of Technology

M.J. Ubbens

June 14, 2023

Faculty of Mechanical, Maritime and Materials Engineering (3mE) · Delft University of Technology

The work in this thesis was supported by Vattenfall. Their cooperation is hereby gratefully acknowledged.

Abstract

Ambitions to limit climate change are incentivizing the expansion of renewable energy. In particular, offshore wind energy is expected to grow rapidly. To harness the full potential of existing as well as prospected offshore wind farms, the limited capacity of the internal cable network of the offshore wind farm, called the collector system, should be efficiently used.

The operation of the collector system during cable outages presents significant potential in this regard. Currently, during these outages, a conservative approach is taken that under-utilizes the capacity of the collector system and consequently limits power production excessively. The available headroom of the system can be unlocked by optimizing the power routing and turbine setpoints. This optimization problem is the topic of the MSc Thesis, carried out within Vattenfall.

Two novel optimization-based rerouting and setpoint decision frameworks are developed for collector systems with arbitrary topologies: an open-loop control strategy and a receding horizon control strategy.

The open-loop control strategy assumes that the network can only be reconfigured at the beginning of the outage. It is formulated as a mixed-integer linear programming problem, in which the cables are modeled as binary control variables and the setpoints as continuous control variables.

The receding horizon control strategy is deployed in real time, leveraging cable temperature measurements and power forecasts to derive optimal control actions dynamically. Dynamic thermal rating is applied, which entails that the power flows are constrained based on the cables' temperatures rather than on a static rating. The resulting control strategy is formulated as a mixed-integer quadratically constrained programming problem.

A case study is performed to compare the performance of the developed strategies to existing strategies. Simulations concerning seven occurred cable outages at an offshore wind farm show an average increase in power production with respect to the industry control strategy of 0.82% for the open-loop control strategy and 4.2% for the receding horizon control strategy.

Table of Contents

Acknowledgements

I would like to express my appreciation to Prof. dr. ir. Bart De Schutter for his valuable support and feedback throughout the course of this thesis. I thoroughly enjoyed our focused conversations, during which you helped me understand that I cannot boil the ocean.

Furthermore, I am truly grateful to Dr. ing. Adel Haghani, who in a very friendly and personal way guided me throughout my quest, and gave me the freedom within Vattenfall to shape this thesis to my interests and ambitions. I highly appreciated the open dialogue and the fresh and creative perspectives you provided.

Thanks should definitely also go to the other team members of the Data Analytics team, who impacted and inspired me. Specifically, I want to thank Robbert and Peter, who have taught me a lot about programming in Python and working with large amounts of data.

I'd also like to recognize the assistance that I received from numerous experts within Vattenfall. In particular, I want to thank Nicholas for his enthusiasm and his valuable feedback on reports and presentations.

Next, I would like to thank Pim for offering me distraction when I needed it and for putting up with me during stressful times.

Last but not least, I would like to thank my parents. I could not have made it so far without their never-ending love and support. Thank you, I am very fortunate to have you in my life.

Delft, University of Technology M.J. Ubbens
June 14, 2023

Chapter 1

Introduction

This chapter introduces the topic of the thesis, which is optimal control of offshore wind farm collector systems during outages. A general introduction is given in Section 1.1, the objective of the work is stated in Section 1.2, and the outline of the report is presented in Section 1.3.

1.1 General introduction

Ambitions to limit climate change are incentivizing the development of renewable energy technologies. One of the most rapidly growing energy markets is offshore wind power. In 2021, its global installed capacity reached 65 GW. In line with the Paris Agreement [61], a UN Global Compact has been signed to commit to the target of 380 GW capacity by 2030 and 2000 GW by 2050 [22]. To meet these ambitious targets, it is vital that the investment costs for Offshore Wind Farms (OWFs) are reduced, and wind power efficiency is increased.

The electrical system of OWFs presents significant potential in this regard. It consists of a collector system and an export system. Within the collector system, inter-array cables transport the power produced by the turbines to the Offshore Substation (OSS). From the OSS, export cables transport the power to shore. Not only does the electrical system constitute a large portion of the capital expenditure, but its cable outages also account for 80% of the financial losses in the offshore wind industry. For example, the failure of one inter-array cable can cost up to €3 million, depending on the type and location of the failure and the weather conditions [20]. These costs are built up of repair costs and costs related to curtailment of power over the duration of the cable outage.

To limit the production losses due to inter-array outages, rerouting can be performed to transport the power produced by the turbines connected to the inoperative cable to the OSS. During standard operation, the collector system is capable of transporting the maximum production capacity within the cable temperature constraints. However, if the power is rerouted, an elongated string of turbines is formed, which introduces the risk of a cable overload. Therefore, rerouting is often paired with new turbine setpoints that ensure that the network's limits will not be exceeded.

Research shows that a conservative approach is currently taken to determine the rerouting and setpoints, resulting in unnecessarily high curtailment levels [11, 54]. Given that inter-array outages typically last more than a month [58], optimizing the rerouting and setpoints can significantly reduce the losses during outages. Moreover, an optimization approach can support the current trend of designing OWFs that are tailored to the site's specifics [1] and OWFs with a larger installed wind power capacity than can be transported via the collector system [11]. Any increase in effectiveness can benefit the entire generating capacity and can aid in realizing the ambitious growth in OWFs targeted.

1.2 Objective

The objective of the thesis is to develop a control strategy for OWF collector systems that maximizes power production during inter-array outages by determining appropriate rerouting actions and turbine setpoints. The corresponding research question is the following:

How can the power production of offshore wind farms be maximized during collector system outages?

1.3 Outline

The thesis is structured as follows. Chapter 2 describes the OWF collector system and discusses existing approaches to the control of collector systems during outages. Two novel strategies are developed in Chapter 3. In Chapter 4, these are applied to a case study concerning outages that occurred at an existing OWF and compared to the method currently used in industry and an approach found in the literature. Subsequently, in Chapter 5, the findings are discussed, and recommendations for future research are given. A conference paper concerning this work can be found in Appendix B.

Chapter 2

Collector system modeling and control

This chapter discusses the modeling and control of the Offshore Wind Farm (OWF) collector system. In Section 2.1, an overview is given of the collector system. Section 2.2 elaborates on the power production of individual turbines. The rating of the cables is discussed in Section 2.3, after which Section 2.4 gives insights into how the power flows through the collector system can be modeled. Subsequently, Section 2.5 presents existing approaches to the control of collector systems during outages. The chapter is summarized in Section 2.6.

2.1 Collector system overview

The main components of the collector system are wind turbines, inter-array cables, and the Offshore Substation (OSS). The inter-array cables enable transportation of the power produced by the turbines to the OSS, from which the power is transported to shore.

Multiple standard configurations of collector systems have been presented in the literature. Typical configurations include radial, double-sided ring, single-sided ring, and star topology, shown in Figure 2.1. The collector system generally contains cables of two or three different sizes. Downstream cables are larger than upstream cables since they transport more power. The only way to control the power routing through the inter-array is via a switchgear. In case of a complete switchgear configuration, each turbine contains one power switch per cable connected to it and an additional one for isolating the turbine in case of malfunctioning [6].

The double-sided and single-sided rings contain cablelinks, which are not fundamentally different from the other cables. During regular operation, these links are not used. When there is an outage, power switches can be switched on to enable routing of the power via a link. At some OWFs, this must be done manually at each turbine. However, modern OWFs are typically equipped with switches that can be controlled remotely from the control center.

Since the electrical system constitutes a significant portion of the capital expenditure, extensive research has been done to optimize the cable layout of OWFs. Factors to be considered are component costs, turbine placement, power production scenarios, electrical losses, and

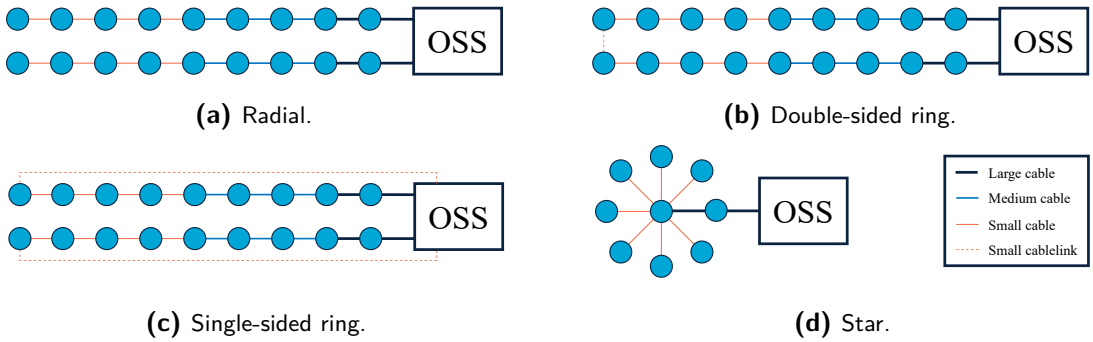

(a) Radial. **(b)** Double-sided ring. **(c)** Single-sided ring. **(d)** Star.

Figure 2.1: Collector system topologies, inspired by [1]. The circles represent the turbines.

environmental factors [1]. Increasingly, collector systems are tailored toward the OWF at hand. By taking into account the different factors while optimizing the collector system, non-standard topologies are chosen. An example of such a collector system is shown in Figure 4.1. As can be seen, different topologies are combined into an irregular array. This may complicate the control of the system, especially during outages.

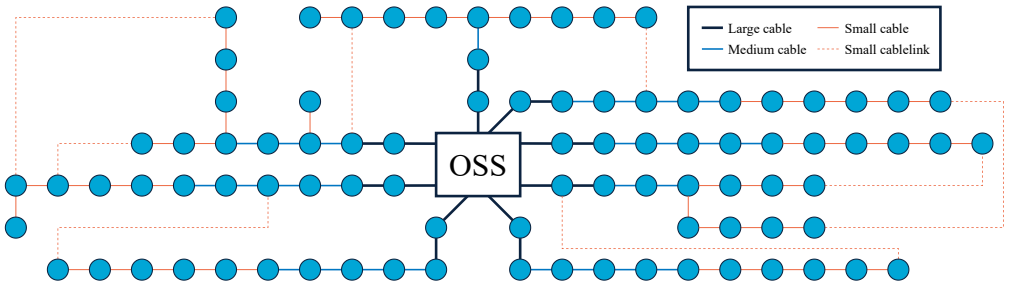

Figure 2.2: Schematic of a meshed collector system. The circles represent the turbines.

These inter-array outages result from failure or preventative maintenance of either terminations or cables. Limited information is available in the literature regarding failure rates and root causes due to confidentiality restrictions [20]. However, the authors of [58] found that for the United Kingdom OWF sector (8.4 GW installed capacity), up to 77% of failures could be attributed to manufacturing and installation. Furthermore, they calculated that the average downtime resulting from inter-array failure and repair was 38 days.

Inter-array cables run through four environments, as shown in Figure 2.3. A large part of the inter-array cables is buried under the seabed. This section spans several hundreds of meters. At the transition between soil and water, the cable protection system shields the cable against currents and sediment. The J-tube protects the cable section that rises from the seabed to the platform of the turbine or OSS [20]. In the hang-off section, the three-core cable is split into three single-core cables so they can be connected to the termination. At the termination, the single-core cables are connected to the switchgear.

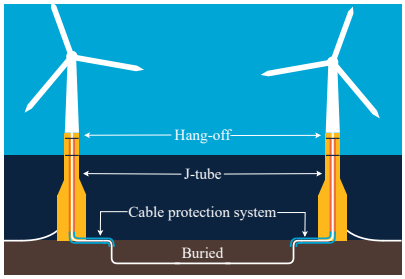

Figure 2.3: Cable environments, inspired by [32].

2.2 Turbine power production

The power production of an OWF depends on its design, the weather conditions, the occurrence of failures, external conditions from the transmission system operator, and energy trading. While the latter three certainly impact power production, the design and the weather are the most significant factors. These can be used to calculate the possible power, which is the power produced when the turbine is functioning with no limitations beyond the ones described in the design specifications [41]. Section 2.2.1 elaborates on how the possible power can be calculated. Subsequently, Section 2.2.2 describes how wind farm operators can influence the turbine power production by applying a setpoint. Approaches to modeling wind power variability are presented in Section 2.2.3.

2.2.1 Possible power

The rated power of turbine i, P_i^{r}, dictates the maximum power that the turbine can produce. The power that can be generated by turbine i when it is operating at full performance is called the possible power, P_i^{poss}. The possible power can be used to assess a turbine's performance and to make informed energy trading decisions. It depends primarily on the wind speed, air density, and turbine design specifications. The possible power can be approximated with the turbine's power curve, which is a function of the wind speed [66].

The turbine producer provides the theoretical power curve based on ideal conditions. An example of a power curve is shown in Figure 2.4a. This curve can serve as an approximation of the possible power production, as shown in Figure 2.4a-2.4c. More accurate deterministic power curves can be obtained by fitting the curve to nacelle wind speed measurements and power data. This is then called the operational power curve.

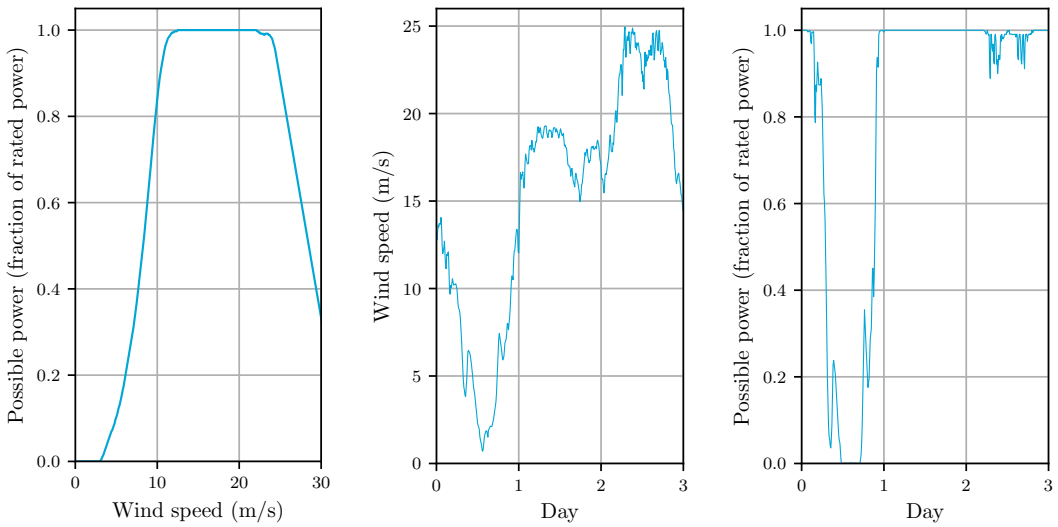

(a) Power curve. **(b)** Wind speed. **(c)** Possible power.

Figure 2.4: Using the power curve (Figure 2.4a) to convert a three-day wind speed profile (Figure 2.4b) to possible power (Figure 2.4c).

Accurate possible power estimates can be derived by using wind speed data from anemometers installed at each turbine. These nacelle wind speed measurements allow for taking into account wake effects. These are velocity deficits and turbulence caused by neighbouring turbines, dependent on the wind direction and speed [1]. When only one anemometer is present at the OWF, the wake effect should be modeled to differentiate between turbine production. The nonlinear Jensen model is most used within optimization. This model is applicable when turbines are spaced at least four rotor diameters apart [38].

2.2.2 Turbine setpoints

The power output of a turbine can be limited by providing a setpoint. The actual power output of the turbine is then given by the minimum of the possible power and the setpoint, P_i^{sp}. This is illustrated in Figure 2.5.

If the possible power exceeds the setpoint, the turbine blades' pitch angle is adjusted to such an extent that the power is limited to the setpoint [29]. It is called curtailment when the production could have been higher than the setpoint [54].

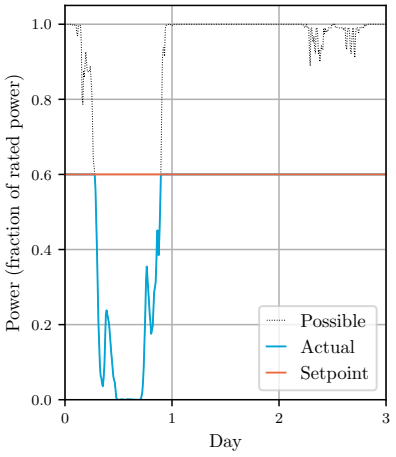

Figure 2.5: Application of a setpoint.

2.2.3 Wind power fluctuations

Wind power generation is inherently volatile and uncertain. It is of paramount importance to take this into account when determining suitable control actions during an outage. Depending on the problem at hand and the available data, different possibilities exist for considering wind stochasticity in such an optimization problem [12, 38].

First of all, the stochasticity can be incorporated probabilistically. Monte Carlo simulation is used in [10, 11, 15]. This entails modeling wind speed or power generation as random variables with known probability density functions. This probability function can be derived via statistical analysis of historical wind data or by setting up the Weibull distribution probability density function with a site-specific shape and scale factor [28]. Combining the power curve with the wind probability density function and the Jensen wake model results in a probability density function of the power generation. This probability density function can also be obtained directly via statistical analysis of historical possible power data. Depending on the application, it might be required to develop multiple probability density functions to account for the seasonal and diurnal patterns that wind speed data show. Wind speeds are typically higher during the daytime and winter [34].

Secondly, stochasticity can be incorporated deterministically. This can be done by directly using historical wind speed or power production data and optimizing over these time series as in [65, 37]. Alternatively, the historical data can be processed to obtain a worst-case time

series, as in [35]. In addition, an average daily pattern can be constructed with historical data to account for diurnal effects, as in [59]. When historical wind power generation data is available, it is more appropriate to use this rather than historical wind speed data as it reflects the actual output of the turbines more accurately [57].

Finally, different wind power forecasting methods can be applied for short-timescale prediction of power production. These typically achieve a Normalized Root Mean Square Error (NRMSE) of 9-14% for 24-hours ahead power predictions. For prediction horizons longer than several days, the accuracy strongly deteriorates due to the uncertainty in wind forecasts [19]. Therefore, the other approaches are more suitable when optimizing over a longer period.

2.3 Cable rating

The rating of the cable dictates the maximum current that the cable can transport. It is limited by the cable's insulation. The maximum conductor temperature for cross-linked polyethylene insulated cables, which are commonly used, is 90 °C. When this temperature limit is exceeded, the aging of the cable takes place at a higher rate than is acceptable in terms of the OWF lifetime [5].

The rating can be calculated for each distinct environment the cable is in. The most limiting section of the cable dictates the rating of the entire cable. This is the section of the J-tube that is in the air, due to its exposure to solar radiation and higher ambient temperatures [32].

Being able to accurately determine the rating of cables is vital for OWF design and operation. Overestimating the rating can lead to cable failure, while a conservative rating might lead to overdimensioned cables or unnecessary curtailment during operations. Different approaches are possible to determine the cable rating. These are elaborated on in Section 2.3.1. In Section 2.3.2, methods to measure and model the cable temperature are discussed.

2.3.1 Approaches to cable rating

In this section, three different cable rating approaches are discussed: Static Thermal Rating (STR), Cyclic Thermal Rating (CTR), and Dynamic Thermal Rating (DTR).

STR entails constraining the power flows by the maximum current that can be transported continuously with the cable. In industry, the internationally recognized IEC standard 60287 [25, 26] is widely used for determining the STR. This standard parametrizes the rating by the thermal resistances, the internal heat losses, and the ambient temperature. The calculations are fast and straightforward. However, the thermal time constant is not considered. For conventional generation plants, applying a static rating does not lead to conservatism, as these are generally operated continuously. In contrast, wind power generation is rather dynamic and shows quick and significant variations. The authors of [8] show that for four OWFs in Scotland, the loading is less than 30% for half of the time, while the loading is bigger than 80% only less than 20% of the time. This results in the cable temperature being much lower than designed for. Inter-array cables are thus often under-utilized when using a STR.

CTR entails constraining the power flows by the maximum fixed current that can be applied as part of a predefined load cycle without violating the conductor temperature. IEC standard 60853-2 calculates the cyclic rating by multiplying the continuous rating with a cyclic rating factor [24]. Cycles of 24 hours are considered. Such a rating might be appropriate for a conventional networks but cannot be applied directly to OWFs as its generation is not accurately represented by a daily cycle. In the literature, several approaches exist that extend CTR to renewable energy sources. The authors of [8] assume alternating periods of fixed low and high load. Low load is given by the current at which a steady-state conductor temperature of 30 °C is realized. Via statistical analysis of one year of wind speed data, the mean duration of low and high load is determined. Compared to the continuous rating, an increase of 17% was achieved for a 33kV cable. Although the approach is rather conservative in that it assumes a load profile consisting of only of low and high load, it is computationally attractive.

DTR is an umbrella term for different methodologies that aim to perform ratings more dynamically. It is a variable current rating that considers actual and predicted conditions. This can entail rating in accordance with time-varying weather conditions ($\text{DTR}_{\text{weather}}$) or loading conditions (DTR_{load}). Traditionally, DTR was based on the former [36]. This can lead to significant improvements in the rating of overhead lines in conventional networks compared to rating according to the worst-case parameters (high ambient temperature and solar radiation, low wind speed). Since the thermal time constant of overhead lines is about 10 to 20 minutes, a steady-state heat balance equation can be used to perform the rating calculations [37]. Recently, DTR has been researched for application to distribution and transmission systems driven by renewable energy sources [33]. Focus of this research is on time-varying loading rather than environmental conditions. The large thermal inertia, in combination with the intermittent loading, enables the uprating of the cables. For these calculations, dynamic cable temperature modeling is required. The authors of [10] use a finite element method approach to obtain a DTR_{load}, while the authors of [33, 35] use a thermo-electric equivalent approach. These models can be used to formulate constraints on the permissible current. Most of the approaches found in the literature use DTR to optimally choose a cable size by taking into account cable and curtailment costs. These papers assume that during actual deployment, curtailment is performed such that the cable temperatures are within limits. How setpoints are adapted and scheduled during real-time operations is not discussed. To the best of the authors' knowledge, only [10, 11] consider how to perform curtailment in accordance with DTR. These approaches entail estimating the 6-hour ahead risk of exceeding an export cable's temperature limit based on the loading of the previous three hours and applying STR for one hour if a risk is identified. For optimal control during outages, it might be more suitable to incorporate the cable temperature dynamics in the optimization formulation directly.

2.3.2 Cable temperature

To ensure safe and efficient operations under DTR, it is vital to be able to measure and model the cable temperatures. In the following sections, these two aspects are discussed.

Cable temperature measurements

Temperature measurements allow for operation closer to the system limits. By monitoring the cable temperature, informed decisions can be made regarding the cable rating. If the temperature is low, the cable rating can be increased. If the temperature nears the limit, curtailment can be performed to ensure safe operation. Furthermore, temperature measurements can be used to correct or validate a temperature model, for instance done in [7]. Additionally, temperature measurements can be analyzed to identify hotspots along the cable. These might indicate cable defects or other anomalies. Inspection can be carried out and if necessary (preventative) maintenance can be performed.

The cable temperatures can be measured using Distributed Temperature Sensing (DTS). An optical laser pulse is sent through the fiber optic cable. Based on the backscattering of light, the fiber temperature can be calculated with a spatial resolution of 0.5 meter. Typically, measurements are averaged over a 30-minute window to improve accuracy and provide the operator sufficient time to respond to temperatures exceeding thresholds. The resulting accuracy of measured DTS temperature is in the range of 1 °C [44]. Other temperature-measuring devices are resistance temperature detectors and thermocouples [31]. Furthermore, phasor measurement unit data can be used to calculate the cable temperature in real time [56].

Cable temperature modeling

Cable temperature models can be used to simulate and predict cable temperatures. The complexity of modeling the conductor temperature stems from the fact that numerous aspects influence the conductor temperature, including cable loading, material properties, cable geometry, and thermal properties of the environment [13]. Currently, three white-box modeling approaches exist that can describe the heat transfer process with reasonable accuracy: the finite element method, thermo-electric equivalent, and step response.

Comparing these three approaches has been done in [44, 45, 43]. This comparison was performed for a single-core high-voltage transmission cable. The results of dynamic temperature simulations are within ± 0.2 °C of each other, indicating similar accuracy. The estimated conductor temperature remains within 2.5 °C of the actual conductor temperature, which is adequate considering the resolution of 1 °C of the fiber optic cable measurements. The thermo-electric equivalent computations were 6 and 20 times faster than step response and finite element method computations, respectively. However, the simulation time is in the order of seconds. For optimal control of the collector system, the temperature of multiple inter-array cables needs to be modeled rather than that of a single export cable. To be able to incorporate it into an optimization framework that is deployed in real time, the model's computational expense should therefore be decreased further.

To this end, the author of [30] proposes a data-driven modeling approach. Four different models are considered: a first order differential equation, a third order state space model, an auto-regressive exogenous model, and a neural network. Each model type is trained and tested on load and cable temperature data pertaining to an existing export cable. The state

space model resulted in the best fit. It is characterized by the following equations:

$$\begin{bmatrix} \dot{T} \\ \ddot{T} \\ \dddot{T} \end{bmatrix} = A \begin{bmatrix} T \\ \dot{T} \\ \ddot{T} \end{bmatrix} + BI^2 + K\varepsilon \tag{2.1a}$$

$$T^{\mathrm{DTS}} = \begin{bmatrix} 1 & 0 & 0 \end{bmatrix} \begin{bmatrix} T \\ \dot{T} \\ \ddot{T} \end{bmatrix} + \varepsilon \tag{2.1b}$$

where T is the cable temperature, T^{DTS} is the DTS measurement, I is the current, A, B, and K are coefficient matrices of which the parameters are estimated using the `System Identification Toolbox` in Matlab, and ε is noise. On the test set, a Normalized Mean Square Error (NMSE) of 82.5% between simulated and actual DTS measurements was achieved for the J-tube section, indicating a reasonable accuracy.

2.4 Network power flow modeling

Typically, inter-array cables are Alternating Current (AC) cables with an operating voltage of 33 kV or 66 kV [20]. Since three-phase cables are concerned, the active power transported through the cables (p) is given by:

$$p = \sqrt{3} V I P_{\mathrm{f}} \tag{2.2}$$

where V is the voltage and P_{f} is the power factor, which is the ratio between the active and apparent power. Eq. (2.2) can be used to determine the rating in terms of admissible power flow rather than current.

Generally, the power flows through the collector system are not measured. They must be derived from the power production at the turbines and the power measurement at the OSS. In the following section, different power flow modeling approaches are presented and evaluated in terms of suitability for collector system power flow analysis within an optimization procedure. Subsequently, the equations pertaining to the linear power flow model are presented. Thereafter, it is discussed how the power switches that enable rerouting can be incorporated into the modeling framework.

2.4.1 Comparison between power flow models

Different models exist that aim to describe the power flow through an electrical grid. The main approaches are listed in Table 2.1.

The transportation model is equivalent to the linear power flow model when radial networks are concerned. In case of a looped network, when multiple paths to the OSS are possible, this model cannot be used to derive power flows [65].

Table 2.1: Characteristics of power flow approaches, based on [38, 48].

Approach	Type	Based on	Limitations
Transportation model	Linear	Kirchoff's 1st law	Ignores losses & reactive power Inadaquate for looped networks
Linear power flow	Linear	Kirchoff's 1st & 2nd law	Ignores losses & reactive power
AC power flow	Non-convex	Full representation	High complexity

The linear power flow model, also called DC power flow, is a linearization of AC power flow. It is based on three assumptions: resistances are negligible compared to reactances, the amplitude of the voltages is similar for all nodes in the system, and voltage angle differences between nodes in proximity to each other are small [67].

The AC power flow model models both active and reactive power flows. In terms of accuracy, AC power flow outperforms the linear power flow method [38].

The severity of the approximation error of linear power flow modeling depends on the system at hand. There is extensive research regarding the suitability of linear power flow for conventional transmission and distribution networks. The authors of [50] attempt to quantify the accuracy for numerous high-voltage transmission networks. In order to stay within 5% of the AC power flow, the resistance should be at least four times smaller than the reactance, the standard deviation of voltage should be limited to 0.01, and the voltage angle should remain lower than 30°. The collector system of an OWF might stay within these boundaries since a relatively low voltage (33 kV) network is concerned, and voltage support and reactive power management at every turbine are in place. This is further affirmed by results from the authors of [65], who found that the maximum voltage drop within the collector system is 0.3 kV, the maximum voltage angle is 0.3°, and the maximum reactive power of a cable is 0.2 Mvar. In addition, the authors of [54] calculated that reactive power constitutes less than 0.34% of the apparent power for typical inter-array cable operation. However, the author recommends further research to assess the accuracy of the linear power flow formulation for OWF collector systems.

For real-time operations of the collector system, accuracy is vital to be able to meet the requirements at the point of connection with the transmission system operator. However, for determining optimal switching actions and generator setpoints during outage periods, the requirement on power flow accuracy is less stringent. In addition, the linearity of the linear power flow method makes it less computationally expensive to use within an optimization framework than the non-convex AC power flow model. In line with this, most approaches in literature regrading OWF collector system design optimization use linear power flow since it makes the problems tractable [39].

2.4.2 Linear power flow model

Let $\mathcal{V}$ denote the set of nodes in the network. Furthermore, let $\mathcal{E}$ denote the set of edges, which contains the cables (i, j) between the nodes. The cable connecting node i and node

j occurs once within the set of edges. The equations concerning linear power flow are the following [63]:

$$P_i - \sum_{j|(i,j)\in\mathcal{E}} p_{ij} + \sum_{j|(j,i)\in\mathcal{E}} p_{ji} = 0 \qquad \text{for } i \in \mathcal{V} \tag{2.3a}$$

$$p_{ij} = b_{ij}(\theta_i - \theta_j) \qquad \text{for } (i,j) \in \mathcal{E} \tag{2.3b}$$

where P_i is the power demand or production of node i, p_{ij} is the power flow through cable (i,j), b_{ij} is the admittance of cable (i,j), and θ_i is the voltage angle of node i. The latter is defined relative to a reference voltage phasor. In the case of the OWF collector system, this is typically the node pertaining to the OSS, of which the voltage angle is then fixed to zero. The power (flow) and admittance are expressed in per-unit values, and the voltage angles in radians. If no connection exists, then $b_{ij} = 0$. In this formulation, the admittance is the reciprocal of the reactance. Accuracy for networks with larger R/X ratio might be improved if the admittance is calculated as $b_{ij} = \frac{x_{ij}}{x_{ij}^2 + r_{ij}^2}$, where x_{ij} and r_{ij} are the reactance and resistance of cable (i,j) [62].

The linear power flow model ignores losses. Depending on the topology and the cable types, the electrical losses in OWFs are 1%-3% of the power production [38]. Losses can be incorporated in the optimization formulation as an approximation in different ways. First of all, power losses can be subtracted from the total power generation in the objective function. Secondly, losses can be modeled as demands in the linear power flow formulation. This entails splitting the power loss over a cable between the corresponding nodes. Both approaches result in the addition of quadratic terms, which increases the computational complexity. Therefore, in some optimization formulations, the losses are approximated with piecewise linear terms to reduce computational expense [53].

When there are no loops in the network, the linear power flow formulation can be reduced to (2.3a). This is called the transportation model [65].

2.4.3 Network reconfiguration

Network reconfiguration involves manually or automatically controlling the power switches in the network to reroute the power. Operators use it to reduce power losses, isolate faults quickly, improve the voltage profile, and increase the power transportation capacity [14].

To be able to incorporate switching actions into the linear power flow model, binary variables z_{ij} can be introduced. Here, $z_{ij} = 1$ if connection (i,j) can be used and $z_{ij} = 0$ if the connection cannot be used. Eq. (2.3b) can then be rewritten as follows [42]:

$$p_{ij} = z_{ij} b_{ij}(\theta_i - \theta_j) \qquad \text{for } (i,j) \in \mathcal{E} \tag{2.4a}$$

$$z_{ij} \in \{0,1\} \qquad \text{for } (i,j) \in \mathcal{E} \tag{2.4b}$$

To prevent the product of continuous and discrete variables, (2.4a) can be replaced by [42]:

$$-M_{ij} z_{ij} \leq p_{ij} \leq M_{ij} z_{ij} \qquad \text{for } (i,j) \in \mathcal{E} \tag{2.5a}$$

$$p_{ij} \leq b_{ij}(\theta_i - \theta_j) + M_{ij}(1 - z_{ij}) \qquad \text{for } (i,j) \in \mathcal{E} \tag{2.5b}$$

$$p_{ij} \geq b_{ij}(\theta_i - \theta_j) - M_{ij}(1 - z_{ij}) \qquad \text{for } (i,j) \in \mathcal{E} \tag{2.5c}$$

where M_{ij} can be selected as $2b_{ij}\theta^{\max}$, in which $\theta^{\max}$ is the maximum voltage angle. In case of a fixed rating, (2.5a) can be replaced by the constraints pertaining to the rating of the cable since these are more stringent:

$$-p_{ij}^{\mathrm{STR}} z_{ij} \leq p_{ij} \leq p_{ij}^{\mathrm{STR}} z_{ij} \qquad \text{for } (i,j) \in \mathcal{E} \tag{2.6}$$

where p_{ij}^{STR} is the power flow limit of the cable as defined by its STR. The same applies when using CTR.

2.5 Existing approaches to collector system control during outages

When there is an inter-array cable failure, an alarm is triggered at the control center. Automatically, all turbines upstream are shut down until an operator intervenes. It is common practice for OWF operators to apply a zero power setpoint to the upstream turbines during the whole outage period, even though power could be rerouted via the links. This has to do with operational security [54]. However, more sophisticated approaches exist that consider power rerouting and setpoint adaptation to limit the loss of production during outages.

In this section, these approaches are discussed. Section 2.5.1 presents the method currently used in industry. The two strategies that have been found in the literature regarding OWF operation during outages are elaborated on in Section 2.5.2 and Section 2.5.3. Subsequently, Section 2.5.4 discusses how methods used in transmission and distribution networks can be leveraged to obtain insights on how to approach the problem at hand.

2.5.1 Industry control strategy

In Figure 2.6, a schematic of part of a collector system is shown. When an outage occurs as indicated in the figure, all turbines in the same string upstream of the inoperative cable are disconnected from the OSS. Power from the downstream turbine is still transported to the OSS.

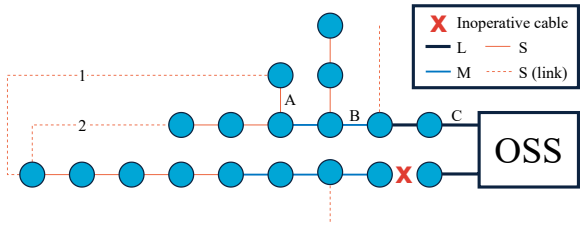

Figure 2.6: Schematic of part of a collector system subject to an outage. The circles represent the turbines.

Links 1 and 2 can connect the disconnected turbines to the OSS. In industry, a single cablelink is activated per outage. This has to do with the power flows. These are not measured and cannot be controlled other than by turning on or off a link. Only the power generated by the turbines and the power at the OSS are known. Under normal circumstances or when only one link is enabled during an outage, the network is radial, which means that the power flows

through the array can easily be derived from the turbine power production. This is no longer straightforward when multiple links are enabled.

If there are multiple options for rerouting the power, all options are assessed. The link that enables the highest amount of power to reach the OSS is activated. In that case, an Elongated String (ELS) is formed. To determine the setpoints, the Full Capacity Cables (FCCs) within the ELS are identified. These are of each size the cables that are furthest downstream in the ELS. If rerouting is performed via link 1, the FCCs are cable A, B, and C. Since STR is concerned, it is assumed that as long as these cables do not exceed their limits, all cables remain within their limits.

For these three FCCs it is calculated by how much the STR would be exceeded if the turbines in the ELS were to produce at rated power. The power flow rating of the FCC with the largest violation, as can be calculated with (2.2), is is divided equally over the turbines in the ELS up to that FCC:

$$P^{\mathrm{sp}} = \frac{\sqrt{3} I^{\mathrm{rated}} \cdot 0.95 V^{\mathrm{nom}} \cdot P_{\mathrm{f}}}{N} \tag{2.7}$$

where P^{sp} is the new setpoint of the turbines, I^{rated} is the rated current of the most limiting FCC, V^{nom} is the nominal voltage (33 kV), and N is the number of turbines provided with a new setpoint. The factor 0.95 stems from the grid codes of the transmission system operator Tennet, dictating a maximum allowable voltage drop of 5% [68]. After these calculations, it is checked whether the calculated setpoints relieve the overload for any smaller-sized FCC as well. If this is not the case, (2.7) is used to derive the setpoints for the turbines connected to this FCC.

While the industry approach taken during inter-array outages is straightforward, easy to implement, and safe, several limitations can be identified:

- Only one link is activated during a cable outage. A higher power transportation capacity is expected to be achieved when using multiple links to distribute the power evenly over the array. Switching of regular cable sections can even be considered, as these are not fundamentally different from the cable links. This way, the power can actively be steered through the entire collector system. As elaborated on in Section 2.4.3, rerouting can be modeled by introducing binary variables.
- STR is used to determine the setpoints. This rating is based on a continuous load profile, while wind power is inherently variable. As discussed in Section 2.3.1, DTR can be used to uprate the cables while adhering to the cable temperature limits.
- The setpoints for the upstream turbines are all fixed to the same value for the entire outage duration. However, the turbines in an OWF do not generate the same power, and their power production fluctuates with the wind speed and direction. As discussed in Section 2.2.3, this should be taken into account.

2.5.2 Dynamic setpoint adaptation based on wind speeds

The authors of [54] consider the volatility of the wind by determining setpoints dynamically based on wind speed measurements. The method aims to maximize power production during outages, taking into account internal power losses. In the approach, wake effects and reactive power flow are neglected.

Similar to the approach used in industry, elaborated on in Section 2.5.1, the FCCs within the ELS are identified. The park's mean wind speed at the beginning of the outage is translated into possible power using the warranted power curve. All turbines in the ELS are provided with this value as a setpoint. Iteratively, new setpoints are calculated based on the violation of the FCC static ratings if the ELS is formed. For the turbine furthest upstream, it is determined if a lower setpoint would eliminate the overload. If so, this setpoint is applied. If not, the turbine is curtailed entirely and the next turbine in the ELS is considered. This process is repeated until the FCCs are within limits. If the wind speed increases significantly, the setpoints are recalculated. Simulations concerning a 60-day outage of the foremost cable in a string with six turbines shows that compared to completely curtailing all six turbines upstream, this approach increases revenue by more than €2 million.

Since downstream turbines are curtailed, power is transmitted over the shortest distance, minimizing losses. Additionally, considering the production at the current wind speed might reduce conservativeness compared to assuming production at rated power. However, it must be noted that if the estimations of possible power are off, turbines might be curtailed excessively since all turbines in the ELS are supplied with this value as a setpoint. In addition, the approach only applies to collector systems with a double-sided ring topology. For these networks, only one link can be used to reroute the power during an outage. The approach cannot be used to determine how the network should be reconfigured for meshed topologies. Moreover, a limitation of the approach is that STR is considered rather than CTR or DTR.

2.5.3 Optimization-based network reconfiguration

The authors of [65] propose a Mixed-Integer Linear Programming (MILP) formulation for minimizing curtailment during outages. It aims to find an optimal power switch configuration of the collector system at the beginning of the outage based on a set of possible power scenarios. The objective function is to maximize the expected power production P^{exp}:

$$\max_{z_{ij}} P^{\text{exp}} = \max_{z_{ij}} \sum_{\forall (i,0) \in \mathcal{E}} \sum_{\forall s \in \mathcal{S}} p_{i0,s} \, \mathbb{P}_s \tag{2.8}$$

where $\mathcal{E}$ is the set of edges and $\mathcal{S}$ is the set of wind scenarios, with $\mathbb{P}_s$ the probability of scenario s. Edges $(i, 0)$ are the cables connected to the OSS.

The authors derive a new formulation of power flow, which they call simplified linear power flow. This formulation is only validated for one OWF topology over a single wind scenario.

The MILP model is tested on a fictitious OWF with 30 turbines, its network containing three double-sided rings and one meshed ring. Wind speed and directions are obtained from [23, 55]. The possible power for the wind scenarios is calculated by applying the Jensen wake model and a linearized power curve. It is shown that by altering the power routing via cable switching, the output of the fictitious OWF can be increased.

Although there is no mention of computation times, the MILP formulation of the optimization problem seems computationally attractive. Furthermore, optimization over the possible power scenarios ensures that the volatility of wind power is taken into account. However, the strategy cannot be used to calculate setpoints dynamically as it simply assumes that during the course of the outage, the setpoints are adjusted such that the STR is met. Another limitation of the approach is that STR is used instead of DTR.

2.5.4 Approaches for transmission and distribution networks

The collector system of an OWF resembles a distribution and transmission network. However, distribution and transmission networks mostly rely on overhead lines to transport electricity, whereas collector systems use submarine cables [46]. This means that research concerning dynamic rating in distribution and transmission networks focuses on $DTR_{weather}$ rather than DTR_{load} since a steady state is reached faster (see Section 2.3.1). Furthermore, most collector system research aims to maximize OWF production. In contrast, for distribution and transmission networks, the focus is put on balancing loads and generation.

Numerous studies have been conducted to optimally perform network reconfiguration and dynamic thermal rating in these networks, amongst others taking into account generation variability and uncertainty. The author consulted the review papers [14, 40, 36] to find existing approaches to network reconfiguration and $DTR_{weather}$ in distribution and transmission networks. In this section, a few of the computationally efficient approaches are highlighted. The efficiency of the approach is of paramount importance since incorporating DTR_{load} will introduce numerous quadratic constraints, increasing the computational complexity.

The authors of [51] present a stochastic receding horizon control approach to minimize the operational cost of a distribution network containing renewable energy sources. The uncertainty of renewable energy production is considered by optimizing over different power production scenarios generated by a neural network over a 10-hour forecasting horizon. AC power flow is used, which leads to a Mixed-Integer Nonlinear Programming (MINLP) problem, solved using a genetic algorithm at an hourly rate. The case study concerning a network with 167 buses and seven switches shows that the operational costs can be decreased. Moreover, it is shown that the application of receding horizon control to network reconfiguration generates robust solutions in the presence of uncertainties. However, it takes 30 minutes to solve the problem. As the problem's computational expense scales exponentially with its size, a convex or linear formulation might be more practical for a system with more switches.

The authors of [3] aim to minimize curtailment and switching costs to remove overload in a distribution network. A relaxation of AC power flow is used, which results in a Mixed-Integer Quadratically Constrained Programming (MIQCP) problem. Results concerning four different distribution systems show that considerable reductions in curtailed generation can be achieved by reconfiguring the network when an overload is detected. The computational times are in the order of seconds. It must be noted that the relaxation of AC power flow can only be used for radially operated networks.

The authors of [37] apply optimal switching and $DTR_{weather}$ for the day-ahead scheduling of a transmission network. The objective of the MILP problem is to minimize the generation and wind curtailment costs, while meeting the load demand. Linear power flow is used to describe the power flow through the system. Results show that coordinated implementation of $DTR_{weather}$ and optimal switching can lead to significant wind power curtailment reduction: 69% reduction was achieved, compared to 29% and 36% when solely applying optimal switching and $DTR_{weather}$ respectively.

2.6 Summary

This chapter provided an overview of the modeling and control of OWF collector systems. The main findings of the chapter are summarized in this section.

Two variables that the operator can control are the state of the power switches, to reroute the power, and the turbine setpoints, that upper-bound the turbine production. During inter-array outages, rerouting needs to be performed to transport the power produced by the turbines connected to the inoperative cable to the OSS. If the power is rerouted, turbine setpoints need to be adjusted to prevent overloading of the cables.

Collector system cables are limited in their capacity by their conductor temperature, which should not exceed 90 °C. Typically, the cables are designed and operated according to their STR. Applying this rating leads to under-utilization of the cables since it disregards the fluctuations in wind power and the thermal constant of the cables. DTR_{load} allows for harvesting the full potential of the cables' capacity by dynamically determining the rating based on the cable temperature measured by DTS and predicted by a dynamic temperature model. Within an optimization problem, a third-order state space model with the squared current as input can be used. Its parameters are to be found by fitting the model to operational data.

The author recommends using linear power flow within a collector system optimization framework. Although it is less accurate than the non-convex AC power flow, findings suggest that the severity of the approximation error might be limited for collector systems. Further research must be conducted to quantify the error. The switches that enable the rerouting of power can be incorporated into the power flow model as binary variables.

In industry, rerouting is performed by enabling a single cablelink and considering STR to determine the setpoints. The authors in [54] extend this approach by taking into account wind speed measurements to derive setpoints dynamically. The authors of [65] develop an approach that considers multiple cables to reroute the power at the beginning of the outage and optimizes over a probability distribution function of possible power. However, their method cannot be used to derive setpoints. Given that inter-array outages typically last more than a month, any improvement in determining suitable control actions can significantly reduce the loss of production during outages. Promising areas of improvement are the incorporation of DTR_{load}, dynamic setpoint adaptation, and dynamic network reconfiguration.

Chapter 3

Optimization-based control of collector systems during outages

In this chapter, two control strategies are derived that aim to maximize power production during outages. Both strategies consider all operable cables for rerouting to actively distribute the power throughout the collector system. Since increasingly the design of collector systems is tailored to the specifics of the site, the control strategies should be applicable to arbitrary topologies. This motivates the need for an optimization-based approach.

The open-loop control strategy, of which the framework is presented in Section 3.1, is intended for Offshore Wind Farms (OWFs) without an automated control system. In contrast, the receding horizon control strategy assumes that such a system is in place. This strategy is elaborated on in Section 3.2. A summary is given in Section 3.3.

3.1 Open-loop control strategy

If there is no automated control system in place, service technicians have to go to the relevant turbines when weather conditions allow it to perform manual switching. In addition, the wind farm operator separately has to log onto each affected turbine to provide a new setpoint. For such an OWF, applying control actions dynamically is inconvenient and costly. To this end, the open-loop control strategy aims to maximize power production during an outage under the constraint that setpoint adaptation and network reconfiguration can only be performed at the beginning of an outage. Due to the long duration of an outage and the uncertainties related to wind power production, Static Thermal Rating (STR) is applied rather than Dynamic Thermal Rating (DTR).

The framework used within the open-loop control strategy to model the collector system is described in Section 3.1.1. The proposed optimization problem is a Mixed-Integer Linear Programming (MILP) problem of which the objective is to maximize the expected power production of the entire wind farm over the outage. This objective function is elaborated

on in Section 3.1.2. Furthermore, the open-loop controller constrains the network to radial operation. The motivation behind this and the pertaining set of constraints is discussed in Section 3.1.3. The STR is adhered to by imposing a constraint on the power flow, as elaborated on in Section 3.1.4. Subsequently, Section 3.1.5 and Section 3.1.6 present constraints related to power balance and power production limits. The full formulation is presented in Section 3.1.7.

3.1.1 Modeling framework

Let $\mathcal{V} = \{0, ..., N\}$ denote the set of nodes pertaining to the Offshore Substation (OSS) and the turbines. Here, N is the number of turbines, and node 0 corresponds to the OSS. The production of turbine i is given by P_i, and the export of the wind farm is given by P_0.

The modeling framework of the open-loop control strategy is depicted in Figure 3.1. The cables are modeled in a directed fashion. To this end, the set $\mathcal{A}$ is introduced, which denotes the set of arcs corresponding to the operative cables between the nodes. The cable connecting node i and node j occurs twice within the set of arcs: as (i, j) and (j, i). Since power can only flow over the same cable in one direction, one of the power flows over the cable connecting node i and j is zero and the other is non-negative.

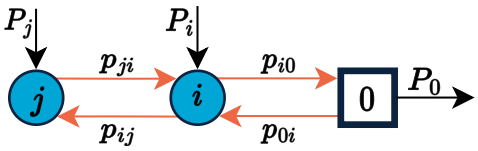

Figure 3.1: Modeling framework of the open-loop control strategy.

3.1.2 Objective function

Within the framework of the open-loop control strategy, power production over an outage is not directly optimized for since the possible power over the outage period is uncertain at the beginning of an outage. As an alternative, a possible power forecast could be incorporated in the framework. However, since an outage on average lasts 38 days [58], and the accuracy of wind power forecasting strongly deteriorates after a couple of days [19], it is chosen not to use the possible power forecasts within this optimization framework. In the following paragraphs, three different objective functions will be discussed in light of their applicability to the problem at hand. Subsequently, an extension to the objective function is presented to penalize unnecessary switching actions.

Maximizing setpoints

The objective function could be to maximize the sum of the turbine setpoints. However, the controller would then be indifferent to the distribution of the setpoints over the network. At certain wind speeds, this could result in unnecessarily low production. Take for instance the network of Figure 3.2 with the parameters listed in Table 3.1. The two turbines each have a rated power of 1.5 MW, and the cables are rated at 2 MW. Maximizing the sum of the turbine setpoints results in an infinite amount of optimal solutions, one of which is applying a setpoint of 0.5 MW to one turbine and 1.5 MW to the other turbine. Another optimal solution is adjusting the setpoints for both turbines to 1 MW. The farm production P_0 is shown for both sets of setpoints for different values of possible power P^{poss} in Figure 3.3.

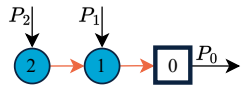

Figure 3.2: An OWF consisting of two turbines and two cables.

Parameters	Value
P_1^{r}, P_2^{r}	1.5 MW
p_{21}^{STR}, p_{10}^{STR}	2 MW

Table 3.1: Parameters of the OWF in Figure 3.2.

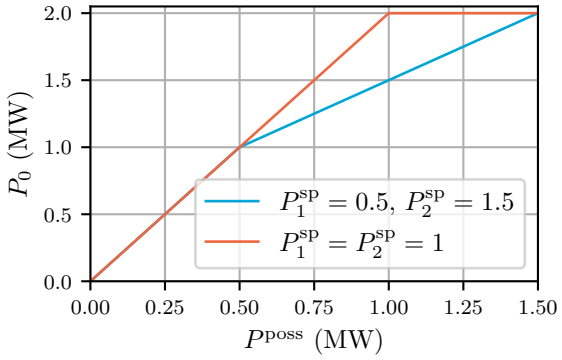

Figure 3.3: Wind farm output P_0 over different possible power scenarios P^{poss}.

As can be seen, the power production is significantly higher under certain possible scenarios when the setpoints are both set to 1 MW. It is thus crucial to consider the distribution of the setpoints over the network.

Maximizing and distributing setpoints

The objective function could be to maximize the sum of the turbine setpoints and subsequently distribute the setpoints as evenly as possible over the turbines. To facilitate this, a two-step approach could be taken, in which first the sum of the setpoints is maximized under the network constraints. Next, the sum of setpoints is constrained to this value, and the optimization problem is rerun with the objective function to distribute the setpoints evenly over the system, for instance by minimizing the 1-norm of the differences between the turbine setpoints. This two-step approach is equivalent to penalizing the former objective function with the same 1-norm accompanied by a sufficiently small penalty coefficient.

However, the distribution of setpoints over the network is not always less important than the sum of the setpoints. This can be shown with the network in Figure 3.4 and its parameters listed in Table 3.2.

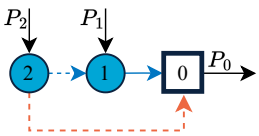

Figure 3.4: An OWF consisting of two turbines and three cables.

Parameters	Value
P_1^{r}, P_2^{r}	1.5 MW
p_{21}^{STR}, p_{10}^{STR}	2.4 MW
p_{20}^{STR}	1 MW

Table 3.2: Parameters of the OWF in Figure 3.4.

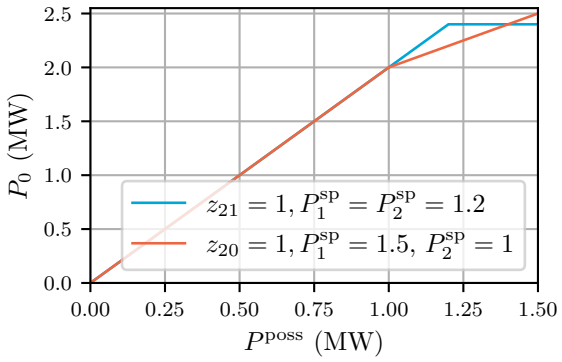

Figure 3.5: Wind farm output P_0 over different possible power scenarios P^{poss}.

Since the network is constrained to operate radially (see Section 3.1.3), either cable $(2,0)$ or $(2,1)$ can be used to transport the power of turbine 2. When cable $(2,0)$ is used ($z_{20}=1$), the sum of the optimal setpoints is 2.5 MW, whereas if cable $(2,1)$ is used ($z_{21}=1$), the sum of the optimal setpoints is 2.4 MW. As shown in Figure 3.5, the network reconfiguration with the lower sum of setpoints ($z_{21}=1$) has a higher output under certain possible power scenarios. The example shows that under certain possible power scenarios the distribution is even more important than the sum of the setpoints.

Maximizing production under scenarios

To incorporate wind power variability into the optimization framework, a probabilistic approach is taken, in which the objective is to maximize the power production over a set of scenarios:

$$\max_{\Xi} \quad \sum_{s\in\mathcal{S}} \sum_{i\in\mathcal{V}\setminus\{0\}} P_{i,s}\mathbb{P}_s \tag{3.1}$$

where Ξ is the vector of decision variables. The set $\mathcal{S}$ denotes the set of possible power production scenarios with for each scenario s a probability $\mathbb{P}_s$ and a possible power production $P_{i,s}^{\text{poss}}$. The actual power output of turbine i at scenario s, $P_{i,s}$, is given by the minimum of the setpoint and the possible power production at that scenario. The resulting control actions are optimal if the set of scenarios is representative of the possible power during the outages.

The scenarios can be generated from historical possible power data. The turbines can be grouped by their warranted power curve and a joint probability distribution function can be created from the average possible power data per turbine type. This approach entails neglecting wake effects. If a certain wind direction is dominant, this will result in sub-optimal solutions to the optimization problem.

Remark 1. To account for wake effects, the turbines can be incorporated individually in the joint probability distribution function. However, a trade-off needs to be made between complexity and performance. As the size of the wind farm increases, setting up a joint probability function containing all individual turbines results in a large set of scenarios over which the optimization has to be performed.

For newly built wind farms, the possible power data can be generated from reanalysis of wind speed data, i.e., ERA5 [18] or MERRA [52]. The input space of the joint probability distribution function is then the wind speed and the wind direction. The probability of each combination of wind speed and direction can be calculated, as well as the pertaining turbine possible power. Wake effects can be taken into account by using the warranted power curve in combination with the Jensen wake model to convert the wind speed and direction into possible power, as described in Section 2.2.1.

The sensitivity of the controller to the set of scenarios can be assessed by comparing the solutions to the optimization problem with different probability distributions. If the open-loop controller proves to be sensitive to the set of scenarios, using a seasonal (joint) probability distribution is beneficial. This allows for the incorporation of the strong seasonal patterns in wind speeds [34], tailoring to the circumstances of the season in which the outage occurs.

Finally, the possible power data should be binned into groups with at least the same resolution as the resolution with which the setpoints can be applied. As an example, consider again the network in Figure 3.2 with the parameters listed in Table 3.1. If the set of scenarios only contains $P_{1,0}^{\text{poss}} = P_{2,0}^{\text{poss}} = 1.5$ MW and $P_{1,1}^{\text{poss}} = P_{2,1}^{\text{poss}} = 0.5$ MW, with equal probability, an optimal solution would be $P_1^{\text{sp}} = 1.5$ MW and $P_2^{\text{sp}} = 0.5$ MW with an objective value of 1.5 MW. However, when the possible power is for instance 1 MW, these setpoints result in unnecessary curtailment, as illustrated in Figure 3.3. Therefore, the set of scenarios should contain all setpoints that can be applied.

Preventing unnecessary switching actions

To prevent switching actions that result in little or no improvement in power production, a penalty term can be added to the objective function of the open-loop control strategy:

$$\max_{\Xi} \quad \left(\sum_{s \in \mathcal{S}} \sum_{i \in \mathcal{V} \setminus \{0\}} P_{i,s} \mathbb{P}_s \right) - c \cdot \sum_{(i,j) \in \mathcal{A}} \left| z_{ij} - z_{ij}^{\text{standard}} \right| \tag{3.2}$$

where c is the penalty coefficient and z_{ij}^{standard} is the configuration of the cable under normal operation. Eq. (3.2) can be reduced to a linear objective function by introducing auxiliary variables ζ_{ij}:

$$\max_{\Xi} \quad \left(\sum_{s \in \mathcal{S}} \sum_{i \in \mathcal{V} \setminus \{0\}} P_{i,s} \mathbb{P}_s \right) - c \cdot \sum_{(i,j) \in \mathcal{A}} \zeta_{ij} \tag{3.3}$$

$$\text{s.t.} \quad -\zeta_{ij} \leq z_{ij} - z_{ij}^{\text{standard}} \leq \zeta_{ij} \qquad \text{for } (i,j) \in \mathcal{A} \tag{3.4}$$

3.1.3 Radiality

In this section it will be shown that the reconfigured network should be radial to guarantee adherence to the STR under the uncertainty of power production over the outage period.

Let p_{ij}^{sp} denote the power flow from node i to node j when all turbines are producing at setpoint. When the turbines are producing at setpoint, the STR must not be violated, i.e., we need ($p_{ij}^{\text{sp}} \leq p_{ij}^{\text{STR}}$ for $(i,j) \in \mathcal{A}$). Moreover, since the power production over the outage period is uncertain, the applied setpoints must ensure that for any power production conforming to these setpoints, the STR is also adhered to. To ensure this, the following relationship must hold:

$$P_i \leq P_i^{\text{sp}} \quad \text{for } i \in \mathcal{V} \setminus \{0\} \implies p_{ij} \leq p_{ij}^{\text{sp}} \quad \text{for } (i,j) \in \mathcal{A} \tag{3.5}$$

Looped network

When loops are present in the network, relationship (3.5) does not necessarily hold. This can be illustrated with an example. The OWF in Figure 3.6 along with the parameters in Table 3.3 is considered. The power flows through the network can be calculated with (2.3). If the cable admittances are all equal and the power productions are $P_1 = P_3 = 1$ MW and

$P_2 = 2$ MW, the power flows are $p_{21} = p_{23} = 1$ MW and $p_{10} = p_{30} = 2$ MW. These power flows all adhere to the cable ratings listed in Table 3.3. However, if these power productions would be applied as setpoints in combination with the topology shown in the figure, there is a risk of exceeding the cable rating. Namely, when for instance $P_3 = 0$ MW, which would be lower than its setpoint, and the other turbines are producing at setpoint, $p_{23} = 1.25$ MW, which exceeds its rating p_{23}^{STR}.

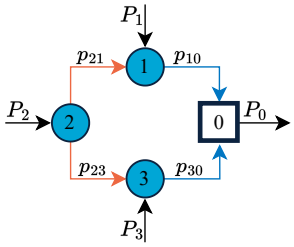

Figure 3.6: An OWF consisting of three turbines.

Parameters	Value
p_{21}^{STR}, p_{23}^{STR}	1 MW
p_{10}^{STR}, p_{30}^{STR}	2 MW

Table 3.3: Parameters of the OWF in Figure 3.6.

This example shows that when loops are present in the network, production conform setpoints is not a sufficient condition to guarantee that the STR is adhered to. Since aside from setpoint adaptation and network reconfiguration there are no other control actions that can be taken during outages, the network must be constrained to radial operation. First, the mathematical formulation for radial operation will be presented, after which it is proven that under radial operation adherence to the cable ratings in case of production at setpoint is a sufficient condition to guarantee that all cable ratings will be adhered to during the entire outage period.

Radiality constraints

To constrain a collector system to radial operation, the sum of the outgoing power flows per turbine should be less or equal than one [17]. This constraint motivates using a set of directed arcs to model the network:

$$z_{ij} \in \{0, 1\} \qquad \text{for } (i,j) \in \mathcal{A} \tag{3.6}$$

$$z_{ij} + z_{ji} \leq 1 \qquad \text{for } (i,j) \in \mathcal{A} \tag{3.7}$$

$$\sum_{j|(i,j)\in\mathcal{A}} z_{ij} \leq 1 \qquad \text{for } i \in \mathcal{V}\backslash\{0\} \tag{3.8}$$

$$0 \leq p_{ij} \leq p_{ij} z_{ij} \qquad \text{for } (i,j) \in \mathcal{A} \tag{3.9}$$

where (3.7) dictates that the power can flow over the same cable in only one direction and (3.9) constrains the power flows to be non-negative, and zero when $z_{ij} = 0$. This set of constraints guarantees radial operation in case there are no power flows from the OSS to the turbines. Since the OSS is the only sink in the network and the nodal balance in (2.3a) must hold, this will be the case.

Proof of adherence to STR in case of radiality

Under the constraints listed above, relationship (3.5) holds. This can be proven by contradiction. Suppose that relationship (3.5) does not hold. Then there exists a scenario in which all turbines are producing at their setpoint and for at least one of the cables, here denoted by cable α, the power flow exceeds the power flow that is present when all turbines are producing at their setpoint:

$$P_i \leq P_i^{\text{sp}} \qquad \text{for } i \in \mathcal{V}\backslash\{0\} \tag{3.10}$$

$$p_\alpha > p_\alpha^{\text{sp}} \tag{3.11}$$

$$p_{ki} \leq p_{ki}^{\text{sp}} \qquad \text{for } (k,i) \in \mathcal{A}\backslash\{\alpha\} \tag{3.12}$$

where (3.12) dictates that for all other cables the power flows are within the power flows that are present when all turbines are producing at their setpoint. Since the network is operated in a radial manner, the transportation model, (2.3a), can be used to describe the network. Furthermore, due to (3.8) and (3.9) there will will be only one outgoing power flow per node in the system. Therefore, the following holds:

$$p_{ij}^{\text{sp}} = P_i^{\text{sp}} + \sum_{k|(k,i)\in\mathcal{A}} p_{ki}^{\text{sp}} \qquad \text{for } (i,j) \in \mathcal{A} \tag{3.13}$$

$$p_{ij} = P_i + \sum_{k|(k,i)\in\mathcal{A}} p_{ki} \qquad \text{for } (i,j) \in \mathcal{A} \tag{3.14}$$

For node $i|(i,j) = \alpha$, the following then must hold to adhere to (3.11):

$$P_i + \sum_{k|(k,i)\in\mathcal{A}} p_{ki} > P_i^{\text{sp}} + \sum_{k|(k,i)\in\mathcal{A}} p_{ki}^{\text{sp}} \qquad \text{for } i|(i,j) = \alpha \tag{3.15}$$

In combination with (3.10) this results in the following constraint:

$$\sum_{k|(k,i)\in\mathcal{A}} p_{ki} > \sum_{k|(k,i)\in\mathcal{A}} p_{ki}^{\text{sp}} \qquad \text{for } i|(i,j) = \alpha \tag{3.16}$$

which contradicts (3.12). Therefore, relationship (3.5) must hold.

3.1.4 Power flow limits

As was proven in Section 3.1.3, radial operation guarantees that the power flows during the outage will never exceed the power flows present when producing at setpoint. Hence, the power flow constraints only need to be formulated for production at setpoint:

$$0 \leq p_{ij}^{\text{sp}} \leq p_{ij}^{\text{STR}} z_{ij} \qquad \text{for } (i,j) \in \mathcal{A} \tag{3.17}$$

3.1.5 Power balance

Since a radial network is concerned, the transportation model and linear power flow model are equivalent. It is chosen to model the power flows for production at setpoint with the transportation model since it involves less variables:

$$P_i^{\text{sp}} - \sum_{j|(i,j)\in\mathcal{A}} p_{ij}^{\text{sp}} + \sum_{i|(j,i)\in\mathcal{A}} p_{ji}^{\text{sp}} = 0 \qquad \text{for } i \in \mathcal{V} \tag{3.18}$$

3.1.6 Power production limits

It is assumed that turbines only produce power rather than consume power. The power output of a turbine at a scenario, $P_{i,s}$, is given by the minimum of the setpoint and the possible power production at that scenario:

$$0 \leq P_{i,s} \leq P_s^{\text{poss}} \qquad \text{for } i \in \mathcal{V}\backslash\{0\},\ s \in \mathcal{S} \tag{3.19}$$

$$P_{i,s} \leq P_i^{\text{sp}} \qquad \text{for } i \in \mathcal{V}\backslash\{0\},\ s \in \mathcal{S} \tag{3.20}$$

When it is known that a turbine will be inoperative during the entire outage period, it might be possible to increase the setpoints of the operative turbines. This can be incorporated into the mathematical formulation as follows:

$$P_i^{\text{sp}} = 0 \qquad \text{for } i \in \mathcal{T} \tag{3.21}$$

where $\mathcal{T}$ denotes the set of inoperative turbines.

3.1.7 Full formulation

The resulting MILP problem is the following:

$$\max_{\Xi} \quad \left(\sum_{s\in\mathcal{S}} \sum_{i\in\mathcal{V}\backslash\{0\}} P_{i,s}\mathbb{P}_s\right) - c \cdot \sum_{(i,j)\in\mathcal{A}} \zeta_{ij} \tag{3.22a}$$

$$\text{s.t.} \quad -\zeta_{ij} \leq z_{ij} - z_{ij}^{\text{standard}} \leq \zeta_{ij} \qquad \text{for } (i,j) \in \mathcal{A} \tag{3.22b}$$

$$z_{ij} \in \{0,1\} \qquad \text{for } (i,j) \in \mathcal{A} \tag{3.22c}$$

$$z_{ij} + z_{ji} \leq 1 \qquad \text{for } (i,j) \in \mathcal{A} \tag{3.22d}$$

$$\sum_{j|(i,j)\in A} z_{ij} \leq 1 \qquad \text{for } i \in \mathcal{V} \tag{3.22e}$$

$$0 \leq p_{ij}^{\text{sp}} \leq p_{ij}^{\text{STR}} z_{ij} \qquad \text{for } (i,j) \in \mathcal{A} \tag{3.22f}$$

$$P_i^{\text{sp}} - \sum_{j|(i,j)\in\mathcal{A}} p_{ij}^{\text{sp}} + \sum_{i|(j,i)\in\mathcal{A}} p_{ji}^{\text{sp}} = 0 \qquad \text{for } i \in \mathcal{V} \tag{3.22g}$$

$$0 \leq P_{i,s} \leq P_s^{\text{poss}} \qquad \text{for } i \in \mathcal{V}\backslash\{0\},\ s \in \mathcal{S} \tag{3.22h}$$

$$P_{i,s} \leq P_i^{\text{sp}} \qquad \text{for } i \in V\backslash\{0\},\ s \in \mathcal{S} \tag{3.22i}$$

$$P_i^{\text{sp}} = 0 \qquad \text{for } i \in \mathcal{T} \tag{3.22j}$$

where Ξ is a vector that contains all values of P_i^{sp}, z_{ij}, $P_{i,s}$, p_{ij}^{sp}, and ζ_{ij}. The problem can be solved using a branch-and-bound algorithm [47].

3.2 Receding horizon control strategy

The receding horizon control strategy assumes that an automated control system is in place that can directly apply setpoint adaptation and network reconfiguration at any given time during the outage. By performing online calculations, cable temperature measurements and power forecasts can be taken into account to tailor the control actions to the specifics of the hour. This allows for constraining the power flows based on the cable temperature limits rather than based on the STR.

The control strategy consists of solving two optimization problems at each hour. The first stage is a Mixed-Integer Quadratically Constrained Programming (MIQCP) problem that entails finding optimal turbine productions and network topologies over a moving horizon based on the power forecasts. In this problem, it is assumed that the power forecast is perfect. The second stage then deals with uncertainty in the forecast to prevent unnecessary curtailment if the forecast is too low. The corresponding Quadratically Constrained Linear Programming (QCLP) problem aims at finding the optimal setpoints for the current hour. While the problems could be merged into one, they are kept separate for clarity.

The framework used to model the collector system is described in Section 3.2.1. The first stage is elaborated on in Section 3.2.2, and the second stage is discussed in Section 3.2.3. Finally, the full formulation is presented in Section 3.2.4.

3.2.1 Modeling framework

The receding horizon control strategy uses the same set $\mathcal{V}$ as the open-loop control strategy for describing the nodes in the network. However, a different set is used to describe the cables.

A radiality constraint as in (3.8) is no longer posed on the network since taking into account forecasts will allow calculating more precisely how the power will flow through any loops in the network. Deviations from the estimation will not accumulate since these will be reflected in the temperature measurements. Therefore, a different set, $\mathcal{E}$, is used to describe the cables than for the open-loop control strategy. In this set of edges, the cable connecting node i and node j occurs only once, limiting the number of binary variables. The corresponding modeling framework is shown in Figure 3.7.

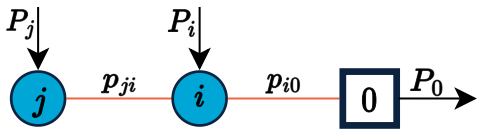

Figure 3.7: Modeling framework of the receding horizon control strategy.

3.2.2 Stage 1: network reconfiguration

The first stage aims to find optimal network configurations over a prediction window. At each hour t, the optimization problem is formulated using the most recent power forecasts and the measured cable temperatures, since these are available at an hourly rate. The optimal network configuration pertaining to the current hour is applied to the network. The second stage uses this configuration as input to calculate the optimal setpoints for the current hour. At the next iteration, the optimization problem is reformulated using the updated measurements.

For the first stage, a multi-rate framework is proposed that uses two different time intervals within the prediction window. Close to hour t, DTR is applied to unlock the available headroom of the network (see Section 2.3.1). These quadratic constraints are only formulated for time steps concerning the near future. It might be of importance to also look at time steps further in the future to be able to prevent an excessive number of switching actions. The power flows in the far future are constrained linearly by the Cyclic Thermal Rating (CTR) (see Section 2.3.1) to decrease the computational burden. While this might introduce prediction inaccuracies within the receding horizon control strategy, the impact on the control actions being taken is expected to be limited since only the network reconfiguration pertaining to the current hour is applied to the network. The choice of CTR for the far future is further motivated by the growing uncertainty of the power forecast over the prediction window and the relatively short thermal time constant of the cables (5 hours, [30]).

The time interval h concerning the time steps in the near future is short (1 hour) to be able to model the temperature dynamics. To this end, the set $\mathcal{H}_t = \{t, t+h, ..., t+N_{\mathrm{p}}^{\mathrm{short}}-1\}$ is introduced, where $N_{\mathrm{p}}^{\mathrm{short}}$ is the length of the prediction window for the short-term model.

For the time steps concerning the far future, a longer time interval l is selected (1 day). Furthermore, the set $\mathcal{L}_t = \{t+N_{\mathrm{p}}^{\mathrm{short}}, t+N_{\mathrm{p}}^{\mathrm{short}}+l, ..., t+N_{\mathrm{p}}^{\mathrm{short}}+N_{\mathrm{p}}^{\mathrm{long}}-1\}$ is introduced, where $N_{\mathrm{p}}^{\mathrm{long}}$ is the length of the prediction window for the long-term model.

In the following sections, the objective function, power flow, power balance, and power production constraints of the first stage will be elaborated on.

Objective function

The objective function at hour t aims to maximize the expected power production over the prediction window:

$$\max_{\Xi_{t,1}} \quad \sum_{k\in\mathcal{H}_t\cup\mathcal{L}_t} \sum_{i\in\mathcal{V}\setminus\{0\}} P_{i,k} \tag{3.23}$$

where $\Xi_{t,1}$ is the vector of decision variables and $P_{i,k}$ is the power production of turbine i at time step k under the assumption of a perfect forecast. A term is added to the objective function to penalize switching actions:

$$\max_{\Xi_{t,1}} \quad \sum_{k\in\mathcal{H}_t\cup\mathcal{L}_t} \left(\sum_{i\in\mathcal{V}\setminus\{0\}} P_{i,k} - c_1 \cdot \sum_{(i,j)\in\mathcal{A}} |z_{ij,k} - z_{ij,k-1}| \right) \tag{3.24}$$

where c_1 is the penalty coefficient and $z_{ij,k}$ is the on/off status of cable (i,j) at time step k. Eq. (3.24) can be reduced to a linear objective function by introducing auxiliary variables $\zeta_{ij,k}$:

$$\max_{\Xi_{t,1}} \quad \sum_{k\in\mathcal{H}_t\cup\mathcal{L}_t} \left(\sum_{i\in\mathcal{V}\setminus\{0\}} P_{i,k} - c_1 \cdot \sum_{(i,j)\in\mathcal{A}} \zeta_{ij,k} \right) \tag{3.25}$$

$$\text{s.t.} \quad -\zeta_{ij,k} \le z_{ij,k} - z_{ij,k-1} \le \zeta_{ij,k} \qquad \text{for } (i,j)\in\mathcal{E},\ k\in\mathcal{H}_t\cup\mathcal{L}_t \tag{3.26}$$

Furthermore, a penalty term is added that aims to distribute the deviations from the power forecast evenly over the network:

$$\max_{\Xi_{t,1}} \quad \sum_{k\in\mathcal{H}_t\cup\mathcal{L}_t}\left(\sum_{i\in\mathcal{V}\setminus\{0\}} P_{i,k} - c_1\cdot\sum_{(i,j)\in\mathcal{E}}\zeta_{ij,k} - c_2\cdot \right.$$
$$\left.\sum_{i\in\mathcal{V}\setminus\{0\}}\sum_{j\in\mathcal{V}:j>i}|P_{i,k} - P^{\text{forecast}}_{i,k|t} - P_{j,k} + P^{\text{forecast}}_{j,k|t}|\right) \tag{3.27}$$

where c_2 is the penalty coefficient and $P^{\text{forecast}}_{i,k|t}$ is the power forecast of turbine i made at hour t concerning time step k. Eq. (3.27) can be reduced to a linear objective function by introducing auxiliary variables $\psi_{i,j,k}$:

$$\max_{\Xi_{t,1}} \quad \sum_{k\in\mathcal{H}_t\cup\mathcal{L}_t}\left(\sum_{i\in\mathcal{V}\setminus\{0\}} P_{i,k} - c_1\cdot\sum_{(i,j)\in\mathcal{E}}\zeta_{ij,k} - c_2\cdot\sum_{i\in\mathcal{V}\setminus\{0\}}\sum_{j\in\mathcal{V}:j>i}\psi_{i,j,k}\right) \tag{3.28}$$

$$\text{s.t.} \quad -\psi_{i,j,k} \le P_{i,k} - P^{\text{forecast}}_{i,k|t} - P_{j,k} + P^{\text{forecast}}_{j,k|t} \le \psi_{i,j,k} \qquad \begin{array}{l}\text{for } i\in\mathcal{V}\setminus\{0\},\\ j\in\mathcal{V}:j>i,\ k\in\mathcal{H}_t\cup\mathcal{L}_t\end{array} \tag{3.29}$$

Power flow limits

For the short prediction window, the power flows are constrained by the cable temperature limit. To this end, the thermal model of (2.1) is used, with as input the power flow instead of the current. As shown in (2.2), the two are linearly related, which entails that they can be interchanged as long as the parameters are fitted with the corresponding quantity as input. The resulting model can be discretized as follows:

$$T_{ij,t+1} = a_{ij}T_{ij,t} + b_{ij}T_{ij,t-1} + c_{ij}T_{ij,t-2} + d_{ij}p^2_{ij,t} + e_{ij} \quad \text{for } (i,j)\in\mathcal{E} \tag{3.30}$$

where $T_{ij,t}$ is the temperature of cable (i,j) at hour t, $p_{ij,t}$ is the power flow through cable (i,j) at hour t, and a_{ij}, b_{ij}, c_{ij}, d_{ij}, and e_{ij} are cable and location-specific parameters that can be found by fitting the model to temperature and power data. With respect to the state-space cable temperature model of [30], the term e_{ij} is added since this turns out to result in a better fit for the data of the case study of Chapter 4. To predict future cable temperatures, the model must be initialized with three Distributed Temperature Sensing (DTS) measurements, $T^{\text{DTS}}_{ij,t}$, $T^{\text{DTS}}_{ij,t-1}$, and $T^{\text{DTS}}_{ij,t-2}$. For the first two hours, the temperatures can then be predicted as follows:

$$T_{t+1|t} = aT^{\text{DTS}}_t + bT^{\text{DTS}}_{t-1} + cT^{\text{DTS}}_{t-2} + dp^2_t + e \tag{3.31}$$
$$T_{t+2|t} = aT_{t+1|t} + bT^{\text{DTS}}_t + cT^{\text{DTS}}_{t-1} + dp^2_{t+1} + e = \tag{3.32}$$
$$(a^2+b)T^{\text{DTS}}_t + (ab+c)T^{\text{DTS}}_{t-1} + acT^{\text{DTS}}_{t-2} + adp^2_t + dp^2_{t+1} + ae + e$$

in which the index ij is dropped for clarity. The power flow constraints for the short prediction window can be formulated without explicitly defining the temperatures, which avoids the use of quadratic equality constraints:

$$F_{ij}\begin{bmatrix} T^{\mathrm{DTS}}_{ij,t} \\ T^{\mathrm{DTS}}_{ij,t-1} \\ T^{\mathrm{DTS}}_{ij,t-2} \end{bmatrix} + G_{ij}\begin{bmatrix} p^2_{ij,t} \\ p^2_{ij,t+1} \\ \vdots \\ p^2_{ij,t+N^{\mathrm{short}}_{\mathrm{p}}-1} \end{bmatrix} + H_{ij} \leq T^{\max}_{N^{\mathrm{short}}_{\mathrm{p}}\times 1} \quad \text{for } (i,j) \in \mathcal{E} \tag{3.33}$$

where $F_{ij} \in \mathbb{R}^{N^{\mathrm{short}}_{\mathrm{p}}\times 3}$, $G_{ij} \in \mathbb{R}^{N^{\mathrm{short}}_{\mathrm{p}}\times N^{\mathrm{short}}_{\mathrm{p}}}$, and $H_{ij} \in \mathbb{R}^{N^{\mathrm{short}}_{\mathrm{p}}\times 1}$ are matrices parameterized by a_{ij}, b_{ij}, c_{ij}, d_{ij}, and e_{ij}, and $T^{\max}$ is the cable temperature limit. Furthermore, $T^{\max}_{N^{\mathrm{short}}_{\mathrm{p}}\times 1}$ is a vector of length $N^{\mathrm{short}}_{\mathrm{p}}$, each element being $T^{\max}$. For $N^{\mathrm{short}}_{\mathrm{p}} = 5$, the matrices are the following (for clarity the index ij is dropped):

$$F = \begin{bmatrix} a & b & c \\ a^2{+}b & ab{+}c & ac \\ a^3{+}2ab{+}c & a^2b{+}ac{+}b^2 & a^2c{+}bc \\ a^4{+}3a^2b{+}2ac{+}b^2 & a^3b{+}a^2c{+}2ab^2{+}2bc & a^3c{+}2abc{+}c^2 \\ a^5{+}4a^3b{+}3a^2c{+}3ab^2{+}2bc & a^4b{+}a^3c{+}3a^2b^2{+}4abc{+}b^3{+}c^2 & a^4c{+}3a^2bc{+}2ac^2{+}b^2c \end{bmatrix} \tag{3.34}$$

$$G = \begin{bmatrix} d & 0 & 0 & 0 & 0 \\ ad & d & 0 & 0 & 0 \\ a^2d{+}bd & ad & d & 0 & 0 \\ a^3d{+}2abd{+}cd & a^2d{+}bd & ad & d & 0 \\ a^4{+}3a^2bd{+}2acd{+}b^2d & a^3d{+}2abd{+}cd & a^2d{+}bd & ad & d \end{bmatrix} \tag{3.35}$$

$$H = \begin{bmatrix} e \\ (a{+}1)e \\ (a^2{+}a{+}b{+}1)e \\ (a{+}b{+}c{+}2ab{+}a^2{+}a^3{+}1)e \\ (a{+}b{+}c{+}2ab{+}2ac{+}3a^2b{+}a^2{+}a^3{+}a^4{+}b^2{+}1)e \end{bmatrix} \tag{3.36}$$

For the long prediction window, the power flows are constrained by the CTR:

$$-p^{\mathrm{CTR}}_{ij} z_{ij,l} \leq p_{ij,l} \leq p^{\mathrm{CTR}}_{ij} z_{ij,l} \qquad \text{for } (i,j) \in \mathcal{E},\ l \in \mathcal{L}_t \tag{3.37}$$

where p^{CTR}_{ij} is the power flow limit through cable (i,j) as defined by its CTR.

Power balance

The linear power flow model of (2.3a) and (2.5) is used to model the power flows in the system:

$$P_{i,k} - \sum_{j|(i,j)\in\mathcal{E}} p_{ij,k} + \sum_{j|(j,i)\in\mathcal{E}} p_{ji,k} = 0 \qquad \text{for } i \in \mathcal{V},\ k \in \mathcal{H}_t \cup \mathcal{L}_t \tag{3.38}$$

$$z_{ij,k} \in \{0,1\} \qquad \text{for } (i,j) \in \mathcal{E},\ k \in \mathcal{H}_t \cup \mathcal{L}_t \tag{3.39}$$

$$-M_{ij} z_{ij,h} \leq p_{ij,h} \leq M_{ij} z_{ij,h} \qquad \text{for } (i,j) \in \mathcal{E},\ h \in \mathcal{H}_t \tag{3.40}$$

$$p_{ij,k} \leq b_{ij}(\theta_{i,k} - \theta_{j,k}) + M_{ij}(1 - z_{ij,k}) \qquad \text{for } (i,j) \in \mathcal{E},\ k \in \mathcal{H}_t \cup \mathcal{L}_t \tag{3.41}$$

$$p_{ij,k} \geq b_{ij}(\theta_{i,k} - \theta_{j,k}) - M_{ij}(1 - z_{ij,k}) \qquad \text{for } (i,j) \in \mathcal{E},\ k \in \mathcal{H}_t \cup \mathcal{L}_t \tag{3.42}$$

$$\theta_{0,k} = 0 \qquad \text{for } k \in \mathcal{H}_t \cup \mathcal{L}_t \tag{3.43}$$

where $\theta_{i,k}$ is the voltage angle of node i at step k. Eq. (3.40) is not posed for time steps concerning the long prediction window as (3.37) is more stringent.

Power production limits

In this stage, it is assumed that the power forecast is perfect. Hence, the forecast can be treated as the possible power, leading to:

$$0 \leq P_{i,k} \leq P^{\text{forecast}}_{i,k|t} \qquad \text{for } i \in \mathcal{V}\backslash\{0\},\ k \in \mathcal{H}_t \cup \mathcal{L}_t \tag{3.44}$$

If there are inoperative turbines at the OWF, this will be reflected in the power forecast.

Due to the power forecast uncertainty, applying $P_{i,t}$ as setpoints would not be optimal. If the power forecast concerning hour t is lower than the possible power at that hour, it might be that the turbines are curtailed unnecessarily. Therefore, a second stage is required to find the optimal setpoints for hour t.

3.2.3 Stage 2: setpoint adaptation

The second stage aims to find the optimal setpoints for hour t. Similar to the first stage, the optimization problem is formulated at each hour t using the measured cable temperatures and the most recent power forecast. Furthermore, the values of $z_{ij,t}$ found in stage 1 are set as parameters. In addition, the power production conforming to the power flow limits under the assumption of a perfect forecast, $P_{i,t}$, is passed to the second stage. The optimal setpoints found by solving the QCLP problem of the second stage are applied to the network. At the next iteration, the optimization problem is reformulated using the updated measurements and the solutions from the first stage.

In the following sections, the objective function, power flow, power balance, and power production constraints of the second stage will be elaborated on.

Objective function

The objective function is to maximize the turbine setpoints while attempting to distribute the deviations from the power forecast evenly over the network:

$$\max_{\Xi_{t,2}} \quad \sum_{i \in \mathcal{V}\backslash\{0\}} P^{\text{sp}}_{i,t} - c_3 \cdot \sum_{i \in \mathcal{V}\backslash\{0\}} \sum_{j \in \mathcal{V}: j > i} \varrho_{i,j,t} \tag{3.45}$$

$$\text{s.t.} \quad -\varrho_{i,j,t} \leq P^{\text{sp}}_{i,t} - P^{\text{forecast}}_{i,t|t} - P^{\text{sp}}_{j,t} + P^{\text{forecast}}_{j,t|t} \leq \varrho_{i,j,t} \qquad \text{for } i \in \mathcal{V}\backslash\{0\},\ j \in \mathcal{V} : j > i \tag{3.46}$$

where $\Xi_{t,2}$ is the vector of decision variables, $P^{\text{sp}}_{i,t}$ is the setpoint of turbine i at hour t, and $\varrho_{i,j,t}$ is an auxiliary variable that ensures linearity of the objective function, similar to $\psi_{i,j,k}$ of the first stage. By distributing the deviations from the power forecast evenly over the network, it is assumed that an incorrect forecast affects the turbines to the same extent. When the wind direction forecast is inaccurate, this might result in sub-optimal solutions.

Power flow limits

The power flows at hour t must ensure that the cable temperature at $t+1$ does not violate the cable temperature limit:

$$T_{ij,t+1} = a_{ij}T^{\mathrm{DTS}}_{ij,t} + b_{ij}T^{\mathrm{DTS}}_{ij,t-1} + c_{ij}T^{\mathrm{DTS}}_{ij,t-2} + d_{ij}(p^{\mathrm{sp}}_{ij,t})^2 + e_{ij} \leq T^{\max} \quad \text{for } (i,j) \in \mathcal{E} \tag{3.47}$$

When the network is not constrained to radial operation, there is a risk of the actual power flow exceeding the power flow limits, see Section 3.1.3. However, the receding horizon control strategy ensures that the power flows adhere to the limits for production at forecast (stage 1) and production at setpoint (stage 2). Therefore, the chance of exceeding the limits for the actual power production is limited. Moreover, if large deviations from the power forecast occur, severe violations of the cable temperature limits can be prevented by taking into account the new cable temperature measurements at the next hour.

Power balance

The linear power flow model of (2.3a) and (2.4a) is used to model the power flows in the system:

$$P^{\mathrm{sp}}_{i,t} - \sum_{j|(i,j)\in\mathcal{E}} p^{\mathrm{sp}}_{ij,t} + \sum_{j|(j,i)\in\mathcal{E}} p^{\mathrm{sp}}_{ji,t} = 0 \qquad \text{for } i \in \mathcal{V} \tag{3.48}$$

$$p^{\mathrm{sp}}_{ij,t} = z_{ij,t}b_{ij}(\theta^{\mathrm{sp}}_{i,t} - \theta^{\mathrm{sp}}_{j,t}) \qquad \text{for } (i,j) \in \mathcal{E} \tag{3.49}$$

$$\theta^{\mathrm{sp}}_{0,t} = 0 \tag{3.50}$$

where $p^{\mathrm{sp}}_{ij,t}$ is the power flow at hour t for production at setpoint and $\theta^{\mathrm{sp}}_{i,t}$ is the voltage angle of turbine i at hour t for production at setpoint. Since in this stage $z_{ij,t}$ is a parameter rather than a control variable, there is no need to rewrite (3.49).

Power production limits

The setpoints must make it possible to produce at least the power production conforming to the power flow limits under the assumption of a perfect forecast, $P_{i,t}$, found in the first stage. Furthermore, the setpoints should be non-negative and should adhere to the turbine rated power:

$$P_{i,t} \leq P^{\mathrm{sp}}_{i,t} \qquad \text{for } i \in \mathcal{V}\backslash\{0\} \tag{3.51}$$

$$0 \leq P^{\mathrm{sp}}_{i,t} \leq P^{\mathrm{r}}_{i} \qquad \text{for } i \in \mathcal{V}\backslash\{0\} \tag{3.52}$$

If there are inoperative turbines at the OWF, a different setpoint configuration might be optimal. This can be considered by constraining the setpoints of the inoperative turbines to zero:

$$P^{\mathrm{sp}}_{i,t} = 0 \qquad \text{for } i \in \mathcal{T} \tag{3.53}$$

3.2.4 Full formulation

A block diagram of the receding horizon control strategy is shown in Figure 3.8. In the following sections, the mathematical formulations of both stages are presented in their entirety.

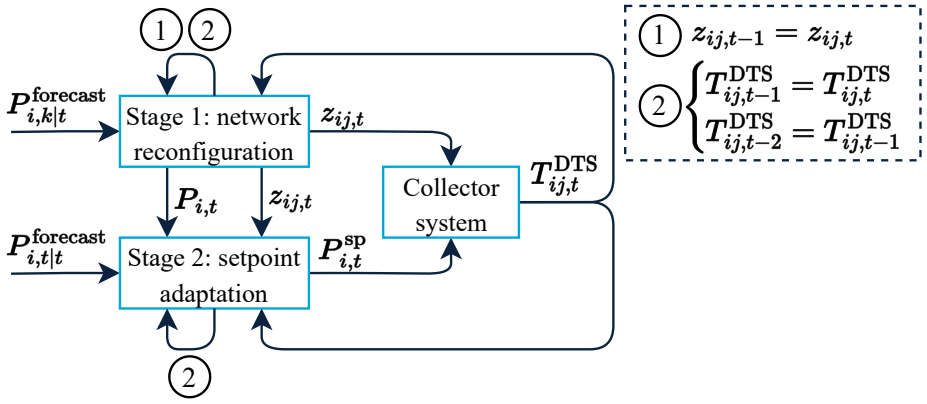

Figure 3.8: Block diagram of the receding horizon control strategy.

Stage 1: network reconfiguration

$$\max_{\Xi_{t,1}} \quad \sum_{k\in\mathcal{H}_t\cup\mathcal{L}_t}\left(\sum_{i\in\mathcal{V}\setminus\{0\}} P_{i,k} - c_1\cdot\sum_{(i,j)\in\mathcal{E}}\zeta_{ij,k} - c_2\cdot\sum_{i\in\mathcal{V}\setminus\{0\}}\sum_{j\in\mathcal{V}:j>i}\psi_{i,j,k}\right) \tag{3.54a}$$

s.t.

$$-\zeta_{ij,k} \le z_{ij,k} - z_{ij,k-1} \le \zeta_{ij,k} \qquad \text{for } (i,j)\in\mathcal{E},\ k\in\mathcal{H}_t\cup\mathcal{L}_t \tag{3.54b}$$

$$-\psi_{i,j,k} \le P_{i,k} - P^{\text{forecast}}_{i,k|t} - P_{j,k} + P^{\text{forecast}}_{j,k|t} \le \psi_{i,j,k} \qquad \text{for } i\in\mathcal{V}\setminus\{0\},\ j\in\mathcal{V}:j>i,\ k\in\mathcal{H}_t\cup\mathcal{L}_t \tag{3.54c}$$

$$F_{ij}\begin{bmatrix} T^{\text{DTS}}_{ij,t} \\ T^{\text{DTS}}_{ij,t-1} \\ T^{\text{DTS}}_{ij,t-2}\end{bmatrix} + G_{ij}\begin{bmatrix} p^2_{ij,t} \\ p^2_{ij,t+1} \\ \vdots \\ p^2_{ij,t+N_{\text{p,h}}-1}\end{bmatrix} + H_{ij} \le T^{\max}_{N_{\text{p}}\times 1} \qquad \text{for } (i,j)\in\mathcal{E} \tag{3.54d}$$

$$-p^{\text{CTR}}_{ij} z_{ij,l} \le p_{ij,l} \le p^{\text{CTR}}_{ij} z_{ij,l} \qquad \text{for } (i,j)\in\mathcal{E},\ l\in\mathcal{L}_t \tag{3.54e}$$

$$P_{i,k} - \sum_{j|(i,j)\in\mathcal{E}} p_{ij,k} + \sum_{j|(j,i)\in\mathcal{E}} p_{ji,k} = 0 \qquad \text{for } i\in\mathcal{V},\ k\in\mathcal{H}_t\cup\mathcal{L}_t \tag{3.54f}$$

$$z_{ij,k}\in\{0,1\} \qquad \text{for } (i,j)\in\mathcal{E},\ k\in\mathcal{H}_t\cup\mathcal{L}_t \tag{3.54g}$$

$$-M_{ij} z_{ij,h} \le p_{ij,h} \le M_{ij} z_{ij,h} \qquad \text{for } (i,j)\in\mathcal{E},\ h\in\mathcal{H}_t \tag{3.54h}$$

$$p_{ij,k} \le b_{ij}(\theta_{i,k} - \theta_{j,k}) + M_{ij}(1 - z_{ij,k}) \qquad \text{for } (i,j)\in\mathcal{E},\ k\in\mathcal{H}_t\cup\mathcal{L}_t \tag{3.54i}$$

$$p_{ij,k} \ge b_{ij}(\theta_{i,k} - \theta_{j,k}) - M_{ij}(1 - z_{ij,k}) \qquad \text{for } (i,j)\in\mathcal{E},\ k\in\mathcal{H}_t\cup\mathcal{L}_t \tag{3.54j}$$

$$\theta_{0,k} = 0 \qquad \text{for } k\in\mathcal{H}_t\cup\mathcal{L}_t \tag{3.54k}$$

$$0 \le P_{i,k} \le P^{\text{forecast}}_{i,k|t} \qquad \text{for } i\in\mathcal{V}\setminus\{0\},\ k\in\mathcal{H}_t\cup\mathcal{L}_t \tag{3.54l}$$

where $\Xi_{t,1}$ is a vector that contains all values of $P_{i,k}$, $z_{ij,k}$, $p_{ij,k}$, $\theta_{i,k}$, $\zeta_{ij,k}$, and $\psi_{i,j,k}$.

Stage 2: setpoint adaptation

$$\max_{\Xi_{t,2}} \quad \sum_{i\in\mathcal{V}\backslash\{0\}} P^{\mathrm{sp}}_{i,t} - c_3 \cdot \sum_{i\in\mathcal{V}\backslash\{0\}} \sum_{j\in\mathcal{V}:j>i} \varrho_{i,j,t} \tag{3.55}$$

$$\text{s.t.} \quad -\varrho_{i,j,t} \leq P^{\mathrm{sp}}_{i,t} - P^{\mathrm{forecast}}_{i,t|t} - P^{\mathrm{sp}}_{j,t} + P^{\mathrm{forecast}}_{j,t|t} \leq \varrho_{i,j,t} \qquad \text{for } i \in \mathcal{V}\backslash\{0\}, \; j \in \mathcal{V} : j > i \tag{3.56}$$

$$a_{ij}T^{\mathrm{DTS}}_{ij,t} + b_{ij}T^{\mathrm{DTS}}_{ij,t-1} + c_{ij}T^{\mathrm{DTS}}_{ij,t-2} + d_{ij}(p^{\mathrm{sp}}_{ij,t})^2 + e_{ij} \leq T^{\max} \qquad \text{for } (i,j) \in \mathcal{E} \tag{3.57}$$

$$P^{\mathrm{sp}}_{i,t} - \sum_{j|(i,j)\in\mathcal{E}} p^{\mathrm{sp}}_{ij,t} + \sum_{j|(j,i)\in\mathcal{E}} p^{\mathrm{sp}}_{ji,t} = 0 \qquad \text{for } i \in \mathcal{V} \tag{3.58}$$

$$p^{\mathrm{sp}}_{ij,t} = z_{ij,t}b_{ij}(\theta^{\mathrm{sp}}_{i,t} - \theta^{\mathrm{sp}}_{j,t}) \qquad \text{for } (i,j) \in \mathcal{E} \tag{3.59}$$

$$\theta^{\mathrm{sp}}_{0,t} = 0 \tag{3.60}$$

$$P_{i,t} \leq P^{\mathrm{sp}}_{i,t} \qquad \text{for } i \in \mathcal{V}\backslash\{0\} \tag{3.61}$$

$$0 \leq P^{\mathrm{sp}}_{i,t} \leq P^{\mathrm{r}}_{i} \qquad \text{for } i \in \mathcal{V}\backslash\{0\} \tag{3.62}$$

$$P^{\mathrm{sp}}_{i,t} = 0 \qquad \text{for } i \in \mathcal{T} \tag{3.63}$$

where $\Xi_{t,2}$ is a vector that contains all values of $P^{\mathrm{sp}}_{i,t}$, $p^{\mathrm{sp}}_{ij,t}$, $\theta^{\mathrm{sp}}_{i,t}$, and $\varrho_{i,j,t}$.

3.3 Summary

In this chapter, two novel optimization-based control strategies are developed for collector systems during cable outages.

The open-loop control strategy aims at maximizing the power production during outages under the constraint that the network and setpoints can only be reconfigured at the beginning of the outage. It is shown that the network must remain radial after the reconfiguration to guarantee adherence to the STR under every production scenario. A probabilistic approach is taken to formulate the objective function. The result is a MILP problem.

The receding horizon control strategy aims to maximize the power production during outages by calculating optimal setpoints and network configurations online over a receding horizon. In doing so, it allows for taking into account cable temperature measurements and power forecasts. Power flows are constrained quadratically based on the cable temperature limit rather than the STR. The control strategy consists of solving two stages at each time step. The first stage is a MIQCP problem that finds optimal network configurations over a receding horizon. To decrease the computational burden, the power flows for time steps further in the future are constrained by the CTR. The second stage is a QCLP problem that finds the optimal setpoints for the current hour.

Chapter 4

Case study: control of an existing collector system during outages

The control strategies developed in this work are tested on a case study and compared to existing control strategies based on the simulation results. A description of the case study is given in Section 4.1. The implementation of the four control strategies is elaborated on in Section 4.2. Subsequently, Section 4.3 presents the results. The chapter is summarized in Section 4.4.

4.1 Case study description

The open-loop and receding horizon control strategy are applied to a case study. The case study concerns an existing Offshore Wind Farm (OWF) that comprises 70 to 100 turbines. Its layout is meshed and contains three distinct cable sizes. The cable ratings, resistances, reactances, and lengths are obtained from datasheets provided by Vattenfall. A fictitious, comparable layout is shown in Figure 4.1.

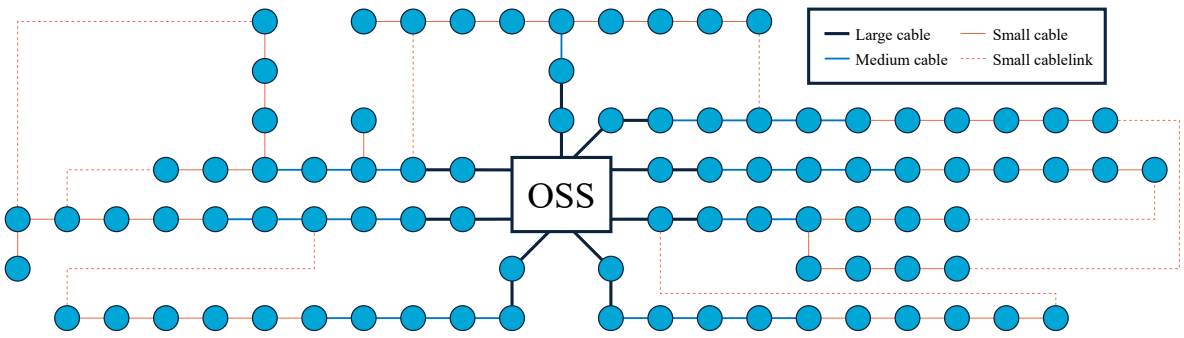

Figure 4.1: Schematic of a meshed OWF collector system that resembles the layout of the case study OWF. The circles represent the turbines.

The strategies are benchmarked against existing control strategies. Only one approach was found in literature that describes how to determine setpoints during inter-array outages, namely [54], hereafter referred to as the literature control strategy. Both this approach and the industry approach are considered in the case study. An overview of the strategies is given in Table 4.1.

Table 4.1: Control strategies considered in the case study.

Strategy	Rating	Input	Output
Industry	STR	Inoperative cable	Fixed setpoints, fixed topology (single link per cable outage)
Literature [54]	STR	Inoperative cable, park mean wind speed	Dynamic setpoints
Open-loop	STR	Inoperative cable	Fixed setpoints, fixed topology
Receding horizon	DTR_{load} & CTR	Inoperative cable, power forecast, DTS measurement	Dynamic setpoints, dynamic topology

The performance of the controllers is assessed for seven occurred outages. These outages all concern different cable sections. An overview of the different outages is given in Table 4.2. As can be seen, one of the outages concerns two cables.

Table 4.2: Details of the outages considered in the case study. Base case power refers to the percentual gap with the possible power if all turbines connected to the inoperative cable are curtailed, and no further control actions are taken.

ID	Duration (days)	Size of affected cable(s)	Base case power
1	26.5	Medium	-8.69%
2	5	Medium and large	-18.7%
3	9.5	Medium	-7.13%
4	9	Medium	-6.19%
5	18	Large	-11.1%
6	10.5	Large	-9.75%
7	144.5	Large	-9.60%

The size of the affected cable gives an indication of the location of the cable outage. During an outage concerning a large-sized cable, more turbines are affected than during an outage of a medium-sized cable.

This is also reflected in the base case power, which is indicative of the loss in production if all turbines connected to the inoperative cable were curtailed entirely and no further no control actions would have been taken.

The percentual gap between power produced during the outage and the possible power can be translated into monetary losses. With an average European offshore wind farm size of 325.5 MW [2], an average capacity factor of 0.42 [2], and an average outage duration of 38 days [58], a 1% decrease in production with respect to the possible power equates to 1.25 GWh of losses during the outage. With a feed-in remuneration of €194/MWh [54], this translates into a loss of €0.24 million per percentual decrease.

Possible power, wind speed, cable temperature, and power forecasting data are required to implement the control strategies and to perform simulations. All data is supplied by Vattenfall. Due to confidentiality restrictions, the data cannot be made publicly available. In the following sections, it will be elaborated on why this data is needed and how the data is obtained.

4.1.1 Possible power data

Possible power data is needed to set up a probability density function of possible power for the open-loop control strategy. Moreover, the possible power data will be used to perform simulations.

The possible power is taken to be the maximum of the active power output of the turbines and a possible power signal calculated by Vattenfall. This possible power signal is derived from nacelle wind speed measurements and the operational power curve. The possible power is given per turbine per 10 minutes.

At a 10-minute interval over the outage period, the simulated power production of a turbine is then the minimum of its possible power and the setpoint that the control strategy applies to the turbine.

4.1.2 Wind speed data

Implementation of the controller proposed by [54] requires park wind speed data. Following the description in the paper, this data is obtained by taking the mean of the wind speed measurements throughout the park and rounding to one decimal.

The frequency of the wind speed data used in [54] is not reported. However, the paper mentions that the operator should manually change the wind speed input value if it increases with respect to the previous value used for calculations. Therefore, it is assumed that the frequency of the data used in [54] is rather low. The same frequency as the receding horizon control strategy is used, which is one hour, facilitating a fair comparison.

4.1.3 Cable temperature data

Distributed Temperature Sensing (DTS) data is required as input to each iteration of the receding horizon control strategy. Since, for the case study, the control strategy will only be applied to the system in simulation, the temperature measurements need to be mimicked. Although the case study serves as a proof of concept, the accuracy of the synthetic measurements is relevant. Suppose the synthetic measurements are consistently lower than would actually be measured under the loading conditions. In that case, the receding horizon control strategy will derive unrealistically high setpoints that would lead to high simulated power production but also to exceeding the cable temperature at the actual OWF. An accurate cable temperature model is thus required to allow for a fair and realistic comparison in performance between the control strategies.

In the following section, the parametric cable temperature model is presented. Subsequently, a description of the power flow and cable temperature data used to fit the model is given.

Finally, the results of the system identification and the equations for the synthetic cable temperature measurements are presented.

Parametric cable temperature model

The thermal model presented in Section 3.2.2 will be used to simulate cable temperature measurements. It can be written in innovations form as follows:

$$\begin{bmatrix} T_{ij,t+1} \\ T_{ij,t} \\ T_{ij,t-1} \end{bmatrix} = \begin{bmatrix} a_{ij} & b_{ij} & c_{ij} \\ 1 & 0 & 0 \\ 0 & 1 & 0 \end{bmatrix} \begin{bmatrix} T_{ij,t} \\ T_{ij,t-1} \\ T_{ij,t-2} \end{bmatrix} + \begin{bmatrix} d_{ij} & e_{ij} \\ 0 & 0 \\ 0 & 0 \end{bmatrix} \begin{bmatrix} p_{ij,t}^2 \\ 1 \end{bmatrix} + \begin{bmatrix} k_{ij} \\ 0 \\ 0 \end{bmatrix} \varepsilon_{ij,t} \tag{4.1}$$

$$T_{ij,t}^{\mathrm{DTS}} = \begin{bmatrix} 1 & 0 & 0 \end{bmatrix} \begin{bmatrix} T_{ij,t} \\ T_{ij,t-1} \\ T_{ij,t-2} \end{bmatrix} + \varepsilon_{ij,t} \tag{4.2}$$

where a_{ij}, b_{ij}, c_{ij}, d_{ij}, and e_{ij} are cable and location-specific parameters that can be found by fitting the model to temperature and power data and $\varepsilon_{ij,t}$ is Gaussian white noise. Due to a lack of information, k_{ij} is set to 1. If additional information on the ratio of process and measurement noise were known, the parameter could be re-evaluated. Note that adjusting k_{ij} will only affect the estimated variance of the noise $\varepsilon_{ij,t}$, not the estimation of the parameters a_{ij}, b_{ij}, c_{ij}, d_{ij}, and e_{ij}.

Power flow and cable temperature data

The input to the parametric cable temperature model is the squared power flow through the cable, and its output is the DTS measurement. To find adequate parameters of the parametric cable temperature models, power flow and cable temperature data are thus required.

For parameter estimation, 4.5 months of hourly cable temperature and power flow data is used. The winter period is chosen since this is when the wind speed and hence power production fluctuates the most, increasing the amount of information that can be derived from the data. Compared to [30], the data set used is five times as large. 80% of the data is used for parameter estimation, while the final 20% is used for evaluating the quality of the model.

DTS measurements are reported at an hourly rate for each half meter of every cable. A single cable is typically several hundreds of meters long [20], and the cable temperature dynamics depend on its location. Therefore, similar to the approach in [30], a single measurement point per cable is used for fitting. Since the J-tube section is the thermal bottleneck of the cable [32], a measurement point in this section is used. Instead of simply selecting the middle point of the section as in [30], per cable, the point with the highest average temperature over the entire data set is selected. This is expected to result in a more conservative temperature model, which is desirable since none of the temperatures along the cable should exceed the temperature limits.

Active turbine power production data is re-sampled to hourly data. The linear power flow equations of (2.3) are used to calculate the power flows through the network.

System identification

For each cable, a separate thermal model is identified. To this end, Matlab's function `greyest` [60] is used, which uses the parameterized model, cable temperature measurements, and squared power flows to identify the system. Furthermore, following physical insights, the parameters a_{ij}, b_{ij}, c_{ij}, and d_{ij} are constrained to be non-negative. In addition to the parameters a_{ij}, b_{ij}, c_{ij}, d_{ij}, and e_{ij}, the variance of the noise is estimated. The focus is set to simulation instead of prediction, which means that the simulation error is minimized rather than the 1-step ahead prediction error. The Gauss–Newton algorithm is used to solve the nonlinear least squares problem [64].

The goodness of fit is evaluated based on the following two metrics [27, 64]:

$$\text{fit}_{\text{NRMSE}} = 100\% \cdot \left(1 - \frac{||\mathbf{T}_{ij}^{\text{DTS}} - \hat{\mathbf{T}}_{ij}^{\text{DTS}}||_2}{||\mathbf{T}_{ij}^{\text{DTS}} - \text{mean}(\mathbf{T}_{ij}^{\text{DTS}})||_2}\right) \tag{4.3}$$

$$\text{fit}_{\text{NMSE}} = 100\% \cdot \left(1 - \frac{||\mathbf{T}_{ij}^{\text{DTS}} - \hat{\mathbf{T}}_{ij}^{\text{DTS}}||_2^2}{||\mathbf{T}_{ij}^{\text{DTS}} - \text{mean}(\mathbf{T}_{ij}^{\text{DTS}})||_2^2}\right) \tag{4.4}$$

where $\hat{\mathbf{T}}_{ij}^{\text{DTS}}$ is the vector of temperature measurements estimated with the identified model. A value of 100% corresponds to a perfect fit, whereas a value of 0% corresponds to a fit that could have been achieved with a straight line (at the mean of the output data). The fit based on the Normalized Mean Square Error (fit_{NMSE}) is calculated since it allows comparison with the results of [30]. The values of the metrics corresponding to the best results on the test set per cable type are shown in Table 4.3.

Table 4.3: Best fit results on the test set per cable type for the cable temperature model. The final row corresponds to the fit reported by [30] concerning an export cable's J-tube section.

Cable type	$\text{fit}_{\text{NRMSE}}$ train	$\text{fit}_{\text{NRMSE}}$ test	fit_{NMSE} train	fit_{NMSE} test
Small	69.6%	52.5%	90.8%	77.4%
Medium	84.7%	73.3%	97.7%	92.8%
Large	81.3%	79.4%	96.5%	95.8%
Export [30]	-	-	88.7%	82.5%

Unfortunately, the test results for the majority of the cables are poor. This is especially pronounced for cables subjected to low power flows. In all likelihood, this stems from the simple nature of the cable temperature model. When the power flows are lower, ambient conditions will play a larger role, which the cable temperature model does not take into account.

The choice is made to use the parameters corresponding to the best fit per cable size for the simulations and the receding horizon control strategy temperature model. Since the case study serves as a proof of concept, it is deemed more appropriate to use reasonable cable temperature models rather than cable temperature models that correspond best to the individual cable data sets. The model corresponding to the medium-sized cable is used for the small-sized cables since, during outages, some of the small-sized cables might experience higher loads than those present in the data set.

Synthetic cable temperature measurements

At each outage, the temperature models are initialized with per cable the actual DTS measurements of the previous three hours. The identified cable temperature model, as presented in (4.1), can be rewritten as follows to simulate the estimated cable temperature at the next time step:

$$T_{ij,t+1} = a_{ij}T_{ij,t} + b_{ij}T_{ij,t-1} + c_{ij}T_{ij,t-2} + d_{ij}p_{ij,t}^2 + e_{ij} + \varepsilon_{ij,t} \tag{4.5}$$

where $\varepsilon_{ij,t}$ is drawn from a zero-mean normal distribution with its variance identified per cable type during system identification. The simulated DTS measurement can then be derived from (4.2) as follows:

$$T_{ij,t+1}^{\text{DTS}} = a_{ij}T_{ij,t} + b_{ij}T_{ij,t-1} + c_{ij}T_{ij,t-2} + d_{ij}p_{ij,t}^2 + e_{ij} + \varepsilon_{ij,t} + \varepsilon_{ij,t+1} \tag{4.6}$$

4.1.4 Power forecasting data

The receding horizon control strategy requires power forecasts as input. Actual historical power forecasting data could not be accessed for this research. Therefore, synthetic power forecasting data has been created.

To this end, perturbations are applied to nacelle wind speed measurements. These perturbations aim to represent the inaccuracy in wind speed and wind direction forecasting. Disturbances are added to the wind speed rather than to the possible power to capture the nonlinearity of the power curve.

At each hour t, the wind speed data of turbine i concerning the future time steps k is selected, denoted by $w_{i,k}$. For $k \in \mathcal{H}_t$, this is the mean of the 10-minute wind speed data concerning the hour following k. For $k \in \mathcal{L}_t$, this is the mean of the 24 hours following k. The following transformation is performed:

$$w_{i,k|t}^{\text{forecast}} = s_k(d_t^{\text{park}} + d_{i,t}^{\text{turbine}})w_{i,k} \tag{4.7}$$

where $w_{i,k|t}^{\text{forecast}}$ is the forecast made at hour t concerning turbine i and prediction step k, $s_k > 0$ is a factor that scales the uncertainty according to the prediction step, $d_t^{\text{park}} \sim \mathcal{N}(0, 0.1)$ is a disturbance added to all nacelle measurements in the park, and $d_{i,t}^{\text{turbine}} \sim \mathcal{N}(0, 0.05)$ is a turbine-specific disturbance added to the individual nacelle measurements. The power forecast $P_{i,k|t}^{\text{forecast}}$ is then found by applying the operational power curve to the wind speed data.

The parameters s_k are found iteratively by assessing the Normalized Root Mean Square Error (NRMSE) of the power forecast per prediction horizon for three years of data. It is attempted to align these with the values reported in [16, 19, 49]. As a result, the NRMSE values of a look-ahead time of one hour, two hours, twelve hours, and one day are 0.146, 0.161, 0.179, and 0.253, respectively.

4.2 Implementation of the control strategies

The control strategies are applied to the case study. The implementation of the four control strategies is discussed in the following sections.

4.2.1 Open-loop control strategy

The open-loop control strategy, as described in Section 3.1, is implemented in Python using the modeling framework Pyomo [4] and is solved with Gurobi [21] on a Vattenfall compute cluster (16 vCPU, 256 GiB, AMD EPYC 7452 2.35 GHz processor).

A probability distribution function of the possible power pertaining to the wind farm of the case study is required to configure the open-loop control strategy. In addition, the penalty term must be selected. In the following sections, these two topics are discussed.

Probability distribution function of possible power

The open-loop control strategy aims to maximize power production over a set of scenarios with their probabilities. To generate this set of scenarios, five years of historical possible power data are used, pertaining to the OWF of the case study. This contains the possible power per turbine per 10 minutes. These five years precede the outage periods considered in the case study. Hence, this data would have been available at the time of the outages.

In accordance with Section 3.1.2, the possible power is rounded to two decimals to limit the number of scenarios while ensuring that the resolution with which the setpoints can be applied is met. The turbines in question all have the same warranted power curve. Hence, the share of each value of possible power is calculated over the entire dataset. This results in a set of possible power scenarios along with their probabilities, as shown in Figure 4.2. It can be seen that production at rated power occurs for a large portion of the time, which is to be expected by looking at the power curve shown in Figure 2.4a.

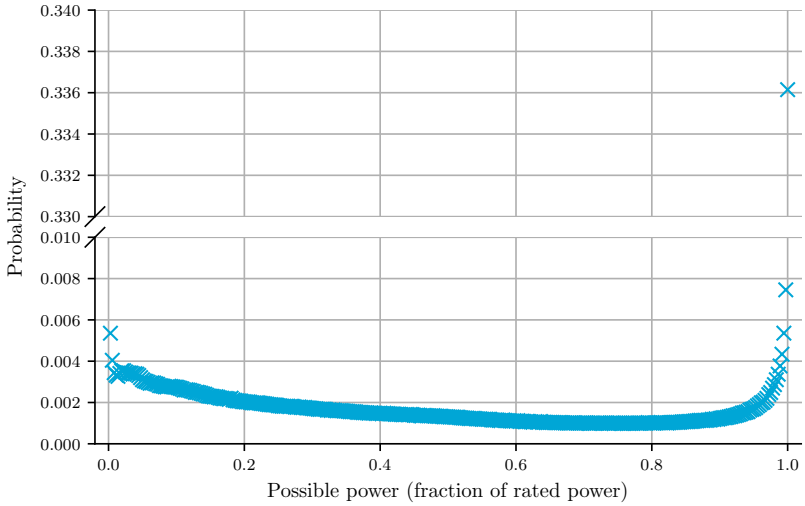

Figure 4.2: The possible power distribution derived for the case study.

To assess the sensitivity of the control strategy with respect to the probability distribution function, a discrete uniform distribution is also applied. This distribution considers all possible power scenarios to be equally likely. In addition, seasonal distributions are derived. To this end, the five years of historical possible power data are grouped into the seasons. For each

season, a separate probability distribution function is generated. This aims to allow the control strategy to take into account the strong seasonal patterns in wind speed [34].

Penalty term weight

As mentioned in Section 3.1.2, a penalty term can be added to prevent unnecessary switching actions. It is chosen to set this parameter to a low value ($c = 0.01$). As a result, the control strategy will recommend performing a switching action for practically any increase in expected production.

4.2.2 Receding horizon control strategy

The receding horizon control strategy, as described in Section 3.2, is implemented in Python using the modeling framework Pyomo [4] and is solved with Gurobi [21] on a Vattenfall compute cluster (16 vCPU, 256 GiB, AMD EPYC 7452 2.35 GHz processor). At each iteration, the following steps are performed:

1. Stage 1 is initialized with DTS measurements and the most recent forecast concerning the prediction horizon.
2. Stage 2 is initialized with DTS measurements and the most recent forecast concerning the current hour.
3. The Mixed-Integer Quadratically Constrained Programming (MIQCP) problem of stage 1 is solved.
4. The optimal values of $z_{ij,t}$ and $P_{i,t}$ are passed as parameters to stage 2.
5. The Quadratically Constrained Linear Programming (QCLP) problem of stage 2 is solved.
6. The optimal setpoints found at stage 2 are used to calculate the power production by taking the minimum of the setpoints and the possible power for each of the 10 minutes. This is aggregated to hourly turbine power productions.
7. The power flows are calculated using the power productions and the optimal topology found at stage 1.
8. The DTS measurements are calculated with (4.6), using the squared power flows as input.
9. The actual cable temperatures are calculated with (4.5). These are stored to be able to calculate the DTS measurements for the next iteration.

The receding horizon control strategy constrains the power flows based on the cable temperatures. To formulate these constraints, cable temperature models are required. In addition, the penalty terms and prediction windows must be set. In the following sections, these three topics are discussed.

Cable temperature constraints

The parameters a_{ij}, b_{ij}, c_{ij}, d_{ij}, and e_{ij} found in Section 4.1.3 are used to define the matrices F_{ij}, G_{ij}, and H_{ij} of the temperature constraints stated in (3.33).

The temperature limit of the cables is 90 °C. However, already at 73 °C, a temperature warning is sent to the control center. Therefore, the maximum temperature $T^{\max}$ is set to 73 °C.

For time steps concerning the far future, CTR is used to constrain the power flows rather than the temperature model. The CTR has not been calculated by Vattenfall for the OWF of the case study. It is assumed that the rating is 17% higher than the STR, following findings from [9].

Penalty term weights

The receding horizon control strategy has three penalty terms that need to be defined.

The weight c_1 defines the magnitude of the penalty term on a switching action between time instances. For a larger prediction window, the increase in the objective value for performing a switching action might be bigger since more time steps are involved. Therefore, different weight magnitudes are assessed per prediction horizon, as shown in Table 4.4.

The weights c_2 (stage 1) and c_3 (stage 2) are part of the penalty terms that aim at distributing the deviations from the forecast evenly over the network. Since this is subordinate to maximizing the expected power production, the terms are set to a low value (0.001).

Prediction windows

Stage 1 of the receding horizon control strategy has two prediction windows that need to be defined, with lengths $N_{\mathrm{p}}^{\mathrm{short}}$ and $N_{\mathrm{p}}^{\mathrm{long}}$.

Tuning of the window length is based on simulations concerning outage 6, since the outage's base case power lies close to the average base case power (see Table 4.2). Furthermore, the outage lasts 10.5 days, which entails that the simulations can be carried out within reasonable time spans (249 iterations). A time limit of 300 seconds is set for solving the problems. If this time limit is reached, the best feasible solution found thus far is returned.

The results of the simulations for different configurations of $N_{\mathrm{p}}^{\mathrm{short}}$, $N_{\mathrm{p}}^{\mathrm{long}}$, and c_1 are given in Table 4.4. The optimality gap is calculated according to:

$$\text{gap} = \frac{|\text{UB} - \text{LB}|}{\text{LB}} \cdot 100\% \tag{4.8}$$

where UB is the upper objective bound, and LB is the lower objective bound.

The power listed in Table 4.4 is the percentual gap with the possible power. The higher (less negative) the percentage, the higher the production. As can be seen, the production is highest for $N_{\mathrm{p}}^{\mathrm{short}} = 3$ hours, $N_{\mathrm{p}}^{\mathrm{long}} = 0$ days, and $c_1 = 3$ (configuration 9).

Configurations with $N_{\mathrm{p}}^{\mathrm{short}} = 0$ result in a lower production than other configurations. For these configurations, the network topology is determined at each iteration based entirely on the CTR rather than on the DTR. Cable temperatures are not considered at the first stage, resulting in sub-optimal network configurations.

As can be seen, the time limit of 300 seconds results in optimality gaps for configurations with long prediction windows. For these configurations, the number of variables is higher, which increases the computational complexity. The production of these configurations is inferior to those with a lower setting of $N_{\mathrm{p}}^{\mathrm{short}}$.

Table 4.4: Simulation results of outage 6 for different prediction windows and penalty terms. Power refers to the percentual gap with the possible power. Time refers to the computation time of stage 1. The optimality gap is calculated according to (4.8).

Config.	$N_{\mathrm{p}}^{\mathrm{short}}$	$N_{\mathrm{p}}^{\mathrm{long}}$	c_1	Power	Switch count	Mean time (s)	Max time (s)	Max optimality gap
1	0	1	1	-2.7%	5	0.154	1.88	0.0%
2	0	3	3	-3.5%	3	0.653	2.88	0.0%
3	0	5	5	-3.5%	3	1.61	4.45	0.0%
4	1	0	1	-0.41%	26	0.202	12.5	0.0%
5	1	0	2	-0.49%	18	0.105	1.27	0.0%
6	2	0	2	-0.41%	17	0.884	73.6	0.0%
7	2	0	4	-0.91%	5	0.563	12.3	0.0%
8	2	2	4	-0.44%	8	0.878	13.9	0.0%
9	3	0	3	-0.36%	11	1.03	29.2	0.0%
10	3	0	5	-0.44%	8	0.660	11.6	0.0%
11	3	1	4	-0.95%	5	8.02	300	0.70%
12	3	3	6	-0.46%	8	1.60	23.1	0.0%
13	5	0	5	-0.88%	5	25.5	300	1.7%
14	8	0	8	-0.87%	9	37.7	300	5.6%
15	8	2	10	-1.2%	7	43.3	300	2.9%
16	12	0	12	-0.96%	5	57.0	300	3.4%

The production results for the short window length configurations with $N_{\mathrm{p}}^{\mathrm{short}} \geq 1$ are rather comparable. For longer prediction windows and higher penalty terms, the number of switching actions is lower.

To assess the sensitivity to the outage scenario, the configurations of the window lengths and penalty term assessed for outage 6 with the most promising results are also implemented for outage 3, which concerns a medium-sized cable rather than a large-sized cable. The results are shown in Table 4.5.

Table 4.5: Simulation results of outage 3 for different configurations of prediction windows and penalty terms. Power refers to the percentual gap with the possible power. Time refers to the computation time of stage 1. The optimality gap is 0.0% for all configurations.

Config.	$N_{\mathrm{p}}^{\mathrm{short}}$	$N_{\mathrm{p}}^{\mathrm{long}}$	c_1	Power	Switch count	Mean time (s)	Max time (s)
4	1	0	1	-2.70%	9	0.082	0.55
5	1	0	2	-2.56%	9	0.076	0.56
6	2	0	2	-2.47%	11	0.21	1.9
8	2	2	4	-2.70%	6	0.62	5.1
9	3	0	3	-2.42%	7	0.42	4.8
10	3	0	5	-2.50%	7	0.43	10
12	3	3	6	-2.72%	6	1.1	21
13	5	0	5	-2.59%	7	1.3	43

As can be seen, for outage 3 the highest production is achieved for $N_{\mathrm{p}}^{\mathrm{short}} = 3$ hours, $N_{\mathrm{p}}^{\mathrm{long}} = 0$ days, and $c_1 = 3$ (configuration 9).

The choice is made to use $N_{\mathrm{p}}^{\mathrm{short}} = 3$ hours, $N_{\mathrm{p}}^{\mathrm{long}} = 0$ days, and $c_1 = 3$ as configuration for the final simulations. Although the difference in performance between configurations is rather limited, this configuration results in the highest production for both outage 3 and outage 6. Additionally, the computation times are acceptable.

4.2.3 Industry control strategy

The switching actions and applied setpoints during outages are obtained from correspondence between cable experts and Offshore Substation (OSS) service leaders. These control actions are checked by manual calculations according to the description in Section 2.5.1.

To allow fair comparison between the control strategies, it was chosen not to use the actual power output of the turbines during the outages to perform simulations with the industry control strategy since the actual power output is dependent on additional factors, such as curtailment due to energy trading and requirements from the Transmission System Operator. Hence, similar to simulations with the other control strategies, per turbine at each 10 minutes the minimum is taken of the possible power and the setpoint to calculate the power production.

4.2.4 Literature control strategy

In Section 2.5.2, the control strategy presented in [54] is introduced. Since this approach is developed for wind farms with a looped rather than a meshed structure, the application of this strategy to the collector system of the case study requires some elaboration.

The literature control strategy is not concerned with the rerouting action that should be taken since in the case of loop connection cables there is only one possibility for rerouting the power during an outage. For the case study, the cable that results in the highest setpoints is activated, similar to the industry strategy. This ensures a radial topology while staying close to the principles of the literature control strategy.

The fundamental idea behind the literature control strategy is that the power production should be maximized while adhering to the STR and minimizing the distance the power travels, thereby reducing power losses. In the case of a meshed network, the latter can be realized by considering the actual cable distances from the turbines to the OSS rather than the positions of the turbines in a string.

The strategy assumes that the wind speed is uniform within the farm, equal to the mean of the nacelle wind speed measurements. The warranted power curve is used to transform this mean wind speed into possible power. The outage-specific wind limit is calculated, which is the highest wind speed for which the turbine power outputs, as calculated by the warranted power curve, do not result in a violation of the STR. At each hour, it is assessed whether the wind speed conforms to or exceeds the wind limit.

If the measured wind speed does not exceed the wind limit, the turbines in the elongated string are all provided with the same setpoint. The authors of [54] suggest applying the power production at the measured wind speed as a setpoint. However, for the case study, in

which the wind profile is not homogeneous within the farm, that would result in unnecessary curtailment. Therefore, the turbines in the Elongated String (ELS) are all given the setpoint corresponding to the power production at the wind limit. This still guarantees adherence to the STR.

If the measured wind speed exceeds the wind limit, all turbines in the ELS are given the setpoint corresponding to power production at the measured wind speed. Moreover, starting at the turbine with the largest cable distance to the OSS, it is determined if an even lower setpoint would eliminate the overload. If so, this setpoint is applied. If not, the turbine is curtailed entirely, and the next turbine in the ELS is considered.

4.3 Results

In this section, the results of the open-loop control strategy and the receding horizon control strategy are presented. Subsequently, the four different control strategies are compared in Section 4.3.3.

4.3.1 Open-loop control strategy

This section discusses the performance of the open-loop control strategy, as well as its sensitivity to the probability distribution function.

The results of the open-loop control strategy are shown in Table 4.6. It can be seen that one cable is activated for every deactivated or inoperative cable. For instance, the open-loop control strategy activates four cables and deactivates two cables for outage 2, during which two cables are inoperative. This is the result of the radiality constraints. Furthermore, more setpoints are adjusted when more cables are used to reroute the power. For outage 3, only one cable is activated, which has to do with the location of the outage and the links.

Table 4.6: Simulation results for the open-loop control strategy. ID refers to the outage, power refers to the percentual gap with the possible power, (de)activated cables refers to the number of cables that have been switched off/on, adjusted setpoints entails the number of turbines that are supplied with an adjusted setpoint, and time corresponds to the computation time.

ID	Power	Activated cables	Deactivated cables	Adjusted setpoints	Time (s)
1	-5.22%	2	1	23	0.22
2	-13.2%	4	2	36	0.48
3	-3.57%	1	0	14	0.18
4	-4.44%	2	1	18	0.20
5	-8.58%	2	1	25	0.22
6	-7.62%	4	3	35	0.83
7	-5.82%	2	1	24	0.23

The relatively large gap between the power produced and the possible power for outage 2 can be attributed to the fact that two cables are affected during this outage. Outage 5 and 6 concern cables of large sizes, which explains these power results. Since the application does not require fast calculations, the average computation time of 0.34 s is satisfactory.

Sensitivity to the probability distribution function

Although the probability of high wind speed is higher in the winter and lower in the summer, using a seasonal probability distribution function does not result in a significantly different output of the open-loop control strategy. The network reconfiguration and the sum of the setpoints per string are identical. The individual turbine setpoints differ by a maximum of 0.01 MW, and those resulting from the seasonal distribution would have also formed a minimum of the objective function when using the original distribution.

This suggests that for the OWF in question, the open-loop control strategy is not very sensitive to the probabilities of the possible power scenarios. This finding is further supported by results obtained by applying a uniform distribution.

4.3.2 Receding horizon control strategy

The receding horizon control strategy is applied to all outages, configured with $N_{\mathrm{p}}^{\mathrm{short}} = 3$ hours, $N_{\mathrm{p}}^{\mathrm{long}} = 0$ days, and $c_1 = 3$. The results are shown in Table 4.7. It can be seen that during outage 7, a large number of switching actions is performed. This can be attributed to the long duration of this outage.

Table 4.7: Simulation results for the receding horizon control strategy. ID refers to the outage, power refers to the percentual gap with the possible power, and switching actions refers to the number of times that cables have been switched on/off, with in parenthesis the number of cables involved. Adjusted setpoints entails the number of turbines that are supplied with an adjusted setpoint at any moment during the outage. The time corresponds to the computation time over all iterations. The maximum temperature is the maximum cable temperature measured during the outage. Between parenthesis, the number of temperature violations is listed.

ID	Power	Switching actions	Adjusted setpoints	Mean time stage 1 (s)	Max time stage 1 (s)	Maximum temperature (°C)
1	-2.85%	6 (3)	27	59	861.4	75.7 (225)
2	-7.21%	11 (9)	47	2.7	36.21	75.0 (25)
3	-2.42%	7 (7)	36	0.42	4.762	75.0 (48)
4	-1.45%	14 (7)	27	0.71	6.230	74.7 (107)
5	-4.77%	2 (2)	27	21	141.1	75.6 (206)
6	-0.358%	11 (10)	49	1.0	29.18	74.8 (48)
7	-2.41%	337 (15)	52	76	2177	76.6 (849)

In addition, there are large variations in computation times for stage 1 between the outages. The mean computation times for all outages are sufficient given that the optimization problem is solved at an hourly rate due to the frequency of the DTS measurements. Across the iterations of all outages, the mean computation time of stage 2 is 0.049 s, with a maximum computation time of 0.82 s.

As can be seen, the temperature limit of 73 °C is violated for all outages. This stems from the relatively large noise terms being added to the temperature measurements. Since the actual cable temperature limit is 90 °C, it is unlikely that the temperature violations will result in damage to the cables.

The temperatures of the four hottest cables during outage 6 are shown in Figure 4.3. As can be seen, the timing of the switches coincides with heating of the cables. By rerouting the power, the power production can be increased while preventing the cables from overheating.

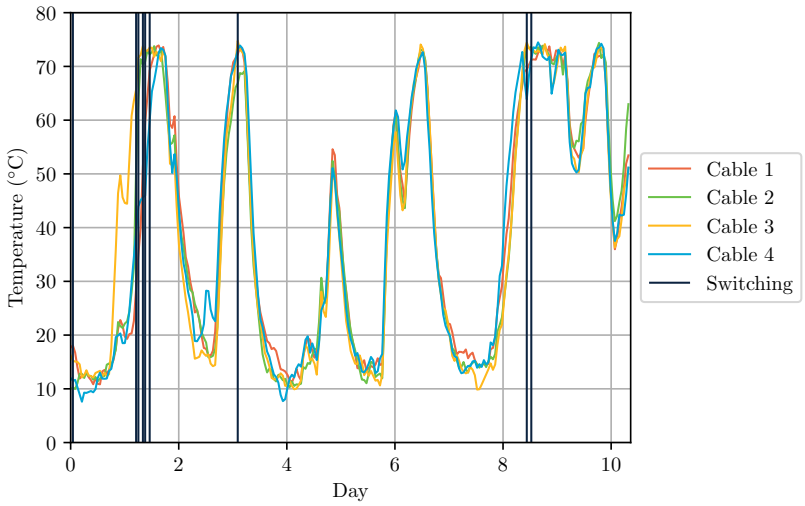

Figure 4.3: The temperature of the four hottest cables during outage 6. The vertical lines indicate the times at which switching actions are performed.

To further assess the performance of the receding horizon control strategy, the following analyses are performed:

- Effect of the rating method: to what extent does DTR impact the performance of the receding horizon control strategy?
- Effect of dynamic switching: to what extent does allowing switching during the outage impact the performance of the receding horizon control strategy?
- Effect of imposing a time limit: to what extent does a computation time limit of 300 seconds for stage 1 impact the performance of the receding horizon control strategy?

Effect of the rating method

To assess the impact of using DTR rather than STR or CTR within the receding horizon control strategy, the simulations for outage 6 are also carried out for these fixed ratings. The results for $N_{\mathrm{p}}^{\mathrm{short}} = 3$ hours, $N_{\mathrm{p}}^{\mathrm{long}} = 0$ days, and $c_1 = 3$ are shown in Figure 4.4.

As can be seen, the production is highest when using DTR, namely 3.6% higher than CTR and 6.1% higher than STR. When looking at the maximum temperatures measured within the wind farm, it can be seen that using CTR results in large violations of the temperature limit at which a warning is sent to the control center. Since the temperatures remain well below the actual cable temperature limit of 90 °C, this will not result in cable damage.

DTR thus allows for increasing the production significantly while limiting the number and magnitude of temperature violations.

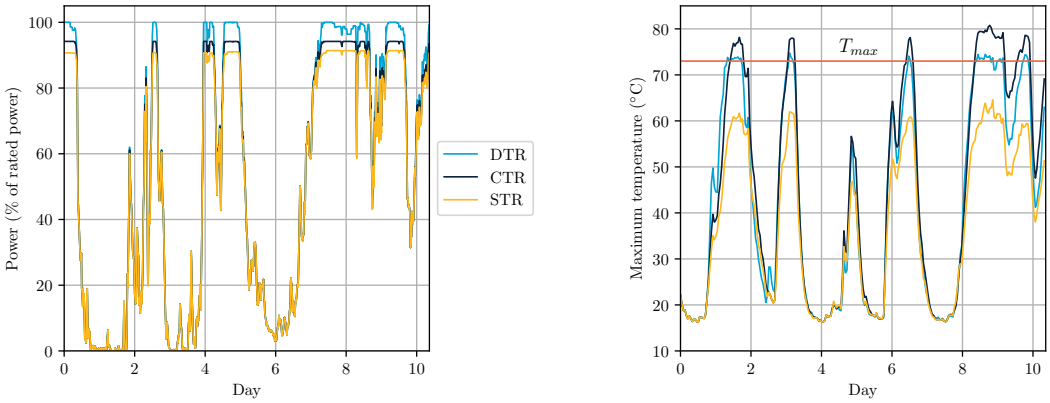

(a) Production relative to rated power.

(b) Maximum cable temperature.

Figure 4.4: Simulation results for different rating methods used within the receding horizon control strategy for outage 6.

Effect of dynamic switching

To analyze the effect of allowing switching actions during the outage, the simulations concerning outage 6 are carried out for a fixed topology. To this end, the network reconfiguration of the open-loop control strategy is applied, and the setpoints are calculated iteratively by solving stage 2 of the receding horizon control strategy. The result is shown in Figure 4.5. As can be seen, enabling dynamic network reconfiguration increases power production. For outage 6, the increase is 1.6%.

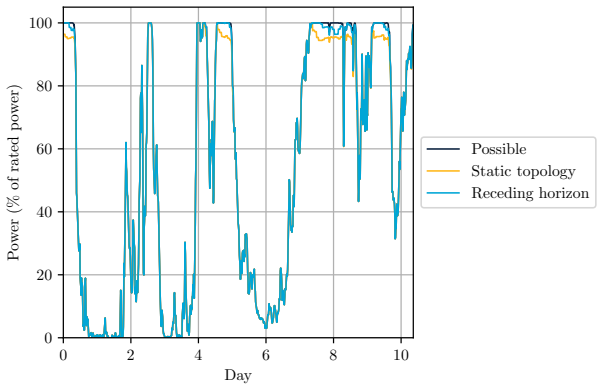

Figure 4.5: Power production relative to rated power for outage 6. Static topology refers to a control strategy that applies the network configuration of the open-loop control strategy and uses stage 2 of the receding horizon control strategy to determine the setpoints dynamically.

Since the number of switching actions during outage 7 is the largest, the same simulations are also performed for this outage. Here, dynamic switching enables an increase of 0.62% with respect to a static topology.

It can be concluded that dynamic switching positively impacts the power production during outages, albeit to a smaller extent than the use of DTR. The increase in power production is likely caused by the network no longer being constrained to radial operation.

Effect of imposing a time limit

Although the mean computation time for stage 1 as listed in Table 4.7 is satisfactory, a time limit might have to imposed for actual implementation, given the maximum computation time of 36 minutes.

To assess the impact of such a time limit on the performance of the receding horizon control strategy, a time limit of 300 seconds is set for solving stage 1. If this time limit is reached, the best feasible solution found thus far is returned. The simulations are performed for outage 1 and outage 7. For the other outages, this time limit was never reached.

For outage 1, this increases power production from -2.85% with respect to the possible power to -2.73%. However, instead of 6 switching actions, 67 are performed. Similarly, for outage 7, this increases power production from -2.41% with respect to the possible power to -2.17%. Instead of 337 switching actions, 515 are performed. The optimality gaps, as can be calculated according to (4.8), are a maximum of 3.0% and 2.3% for outage 1 and outage 7, respectively, rather than 0.01%.

Imposing a time limit thus increases power production at the cost of a much higher number of switching actions. For actual implementation, this might be undesirable.

4.3.3 Comparison between the control strategies

In the following section, a comparison will be made between the different control strategies. The power production and control actions will be discussed.

Power production

For each of the control strategies and outages, the percentual gap with possible power is listed in Table 4.8.

Table 4.8: Relative power production for each control strategy. The percentages indicate the gap with the possible power. A higher (less negative) percentage indicates a higher production. Base case refers to curtailing the turbines connected to the inoperative cable and not applying any further control actions.

ID	Base case	Industry	Literature	Open-loop	Receding horizon
1	-8.69%	-5.22%	-6.05%	-5.12%	-2.85%
2	-18.7%	-13.2%	-15.3%	-12.3%	-7.21%
3	-7.13%	-3.57%	-3.68%	-3.55%	-2.42%
4	-6.19%	-4.44%	-4.52%	-4.15%	-1.45%
5	-11.1%	-8.58%	-8.39%	-7.33%	-4.77%
6	-9.75%	-7.62%	-7.57%	-5.74%	-0.358%
7	-9.60%	-5.82%	-5.93%	-4.97%	-2.41%

As can be seen, the receding horizon control strategy outperforms the other control strategies for all outages. This can be attributed to using DTR instead of STR, which allows for an increase in rating when the cable temperatures are low. In combination with network

reconfigurations during the outage, this results in an increase in production. Moreover, the receding horizon control strategy does not assume a homogeneous wind profile within the wind farm. Instead, it bases its control actions on wind forecasts, allowing for the incorporation of wake effects. This enables tailoring the setpoints to the expected possible power of the individual turbines, maximizing the power production.

Furthermore, the open-loop control strategy results in a higher production than the industry control strategy for all outages. The difference can be attributed to the open-loop control strategy considering multiple cables for rerouting, thereby distributing the setpoints more evenly over the network.

For outage 3, the open-loop control strategy only uses one cable for rerouting, which explains the small difference between the industry and open-loop control strategy. The difference in production between the strategies during this outage can be attributed to the production scenarios of the open-loop control strategy. Since these are already defined at a two-decimal resolution, the strategy finds optimal combinations of these productions. In contrast, the industry strategy calculates the setpoints by dividing the admissible power flow over the turbines and afterward rounding down. For example, when the admissible power flow of the most limiting cable section is 1.01 MW, and there are two turbines connected to it, the industry control strategy will recommend applying a setpoint of 0.50 MW to both turbines. In comparison, the open-loop control strategy would give one of the turbines a setpoint of 0.50 MW and the other a setpoint of 0.51 MW.

As can be seen in Table 4.8, the literature control strategy has the lowest production for nearly all outages. This can be attributed to the assumption of a uniform wind speed throughout the park. When the wind limit is exceeded, all turbines in the elongated string are given the setpoint that corresponds to the power production at the measured mean park wind speed. However, when there are differences in possible power within the farm, for instance due to wake effects or differences in operational power curves, this can result in unnecessary curtailment.

In the simulations, power losses have not been taken into account. It is expected that the literature control strategy results in the lowest losses due to its focus on minimizing the transmission distances. However, electrical losses only account for 1-3% of the power production [20], of which a large part is transformer- rather than cable-related. Hence, the literature control strategy is unlikely to result in a higher production than the proposed control strategies.

The average increase in power production with respect to the industry control strategy is 0.82% and 4.2% for the open-loop and receding horizon control strategy, respectively. Given that only a part of the network is affected during the outage, this is a significant improvement.

With an average European offshore wind farm size of 325.5 MW [2], an average capacity factor of 0.42 [2], and an average outage duration of 38 days [58], the estimated increase in power production per outage is 1.03 GWh for the open-loop control strategy and 5.23 GWh for the receding horizon control strategy. With a feed-in remuneration of €194/MWh [54], this translates into an increase in revenue per outage of €0.20 million and €1.0 million, respectively.

The power production during outage 2 and outage 6 are shown in Figure 4.6 and Figure 4.7, respectively. Similar plots for the other outages can be found in Appendix A. It can be seen that the difference between the control strategies in terms of absolute power production

is more pronounced when the possible power is higher. This can be attributed to the fact that during these periods, the setpoints often dictate the production rather than the possible power.

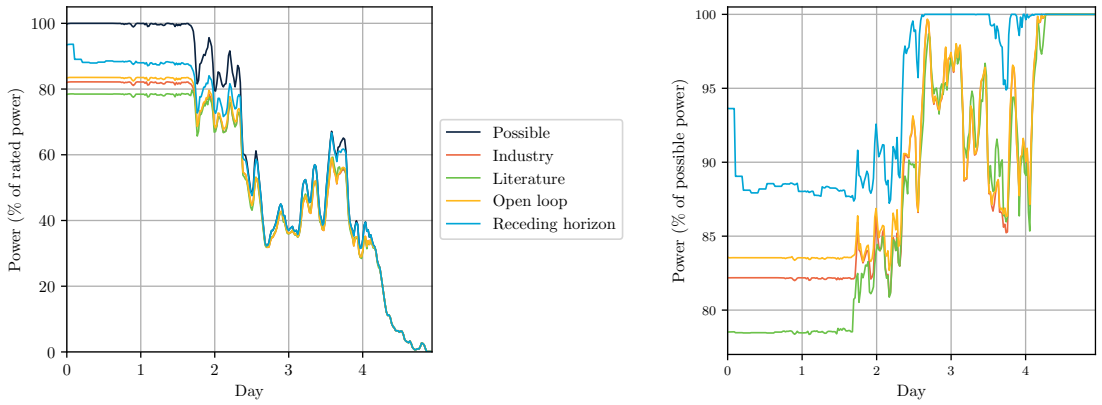

(a) Relative to rated power. **(b)** Relative to possible power.

Figure 4.6: Power production for the different control strategies for outage 2.

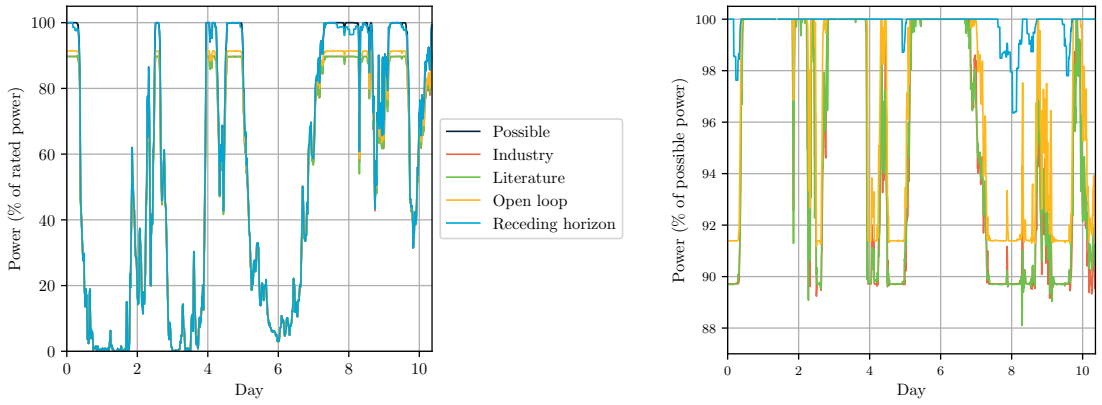

(a) Relative to rated power. **(b)** Relative to possible power.

Figure 4.7: Power production for the different control strategies for outage 6.

In conclusion, both developed strategies outperform the existing control strategies for all outages considered in the case study. In particular, the receding horizon control strategy enables a significant decrease in the loss of production during outages.

Control actions

The number of switching actions per control strategy can be found in Table 4.9. In contrast to the other control strategies, the receding horizon control strategy can reconfigure the network at each hour. As a result, it performs the most switching actions, except during outage 5. Due to the radiality constraint, the open-loop control strategy needs to deactivate one of the cables, whereas the receding horizon control strategy does not.

Table 4.9: The total number of switching actions for each control strategy.

ID	Duration (days)	Industry	Literature	Open-loop	Receding horizon
1	26.5	1	1	3	6
2	5	2	2	6	11
3	9.5	1	1	1	7
4	9	1	1	3	14
5	18	1	1	3	2
6	10.5	1	1	7	11
7	114.5	1	1	3	337

The control actions taken during one of the outages are visualized in Figure 4.8. As can be seen, the receding horizon control strategy alters the setpoint of more turbines throughout the outage compared to the other control strategies. The reason that this strategy nevertheless outperforms the other strategies can be observed in Figure 4.9: it applies much higher setpoints, which enables a higher power production.

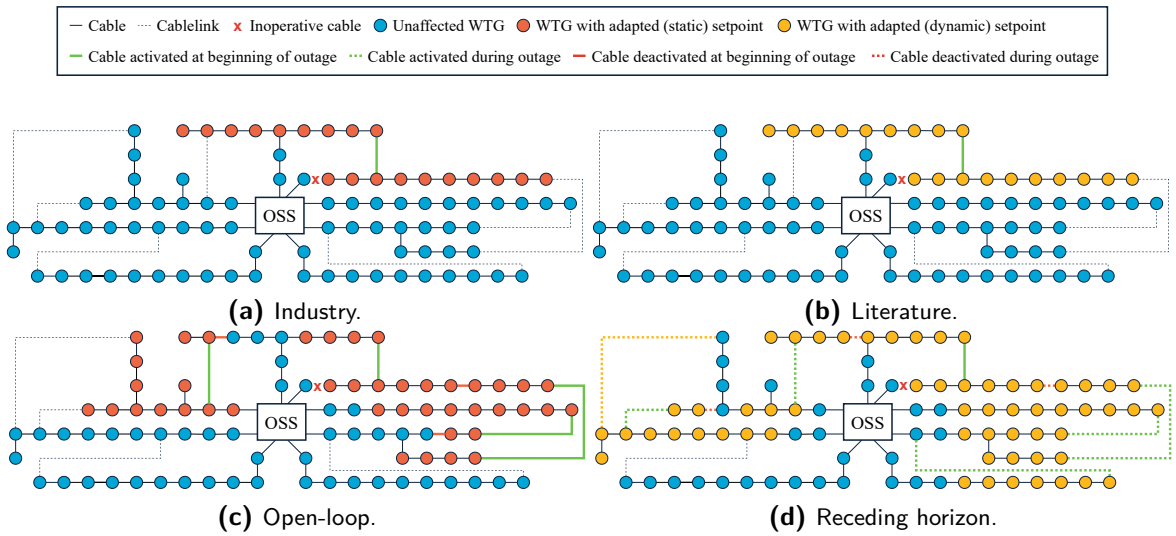

Figure 4.8: Control actions taken by the different control strategies for outage 6.

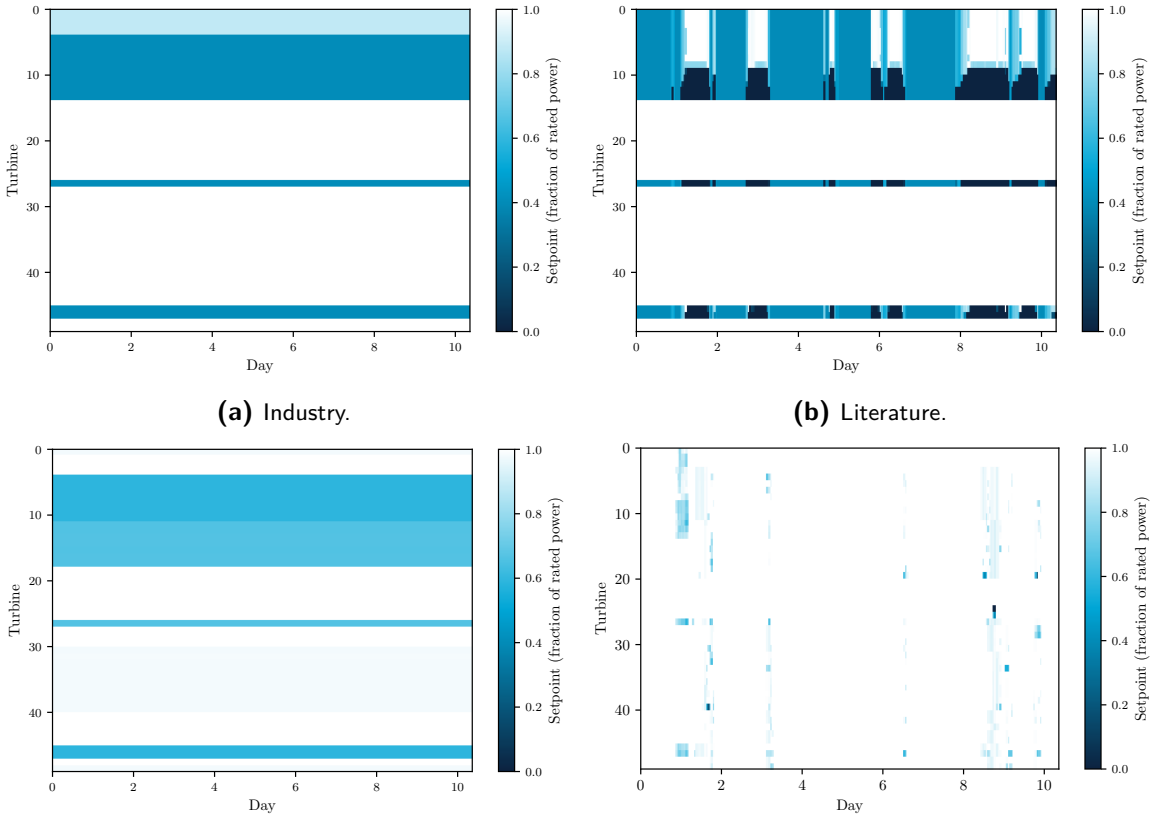

(a) Industry.

(b) Literature.

(c) Open-loop.

(d) Receding horizon.

Figure 4.9: Setpoints applied for the different control strategies for outage 6. Turbines that do not have altered setpoints for any of the control strategies are not shown.

4.4 Summary

In this chapter, the results of a case study concerning seven outages that occurred at an existing OWF are presented. Actual possible power and wind speed data are used to perform the simulations. Cable temperature measurements are obtained by performing simulations with a cable temperature model fitted to cable temperature and power flow data.

The receding horizon control strategy leads to higher production than the other strategies for all outages. This increase in production can mainly be attributed to the use of DTR. Dynamic switching further enables exploiting DTR to the fullest by (de)activating cables during the outage based on the cable temperatures and forecasts.

The open-loop control strategy is a promising alternative if an automated control system is not in place. The strategy outperforms the industry and literature control strategy in terms of production, with fast computation times.

The average increase in power production with respect to the industry control strategy is 0.82% and 4.2% for the open-loop and receding horizon control strategy, respectively. For a typical outage, this can be translated into a revenue increase of €0.20 million and €1.0 million, respectively.

Chapter 5

Conclusions and recommendations

In this chapter, the thesis is reflected upon. In Section 5.1, a summary of the work is given. Section 5.2 highlights the contributions with respect to the literature. Finally, in Section 5.3 the results are discussed and recommendations are given for future research.

5.1 Project summary

This thesis researches the control of Offshore Wind Farm (OWF) collector systems during outages. Specifically, the work aims to answer the following research question:

How can the power production of offshore wind farms be maximized during collector system outages?

To answer this question, the collector system itself is investigated and modeled. Additionally, existing approaches in the literature are reviewed. It is concluded that optimization-based control offers an opportunity for an increase in production with respect to the existing approaches for the collector system. Following this finding, two novel control strategies are developed that aim to maximize the power production of OWF collector systems during outages: the open-loop control strategy and the receding horizon control strategy.

The open-loop control strategy assumes that the network can only be reconfigured once, at the beginning of the outage. It is formulated as a Mixed-Integer Linear Programming (MILP) problem, of which the objective function is to maximize the expected power production. In order to guarantee adherence to the Static Thermal Rating (STR) for the entire duration of the outage, a radiality constraint is posed on the network.

The receding horizon control strategy instead assumes that there is an automated control system in place that is capable of reconfiguring setpoints and power switches during the outage. The strategy leverages current cable temperatures and power forecast information to derive optimal control actions. It is formulated as a two-stage optimization problem that is solved

at an hourly rate. The first stage concerns a Mixed-Integer Quadratically Constrained Programming (MIQCP) problem that determines optimal network configurations over a receding horizon. The optimal setpoints for the current hour are found at the second stage, which is a Quadratically Constrained Linear Programming (QCLP) problem.

Both control strategies are applied to a case study concerning an existing OWF. The developed strategies outperform the approach taken in the industry and the approach proposed in [54] for all seven outages. The average increase in power production with respect to the industry control strategy is 0.82% for the open-loop control strategy. An increase of 4.2% is observed for the receding horizon control strategy. The latter equates to a revenue increase of €1.0 million for a typical outage duration of 38 days at an average capacity OWF. From sensitivity analysis, it can be concluded that this increase can primarily be attributed to determining the setpoints dynamically based on the Dynamic Thermal Rating (DTR) rather than the STR.

5.2 Contributions

To the best of the author's knowledge, there are only two approaches available in the literature that concern the control of collector systems during outages, namely [54] and [65]. This thesis contributes to this existing literature as follows:

- Development of two novel optimization-based rerouting and setpoint decision frameworks for outages at OWF collector systems with arbitrary topologies:
  1. An event-driven method that determines a fixed topology and fixed setpoints while maximizing the expected power production and guaranteeing compliance to the STR during the entire outage.
  2. A receding horizon algorithm that determines the optimal topology and setpoints at each hour by taking into account turbine production forecasts, cable temperature measurements, and cable temperature dynamics. In contrast to the methods of [54] and [65], the receding horizon control strategy applies dynamic network reconfiguration. Moreover, load-based DTR is used to constrain the power flows in the network. This has been implemented in [10, 11], but only for a single export cable.

  Both developed frameworks differ from [54] in that they consider rerouting via multiple cables. Furthermore, the newly proposed frameworks address the computation of the setpoints, whereas the method of [65] simply assumes that the setpoints are adjusted during the outage to meet the static ratings.
- Evaluation and comparison of the closed-loop performance of the two novel frameworks and two existing approaches based on outages that actually occurred at an OWF. In contrast to [54] and [65], OWF possible power data is used rather than a translation of wind speed measurements to possible power via the warranted power curve. By taking this approach, it could be shown that the method in [54] is not capable of dealing well with non-uniform wind speeds within the park and inaccuracies in the warranted power curve. In contrast, it is shown that the developed strategies can cope well with the variability of wind power production.

5.3 Discussion and recommendations for future research

The outcomes of this research show that the loss in production during collector system outages can be decreased significantly by using optimization-based control strategies. This is in line with related research regarding transmission and distribution networks. Nonetheless, the findings of this study have to be seen in light of some limitations.

First of all, linear power flow is used to model and simulate the power flows through the system. It is unknown to what extent this approximation deviates from reality. Further research is needed to establish the accuracy of linear power flow for OWF collector systems. However, the impact of the approximation error is expected to be limited. Since the open-loop control strategy constrains the network to radial operation, the power flows will never exceed those calculated by the control strategy. For the receding horizon control strategy, an approximation error will not accumulate as the cable temperature measurements are updated each hour.

Secondly, this work assumes that the admissible power flows in the collector systems are solely restricted by the cable temperatures. However, transformers, breakers, and other components might set further restrictions on the loadability of the network. It is recommended to investigate if the rating of these components is limiting and, if so, to incorporate these as additional constraints into the framework of the receding horizon control strategy.

In addition, it must be noted that the cable temperature models used in the case study do not form an accurate representation of the actual temperature dynamics. Further experimental investigations are needed to derive more suitable models for the collector system that are fit for optimization. In this regard, taking into account ambient conditions could pose a significant improvement. Alternatively, it would be interesting to look into adaptive receding horizon control, in which the prediction model gradually evolves with time. This would allow for considering changing operating conditions without explicitly providing these changes to the controller.

Finally, this thesis is concerned with the maximization of power production. The control strategies are indifferent to the timing of high and low production. External restrictions can be taken into account by considering load balancing within the objective function of the receding horizon control strategy. This way, constraints from the transmission system operator or energy trading can be considered, allowing even better-tailored dynamic setpoints.

Appendix A

Additional simulation results

In this appendix, the performances of the control strategies are further illustrated. Similar to Figure 4.6 and Figure 4.7, that concern outage 2 and outage 6, the power production for the remaining outages is shown.

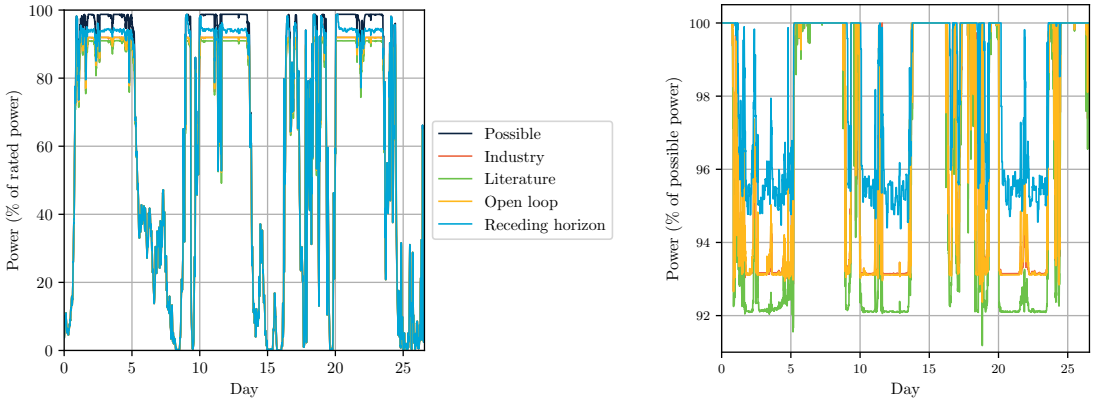

(a) Relative to rated power.

(b) Relative to possible power.

Figure A.1: Power production for the different control strategies for outage 1.

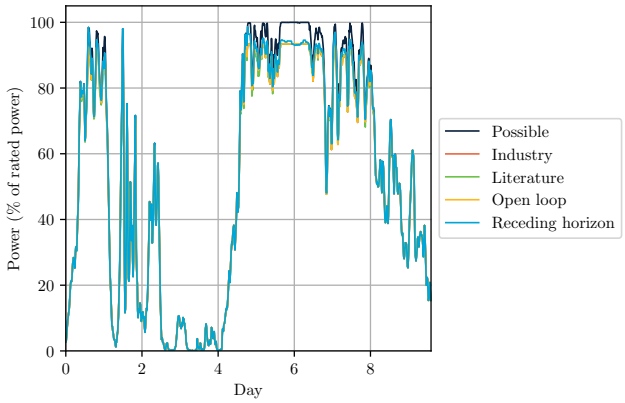

(a) Relative to rated power.

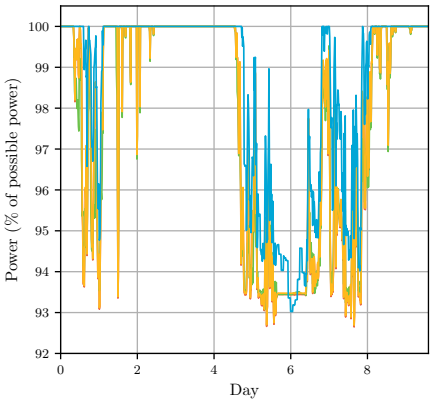

(b) Relative to possible power.

Figure A.2: Power production for the different control strategies for outage 3.

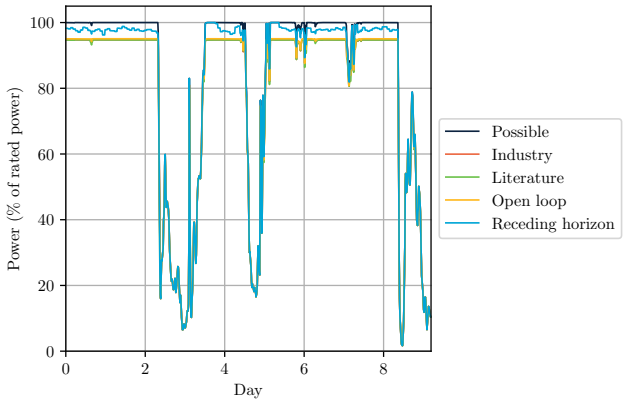

(a) Relative to rated power.

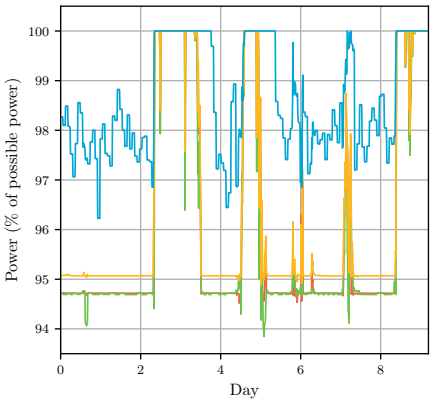

(b) Relative to possible power.

Figure A.3: Power production for the different control strategies for outage 4.

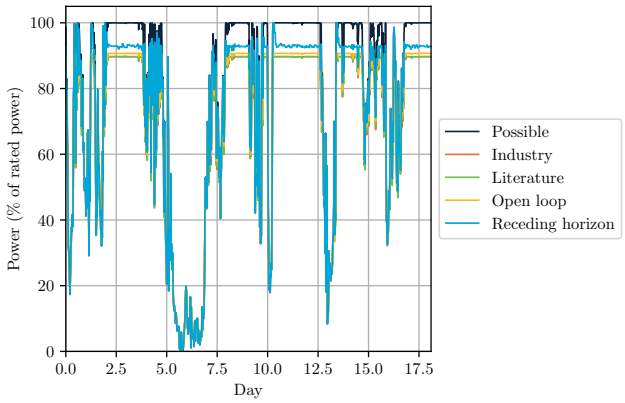

(a) Relative to rated power.

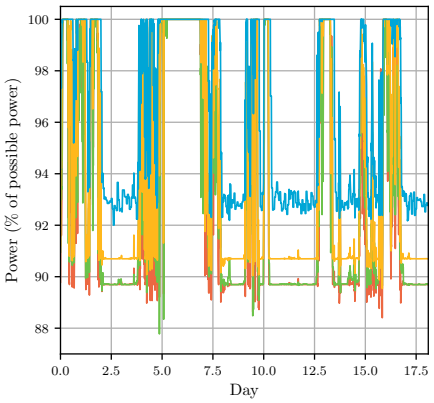

(b) Relative to possible power.

Figure A.4: Power production for the different control strategies for outage 5.

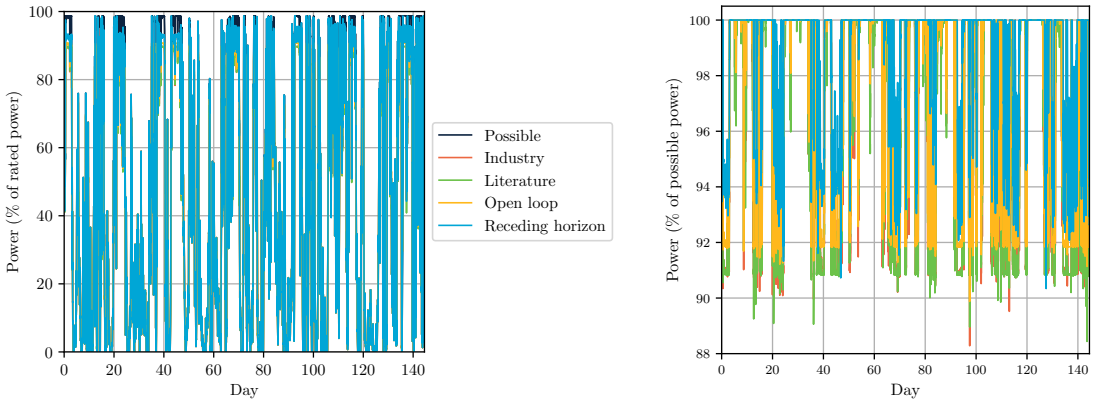

(a) Relative to rated power.

(b) Relative to possible power.

Figure A.5: Power production for the different control strategies for outage 7.

Appendix B

Conference paper

A conference paper has been written on the research presented in this MSc Thesis. It is currently under review for the IEEE SmartGridComm 2023. The following pages contain the submitted paper.

Optimal control of offshore wind farm collector systems during outages

Martiene Ubbens
Business Area Wind
Vattenfall
Amsterdam, The Netherlands
martiene.ubbens@vattenfall.com

Bart De Schutter
Delft Center for Systems and Control
Delft University of Technology
Delft, The Netherlands
b.deschutter@tudelft.nl

***Abstract*—Two optimization-based approaches are proposed to optimize the power routing and turbine setpoints of offshore wind farm (OWF) collector systems during cable outages. The open-loop control strategy assumes that the network can only be reconfigured at the beginning of the outage. In contrast, the receding horizon control strategy is deployed in real time, leveraging cable temperature measurements and power forecasts to derive optimal control actions dynamically. Simulation results concerning occurred outages at an existing OWF prove the practical applicability of the novel approaches and show that both strategies outperform existing approaches.**

***Index Terms*—offshore wind farm operation, collector system outages, optimization-based control, dynamic thermal rating**

I. Introduction

Ambitions to limit climate change are incentivizing the development of renewable energy technologies. One of the most rapidly growing energy markets is offshore wind power. In 2021, its global installed capacity reached 65 GW. In line with the Paris Agreement [1], a UN Global Compact has been signed to commit to the target of 380 GW capacity by 2030 and 2000 GW by 2050 [2]. To meet these ambitious targets, it is vital that the investment costs for Offshore Wind Farms (OWFs) are reduced, and wind power efficiency is increased.

The electrical system of OWFs presents significant potential in this regard. It typically consists of an AC collector system, an example of which is shown in Figure 1, and an export system. Within the collector system, inter-array cables transport the power produced by the turbines to the Offshore Substation (OSS). From the OSS, export cables transport the power to shore. Not only does the electrical system constitute a large portion of the capital expenditure, but its cable outages also account for 80% of the financial losses in the offshore wind industry. For example, the failure of one inter-array cable can cost up to €3 million, depending on the type and location of the failure [3]. These costs are built up of repair costs and costs related to the curtailment of power throughout the outage.

To limit the production losses due to inter-array outages, rerouting can be performed to transport the power produced by the turbines connected to the inoperative cable to the OSS. If the power is rerouted, an elongated string is formed, and turbine setpoints need to be adjusted to prevent overloading of the cables. These setpoints upper-bound the turbine production.

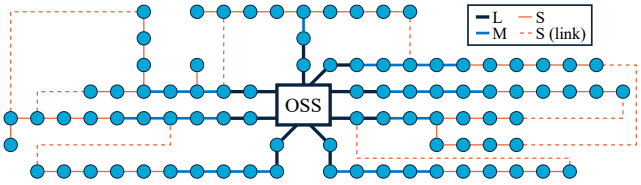

Fig. 1. Schematic of a meshed collector system. The circles represent the turbines. The cable sizes are indicated in the legend. Links are not used during standard operation but are not fundamentally different from the other cables.

In the industry and in [4], a single cable is activated to reroute the power. The authors of [5] develop an optimization-based approach that instead considers the full freedom of the network to distribute the power more evenly over the network. However, their method cannot be used to derive setpoints since it simply assumes that during an outage, curtailment is performed such that the power flow limits are not violated. Like the other mentioned approaches, Static Thermal Rating (STR) is used to constrain the power flows through the network. This rating dictates the maximum amount of power that can flow through the cable continuously. When applied to OWFs, this leads to under-utilization of the network as the fluctuations in wind power are disregarded [6].

Given that inter-array outages typically last more than a month [7], optimizing the rerouting and setpoints can significantly reduce the losses during outages. Moreover, an optimization approach can support the current trend of designing OWFs that are tailored to the site's specifics [8] and OWFs with a larger installed wind power capacity than can be transported via the collector system [6]. Any increase in effectiveness can benefit the entire generating capacity and can aid in realizing the ambitious growth in OWFs targeted.

This work presents two novel control strategies that aim to maximize power production during outages: the open-loop control strategy (Section III) and the receding horizon control strategy (Section IV). The developed control strategies, as well as the approaches taken in the industry and in [4], are applied to a case study (Section V) concerning outages that actually occurred. It is shown that both control strategies outperform the existing approaches in terms of power production.

II. Preliminaries

A. Cable rating

Collector system cables are limited in their capacity by their conductor temperature, which should not exceed 90 °C [9]. Typically, the cables are designed and operated according to their STR. This entails constraining the power flows by the maximum current that can be transported continuously without violating the temperature limit [10]. The calculations used to determine the STR are straightforward but do not consider the thermal time constant of the cables. Given the variability in wind power, this leads to under-utilization of the cables.

The full potential of the cables' capacity can be harvested by dynamically determining the rating based on the cable temperature measured by sensors and predicted by a dynamic temperature model. The authors of [11] use load-based Dynamic Thermal Rating (DTR) to estimate the 6-hour ahead risk of exceeding the temperature limit of an export cable and apply STR for one hour if a risk is identified. For optimal control of collector systems during outages, it might be more suitable to directly incorporate the cable temperature dynamics in the optimization formulation. To this end, a dynamic temperature model fit for optimization must be used, such as the third-order state space model derived in [12]. Its input is the squared current. The parameters are to be found by fitting the model to temperature and loading data.

B. Turbine power production

The rated power of turbine i, P_i^{r}, dictates the maximum power that the turbine can produce. The power that turbine i can generate when operating at full performance is called the possible power, P_i^{poss}. It can be approximated with the turbine's warranted power curve, which is a function of the wind speed. More accurate estimations can be obtained by applying the operational power curve to nacelle wind speed measurements [13].

A setpoint can be applied to limit the power output of a turbine. The actual power output of the turbine is then given by the minimum of the possible power, P_i^{poss}, and the setpoint, P_i^{sp} [4].

C. Power flow

Linear or AC power flow can be used to describe the power flows through the network. Although the linear power flow model is less accurate than the AC power flow model, findings suggest that the severity of the approximation error might be limited for collector systems [4], [5], [14]. In addition, the linearity of the linear power flow method makes it less computationally expensive to use within an optimization framework than the nonlinear AC power flow model. In line with this, most approaches in the literature regarding OWF collector system design optimization use linear power flow since it makes the problems tractable [15]. However, the authors recommend further research to assess the accuracy of the linear power flow formulation for OWF collector systems.

D. Existing control strategies

The method used by the industry performs rerouting via one cable and considers STR to determine the turbine setpoints. The capacity of the most limiting cable in the elongated string is then divided equally over the turbines connected to it.

The authors of [4] extend this approach by considering wind speed measurements to derive setpoints dynamically. The strategy assumes a uniform wind speed within the farm. The warranted power curve is used to transform the park's mean wind speed into possible power. All turbines in the elongated string are provided with this value as a setpoint. Iteratively, new setpoints are calculated based on the violation of the STR if the elongated string is formed. Starting with the turbine that has the largest distance to the OSS, it is determined if an even lower setpoint would eliminate the overload. If so, this setpoint is applied. If not, the turbine is curtailed entirely, and the next turbine in the elongated string is considered. As such, power is transmitted over the shortest distance, minimizing losses.

III. Open-loop control strategy

If there is no automated control system in place, service technicians have to go to the relevant turbines when weather conditions allow it to perform manual switching. In addition, the wind farm operator separately has to log onto each affected turbine to provide a new setpoint. For such an OWF, applying control actions dynamically is inconvenient and costly. To this end, the open-loop control strategy aims to maximize power production during an outage under the constraint that setpoint adaptation and network reconfiguration can only be performed at the beginning of an outage. Due to the long duration of an outage and the uncertainties related to wind power production, STR is applied rather than DTR.

To incorporate the wind power variability into the optimization framework, a probabilistic approach is taken, in which the objective is to maximize the production over a set of scenarios:

$$\max \quad \sum_{s\in\mathcal{S}} \sum_{i\in\mathcal{V}\backslash\{0\}} P_{i,s}\mathbb{P}_s \tag{1}$$

where $\mathcal{V} = \{0, ..., N\}$ denotes the set of nodes pertaining to the OSS and the turbines. Here, N is the number of turbines, and node 0 corresponds to the OSS. The set $\mathcal{S}$ denotes the set of possible power production scenarios, with for each scenario s a probability $\mathbb{P}_s$ and a possible power production $P_{i,s}^{\mathrm{poss}}$. The scenarios can be generated from historical possible power data. The power output of turbine i at scenario s, $P_{i,s}$, is then upper-bounded by the setpoint and the possible power production at that scenario:

$$0 \leq P_{i,s} \leq P_s^{\mathrm{poss}} \qquad \text{for } i \in \mathcal{V}\backslash\{0\},\ s \in \mathcal{S} \tag{2}$$

$$P_{i,s} \leq P_i^{\mathrm{sp}} \qquad \text{for } i \in \mathcal{V}\backslash\{0\},\ s \in \mathcal{S} \tag{3}$$

The resulting control actions are optimal if the set of scenarios is representative of the possible power during the outages.

The STR must not be violated when the turbines are producing at setpoint. Moreover, the applied setpoints must ensure that the STR is also adhered to for any power production conforming to these setpoints. To ensure this under

the uncertainty of the power production over the outage, the network should be operated radially, i.e., a maximum of one outgoing power flow per turbine must be enforced. To this end, a set of arcs, $\mathcal{A}$, is used to describe the operable cables in the network. The cable connecting node i and node j occurs twice within the set of arcs, as (i,j) and (j,i). The radiality constraint can then be captured by the following equations [16]:

$$\sum_{j|(i,j)\in\mathcal{A}} z_{ij} \leq 1 \qquad \text{for } i \in \mathcal{V}\backslash\{0\} \tag{4}$$

$$z_{ij} \in \{0,1\} \qquad \text{for } (i,j) \in \mathcal{A} \tag{5}$$

$$z_{ij} + z_{ji} \leq 1 \qquad \text{for } (i,j) \in \mathcal{A} \tag{6}$$

where the binary variable z_{ij} models the on/off status of cable (i,j). Here, $z_{ij} = 1$ if cable (i,j) can be used and $z_{ij} = 0$ if the cable cannot be used. Equation (6) dictates that power can flow over the same cable in one direction only.

Since radial operation guarantees that the power flows during the outage will never exceed the power flows present when producing at setpoint, the power flow constraints only need to be formulated for the production at setpoint. Furthermore, in the case of radial operation, the linear power flow model can be simplified [5]:

$$0 \leq p_{ij}^{\mathrm{sp}} \leq p_{ij}^{\mathrm{STR}} z_{ij} \qquad \text{for } (i,j) \in \mathcal{A} \tag{7}$$

$$P_i^{\mathrm{sp}} - \sum_{j|(i,j)\in\mathcal{A}} p_{ij}^{\mathrm{sp}} + \sum_{i|(j,i)\in\mathcal{A}} p_{ji}^{\mathrm{sp}} = 0 \qquad \text{for } i \in \mathcal{V} \tag{8}$$

where p_{ij}^{sp} denotes the power flow from node i to node j when all turbines are producing at setpoint and p_{ij}^{STR} is the static thermal rating of cable (i,j).

To prevent switching actions that result in little or no improvement in expected power production, a penalty term can be added to the objective function:

$$\max \quad \left(\sum_{s\in\mathcal{S}} \sum_{i\in\mathcal{V}\backslash\{0\}} P_{i,s}\mathbb{P}_s \right) - c \cdot \sum_{(i,j)\in\mathcal{A}} \zeta_{ij} \tag{9}$$

$$\text{s.t.} \quad -\zeta_{ij} \leq z_{ij} - z_{ij}^{\mathrm{standard}} \leq \zeta_{ij} \quad \text{for } (i,j) \in \mathcal{A} \tag{10}$$

where c is the penalty coefficient, $z_{ij}^{\mathrm{standard}}$ is the configuration of the cable under standard operation and ζ_{ij} is an auxiliary variable. The result is a mixed-integer linear programming (MILP) problem, which can be solved using a brand-and-bound algorithm [17].

IV. Receding horizon control strategy

The receding horizon control strategy assumes that an automated control system is in place that can directly apply setpoint adaptation and network reconfiguration at any given time during the outage. By performing online calculations, cable temperature measurements and power forecasts can be taken into account to tailor the control actions to the specifics of the time step. This allows for constraining the power flows based on the cable temperature limits rather than on the STR.

The control strategy consists of solving two optimization problems at each hour. The first stage is a mixed-integer quadratically constrained programming (MIQCP) problem that finds optimal turbine productions and network topologies over a moving horizon. In this problem, it is assumed that the power forecast is perfect. The second stage then deals with uncertainty in the forecast to prevent unnecessary curtailment if the forecast is too low. The corresponding quadratically constrained linear programming (QCLP) problem aims at finding optimal setpoints for the current hour. While the problems could be merged into one, they are kept separate for clarity.

A radiality constraint as in (4) is no longer posed on the network since taking into account forecasts will allow calculating more precisely how the power will flow through any loops in the network. Deviations from the estimation will not propagate since these will be reflected in the temperature measurements. Therefore, a different set, $\mathcal{E}$, is used to describe the cables than for the open-loop control strategy. In this set of edges, the cable connecting node i and node j occurs only once, limiting the number of binary variables.

A. Stage 1: network reconfiguration

At each hour t, the first stage aims to find optimal network configurations over a prediction window $\mathcal{K}_t = \{t, t+1, ..., t+N_{\mathrm{p}}-1\}$, where N_{p} is the prediction window length. The time interval is 1 hour to be able to model the temperature dynamics. The objective function at hour t aims to maximize the expected power production over the prediction window while penalizing switching actions and distributing curtailment with respect to the power forecast evenly over the network, as stated in (11)-(14). In these equations, $P_{i,k}$ is the power production of turbine i at time step k under the assumption of a perfect forecast, $z_{ij,k}$ is the on/off status of cable (i,j) at time step k, $P_{i,k|t}^{\mathrm{forecast}}$ is the power forecast of turbine i made at hour t concerning time step k, c_1 and c_2 are penalty coefficients, and $\zeta_{ij,k}$ and $\psi_{i,j,k}$ are auxiliary variables. Since

$$\max \quad \sum_{k\in\mathcal{K}_t} \left(\sum_{i\in\mathcal{V}\backslash\{0\}} P_{i,k} - c_1 \cdot \sum_{(i,j)\in\mathcal{E}} \zeta_{ij,k} - c_2 \cdot \sum_{i\in\mathcal{V}\backslash\{0\}} \sum_{j\in\mathcal{V}:j>i} \psi_{i,j,k} \right) \tag{11}$$

$$\text{s.t.} \quad -\zeta_{ij,k} \leq z_{ij,k} - z_{ij,k-1} \leq \zeta_{ij,k} \qquad \text{for } (i,j) \in \mathcal{E},\ k \in \mathcal{K}_t \tag{12}$$

$$0 \leq P_{i,k} \leq P_{i,k|t}^{\mathrm{forecast}} \qquad \text{for } i \in \mathcal{V}\backslash\{0\},\ k \in \mathcal{K}_t \tag{13}$$

$$-\psi_{i,j,k} \leq P_{i,k} - P_{i,k|t}^{\mathrm{forecast}} - P_{j,k} + P_{j,k|t}^{\mathrm{forecast}} \leq \psi_{i,j,k} \qquad \text{for } i \in \mathcal{V}\backslash\{0\},\ j \in \mathcal{V} : j > i,\ k \in \mathcal{K}_t \tag{14}$$

stage 1 assumes that the forecast is perfect, the forecast can be treated as the possible power, leading to (13).

The linear power flow model of [18] is used to model the power flows in the system:

$$P_{i,k} - \sum_{j|(i,j)\in\mathcal{E}} p_{ij,k} + \sum_{j|(j,i)\in\mathcal{E}} p_{ji,k} = 0 \quad \text{for } i \in \mathcal{V},\ k \in \mathcal{K}_t \tag{15}$$

$$z_{ij,k} \in \{0,1\} \quad \text{for } (i,j) \in \mathcal{E},\ k \in \mathcal{K}_t \tag{16}$$

$$-M_{ij} z_{ij,k} \leq p_{ij,k} \leq M_{ij} z_{ij,k} \quad \text{for } (i,j) \in \mathcal{E},\ k \in \mathcal{K}_t \tag{17}$$

$$p_{ij,k} \leq b_{ij}(\theta_{i,k} - \theta_{j,k}) + M_{ij}(1 - z_{ij,k}) \quad \text{for } (i,j) \in \mathcal{E},\ k \in \mathcal{K}_t \tag{18}$$

$$p_{ij,k} \geq b_{ij}(\theta_{i,k} - \theta_{j,k}) - M_{ij}(1 - z_{ij,k}) \quad \text{for } (i,j) \in \mathcal{E},\ k \in \mathcal{K}_t \tag{19}$$

where $p_{ij,k}$ is the power flow through cable (i,j) at time step k, b_{ij} is the admittance of cable (i,j), and $\theta_{i,k}$ is the voltage angle of node i at time step k. The latter is defined relative to a reference voltage phasor. This is typically the node pertaining to the OSS, of which the voltage angle is then fixed to zero. The power (flow) and admittance are expressed in per-unit values and the voltage angles in radians. Furthermore, M_{ij} can be selected as $2b_{ij}\theta^{\max}$, in which $\theta^{\max}$ is the maximum voltage angle.

A discretized version of the thermal model of [12] can be used to estimate future cable temperatures:

$$T_{ij,t+1} = a_{ij}T_{ij,t} + b_{ij}T_{ij,t-1} + c_{ij}T_{ij,t-2} + d_{ij}p_{ij,t}^2 + e_{ij} \tag{20}$$

where $T_{ij,t}$ is the temperature of cable (i,j) at hour t, $p_{ij,t}$ is the power flow through cable (i,j) at hour t, and a_{ij}, b_{ij}, c_{ij}, d_{ij}, and e_{ij} are cable and location-specific parameters that can be found by fitting the model to temperature and power data. With respect to the state-space model of [12], the term e_{ij} has been added since this turns out to result in a better fit for the data of the case study of Section V. To predict future cable temperatures, the model must be initialized with three Distributed Temperature Sensing (DTS) measurements, $T_{ij,t}^{\mathrm{DTS}}$, $T_{ij,t-1}^{\mathrm{DTS}}$, and $T_{ij,t-2}^{\mathrm{DTS}}$. For the first two prediction steps, the future temperatures can then be constrained as follows:

$$T_{t+1|t} = aT_t^{\mathrm{DTS}} + bT_{t-1}^{\mathrm{DTS}} + cT_{t-2}^{\mathrm{DTS}} + dp_t^2 + e \leq T^{\max} \tag{21}$$

$$T_{t+2|t} = aT_{t+1|t} + bT_t^{\mathrm{DTS}} + cT_{t-1}^{\mathrm{DTS}} + dp_{t+1}^2 + e = (a^2+b)T_t^{\mathrm{DTS}} + (ab+c)T_{t-1}^{\mathrm{DTS}} + acT_{t-2}^{\mathrm{DTS}} + adp_t^2 + dp_{t+1}^2 + ae + e \leq T^{\max} \tag{22}$$

where $T^{\max}$ is the cable temperature limit and the index ij is dropped for clarity. The power flow constraints can be formulated without explicitly defining the temperatures, which avoids the use of quadratic equality constraints:

$$F_{ij}\begin{bmatrix} T_{ij,t}^{\mathrm{DTS}} \\ T_{ij,t-1}^{\mathrm{DTS}} \\ T_{ij,t-2}^{\mathrm{DTS}} \end{bmatrix} + G_{ij}\begin{bmatrix} p_{ij,t}^2 \\ p_{ij,t+1}^2 \\ \vdots \\ p_{ij,t+N_{\mathrm{p}}-1}^2 \end{bmatrix} + H_{ij} \leq T_{N_{\mathrm{p}}\times 1}^{\max} \quad \text{for } (i,j) \in \mathcal{E} \tag{23}$$

where $F_{ij} \in \mathbb{R}^{N_{\mathrm{p}}\times 3}$, $G_{ij} \in \mathbb{R}^{N_{\mathrm{p}}\times N_{\mathrm{p}}}$, and $H_{ij} \in \mathbb{R}^{N_{\mathrm{p}}\times 1}$ are matrices parameterized by a_{ij}, b_{ij}, c_{ij}, d_{ij}, and e_{ij}. Furthermore, $T_{N_{\mathrm{p}}\times 1}^{\max}$ is a vector of length N_{p}, each element being $T^{\max}$.

At each hour t, the optimization problem of (11)-(19) and (23) is formulated using the measured cable temperatures and the most recent power forecast. The optimal network configuration pertaining to the current hour is applied to the network.

B. Stage 2: setpoint adaptation

The second stage uses $z_{ij,t}$ and $P_{i,t}$ as input to calculate the optimal setpoints for the current hour. Its objective function is to maximize the setpoints while aiming to distribute the deviations of the turbine setpoints from the power forecast evenly over the network. By doing so, the strategy assumes that any inaccuracy in the power forecast affects the turbines to the same extent. The optimization framework is the following:

$$\max \quad \sum_{i\in\mathcal{V}\setminus\{0\}} P_{i,t}^{\mathrm{sp}} - c_3 \cdot \sum_{i\in\mathcal{V}\setminus\{0\}} \sum_{j\in\mathcal{V}:j>i} \varrho_{i,j,t} \tag{24}$$

$$\text{s.t.} \quad -\varrho_{i,j,t} \leq P_{i,t}^{\mathrm{sp}} - P_{i,t|t}^{\mathrm{forecast}} - P_{j,t}^{\mathrm{sp}} + P_{j,t|t}^{\mathrm{forecast}} \leq \varrho_{i,j,t} \quad \text{for } i \in \mathcal{V}\setminus\{0\},\ j \in \mathcal{V} : j > i \tag{25}$$

$$a_{ij}T_{ij,t}^{\mathrm{DTS}} + b_{ij}T_{ij,t-1}^{\mathrm{DTS}} + c_{ij}T_{ij,t-2}^{\mathrm{DTS}} + d_{ij}(p_{ij,t}^{\mathrm{sp}})^2 + e_{ij} \leq T^{\max} \quad \text{for } (i,j) \in \mathcal{E} \tag{26}$$

$$P_{i,t}^{\mathrm{sp}} - \sum_{j|(i,j)\in\mathcal{E}} p_{ij,t}^{\mathrm{sp}} + \sum_{j|(j,i)\in\mathcal{E}} p_{ji,t}^{\mathrm{sp}} = 0 \quad \text{for } i \in \mathcal{V} \tag{27}$$

$$p_{ij,t}^{\mathrm{sp}} = z_{ij,t} b_{ij}(\theta_{i,t}^{\mathrm{sp}} - \theta_{j,t}^{\mathrm{sp}}) \quad \text{for } (i,j) \in \mathcal{E} \tag{28}$$

$$P_{i,t} \leq P_{i,t}^{\mathrm{sp}} \quad \text{for } i \in \mathcal{V}\setminus\{0\} \tag{29}$$

$$0 \leq P_{i,t}^{\mathrm{sp}} \leq P_i^{\mathrm{r}} \quad \text{for } i \in \mathcal{V}\setminus\{0\} \tag{30}$$

In these equations, the variables with the superscript sp denote the previously introduced variables in case of production at setpoint. Furthermore, c_3 is a penalty coefficient, and $\varrho_{i,j,t}$ is an auxiliary variable.

Since for this stage, $z_{ij,t}$ are parameters rather than optimization variables, the linear power flow model introduced in (15)-(19) can be reduced to (28) while preserving linearity. Furthermore, the setpoints must make it possible to produce at least the power production conforming to the power flow limits under the assumption of a perfect forecast, $P_{i,t}$, found in the first stage. This is dictated by (29).

The setpoints found by the second stage are applied to the turbines. The optimization problems of both stages are reformulated at the next iteration using the updated measurements.

V. Case study

The novel strategies and existing strategies, described in Section II-D, are applied to a case study concerning seven outages that occurred at an existing OWF with a meshed layout. The farm comprises 70 to 100 turbines and contains three distinct cable sizes.

A. Data

Possible power, cable temperature, wind speed, and power forecasting data are required to implement the control strategies and to perform simulations. All data is supplied by Vattenfall. Due to confidentiality restrictions, the data cannot be made publicly available.

The possible power is taken to be the maximum of the active power output of the turbine and a possible power signal derived from nacelle wind speed measurements and the operational power curve. The possible power is given per turbine per 10 minutes. Possible power data is also needed to generate the scenarios for the open-loop control strategy. To this end, five years of historical possible power data are binned into groups, for each of which the probability is calculated.

A cable temperature model fitted to cable temperature and power flow data is used to generate synthetic cable temperature measurements during the simulations. With respect to (20), noise terms are added to simulate process and measurement noise:

$$T_{ij,t+1} = a_{ij}T_{ij,t} + b_{ij}T_{ij,t-1} + c_{ij}T_{ij,t-2} + d_{ij}p^2_{ij,t} + e_{ij} + \varepsilon_{ij,t} \quad (31)$$

$$T^{\mathrm{DTS}}_{ij,t} = T_{ij,t} + \varepsilon_{ij,t} \quad (32)$$

where $\varepsilon_{ij,t}$ is drawn from a zero-mean normal distribution with its variance identified per cable during system identification.

During outages, cables might experience higher power flows than under standard operation. Therefore, per cable size, the cable that experiences the highest power flow is used for identifying a thermal model. The model corresponding to the medium-sized cable is used for the small-sized cables since, during outages, some of the small-sized cables might experience much higher loads than those in the data set.

For parameter estimation, 4.5 months of hourly cable temperature and power flow data are used. 80% of the data is used for system identification, while the final 20% is used for evaluating the quality of the model.

Matlab's function `greyest` [19] is used, which applies nonlinear least squares identification for the problem at hand. The focus is set to simulation instead of prediction, which means that the simulation error is minimized rather than the 1-step ahead prediction error. For the medium- and large-sized cable, the resulting Normalized Mean Square Error (NMSE) fit is 92.8% and 95.8%, respectively. For comparison, note that in [12], a fit of 82.5% to export cable data was reported.

B. Implementation

The novel control strategies are implemented in Python using the modeling framework Pyomo [20] and are solved with Gurobi [21] on a Vattenfall compute cluster (16 vCPU, 256 GiB, AMD EPYC 7452 2.35 GHz processor).

The length N_{p} of the prediction window and the penalty coefficient c_1 of the receding horizon control strategy have been selected based on manual tuning. Here, $N_{\mathrm{p}} = 3$ h and $c_1 = 3$ were the most suited. The remainder of the penalty coefficients are set to $c = 0.01$, $c_2 = 0.001$, and $c_3 = 0.001$.

The strategy of [4], hereafter referred to as the literature control strategy, is derived for OWFs with loop connection cables. For those OWFs, only one cable can be used to reroute the power. The strategy does not consider how to perform rerouting for meshed networks. For the case study, the cable that results in the highest setpoints is activated, similar to the industry strategy. Furthermore, if further reduction in setpoint is not necessary at the measured wind speed, the highest turbine power for which the STR is not violated is applied as setpoint. This approach differs from [4], which applies the power production at measured wind speed as a setpoint. However, for the case study, in which the wind profile is not homogeneous within the farm, that would result in unnecessary curtailment.

In addition, it is calculated what the production would have been if all turbines connected to the inoperative cable were curtailed and no further control actions were taken. This is referred to as the base strategy.

C. Results

For each control strategy and outage, the percentual gap with possible power is listed in Table I. By way of illustration, the power production during outages 2 and 6 is shown in Figure 2 and Figure 3, respectively. As can be seen, the receding horizon control strategy outperforms the other control strategies for all outages.

The increase in production can mainly be attributed to the use of DTR. Dynamic switching further enables exploiting DTR to the fullest by (de)activating cables during the outage based on the cable temperatures and forecasts. The computa-

TABLE I
POWER PRODUCTION RELATIVE TO THE POSSIBLE POWER FOR EACH OUTAGE AND CONTROL STRATEGY.

	Base	Industry	Literature	Open-loop	Receding horizon
1	-8.69%	-5.22%	-6.05%	-5.12%	-2.85%
2	-18.72%	-13.21%	-15.28%	-12.30%	-7.21%
3	-7.13%	-3.57%	-3.68%	-3.55%	-2.42%
4	-6.19%	-4.44%	-4.52%	-4.15%	-1.45%
5	-11.10%	-8.58%	-8.39%	-7.33%	-4.77%
6	-9.75%	-7.62%	-7.57%	-5.74%	-0.36%
7	-9.60%	-5.82%	-5.93%	-4.97%	-2.41%

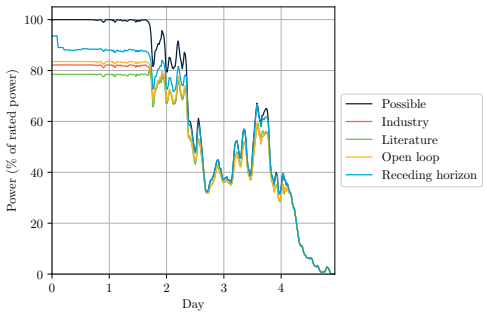

Fig. 2. Power production for outage 2.

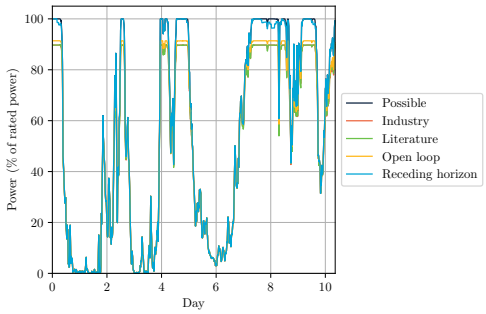

Fig. 3. Power production for outage 6.

tions for one time step are performed within 23 s on average, with a maximum computation time of 35 minutes.

The open-loop control strategy is a promising alternative if there is no automated control system. This strategy outperforms the industry strategy and the literature strategy in terms of production, with fast computations, i.e., on average 0.34 s.

By using real possible power data that differentiates between turbines, it could be shown that the method in [4] cannot deal well with non-uniform wind speeds within the park and inaccuracies in the warranted power curve.

The average increase in power production with respect to the industry control strategy is 0.82% and 4.2% for the open-loop and receding horizon control strategy, respectively. With an average offshore wind farm size of 301 MW [22], an average capacity factor of 0.42 [22], and an average outage duration of 38 days [7], the estimated increase in power production per outage is 951 MWh for the open-loop and 4.84 GWh for the receding horizon control strategy. With a feed-in remuneration of €194/MWh [4], this translates into a revenue increase per outage of €0.18 million and €0.94 million, respectively.

VI. Conclusions

We have presented two novel optimization-based rerouting and setpoint decision frameworks for outages in OWF collector systems with arbitrary topologies: the open-loop control strategy and the receding horizon control strategy. The performance of these strategies is compared to existing control strategies by simulations with real data from occurred outages. It is shown that both developed strategies outperform the existing control strategies. In particular, the receding horizon control strategy enables a significant decrease in the loss of production during outages.

Future work will focus on incorporating DTR in the operations of collector systems. The thermal model should be fitted per cable to account for location-specific properties instead of using the same parameters per cable size. Ambient conditions can be considered by applying adaptive receding horizon control, in which the temperature model gradually evolves with time. This would allow for considering changing operating conditions without explicitly providing these to the controller.

Acknowledgment

We want to thank Adel Haghani from Vattenfall BA Wind for his valuable feedback and support.

References

[1] UNFCCC, "The Paris Agreement," 2015. UNTC XXVII 7.d.
[2] GWEC, "Global offshore wind report 2022," Tech. rep., Global Wind Energy Council, 2022. https://gwec.net/gwecs-global-offshore-wind-report, accessed December 2022.
[3] E. Gulski, G. J. Anders, R. A. Jongen, J. Parciak, J. Siemiński, E. Piesowicz, S. Paszkiewicz, and I. Irska, "Discussion of electrical and thermal aspects of offshore wind farms' power cables reliability," *Renewable and Sustainable Energy Reviews*, vol. 151, p. 111580, 2021.
[4] J. Scholz, E. Wiebe, V. Scheffer, and C. Becker, "Economic power control for offshore wind farms with loop connection cables," *Automatisierungstechnik*, vol. 68, no. 9, pp. 765–780, 2020.
[5] B. Wang, X. Wang, Z. Song, L. Zhang, S. Wang, and C. Xin, "Fault state operation analysis for offshore wind farm with ring-topology collector system: An OPF and topology optimization method," in *2021 IEEE 5th Conference on Energy Internet and Energy System Integration (EI2)*, pp. 119–124, 2021.
[6] M. A. H. Colin and J. A. Pilgrim, "Cable thermal risk estimation for overplanted wind farms," *IEEE Transactions on Power Delivery*, vol. 35, no. 2, pp. 609–617, 2019.
[7] C. Strang-Moran, "Subsea cable management: Failure trending for offshore wind," *Wind Energy Science Discussions*, pp. 1–11, 2020.
[8] O. Anaya-Lara, "Offshore wind farm arrays," in *Offshore Wind Farms*, pp. 389–417, Elsevier, 2016.
[9] S. Catmull, R. D. Chippendale, J. A. Pilgrim, G. Hutton, and P. Cangy, "Cyclic load profiles for offshore wind farm cable rating," *IEEE Transactions on Power Delivery*, vol. 31, pp. 1242–1250, 2016.
[10] IEC, "IEC 60287-1: Electric cables – calculation of the current rating, Part 1: Current rating equations (100% load factor) and calculation of losses," International standard, International Electrotechnical Organization, 2014.
[11] M. A. H. Colin, J. Dix, and J. A. Pilgrim, "Export cable rating optimisation by wind power ramp and thermal risk estimation," *IET Renewable Power Generation*, vol. 15, pp. 1564–1581, 2021.
[12] S. H. H. Kazmi, *Dynamic Rating Based Design and Operation of Offshore Windfarm Export Systems*. PhD thesis, Technical University of Denmark, 2021.
[13] Y. Wang, Q. Hu, L. Li, A. M. Foley, and D. Srinivasan, "Approaches to wind power curve modeling: A review and discussion," *Renewable and Sustainable Energy Reviews*, vol. 116, p. 109422, 2019.
[14] K. Purchala, L. Meeus, D. Van Dommelen, and R. Belmans, "Usefulness of DC power flow for active power flow analysis," in *IEEE Power Engineering Society General Meeting, 2005*, pp. 454–459 Vol. 1, 2005.
[15] S. Lumbreras, A. Ramos, and P. Sánchez-Martin, "Offshore wind farm electrical design using a hybrid of ordinal optimization and mixed-integer programming," *Wind Energy*, vol. 18, no. 12, pp. 2241–2258, 2015.
[16] M. Fischetti and D. Pisinger, "Optimizing wind farm cable routing considering power losses," *European Journal of Operational Research*, vol. 270, no. 3, pp. 917–930, 2018.
[17] V. Paschos, *Concepts of Combinatorial Optimization*. Wiley, 2014.
[18] E. B. Fisher, R. P. O'Neill, and M. C. Ferris, "Optimal transmission switching," *IEEE Transactions on Power Systems*, vol. 23, no. 3, pp. 1346–1355, 2008.
[19] The MathWorks, Inc., "greyest." https://nl.mathworks.com/help/ident/ref/greyest.html, accessed May 2023.
[20] M. L. Bynum, G. A. Hackebeil, W. E. Hart, and C. D. Laird, *Pyomo–Optimization Modeling in Python*, vol. 67. Springer Science & Business Media, third ed., 2021.
[21] Gurobi Optimization, LLC, "Gurobi Optimizer Reference Manual," 2023. https://www.gurobi.com.
[22] M. Bilgili and H. Alphan, "Global growth in offshore wind turbine technology," *Clean Technologies and Environmental Policy*, vol. 24, no. 7, pp. 2215–2227, 2022.

Bibliography

[1] O. Anaya-Lara. Offshore wind farm arrays. In *Offshore Wind Farms*, pages 389–417. Elsevier, 2016.

[2] M. Bilgili and H. Alphan. Global growth in offshore wind turbine technology. *Clean Technologies and Environmental Policy*, 24(7):2215–2227, 2022.

[3] I. Bilibin and F. Capitanescu. Contributions to thermal constraints management in radial active distribution systems. *Electric Power Systems Research*, 111:169–176, 2014.

[4] M. L. Bynum, G. A. Hackebeil, W. E. Hart, and C. D. Laird. *Pyomo–Optimization Modeling in Python*, volume 67. Springer Science & Business Media, third edition, 2021.

[5] S. Catmull, R. D. Chippendale, J. A. Pilgrim, G. Hutton, and P. Cangy. Cyclic load profiles for offshore wind farm cable rating. *IEEE Transactions on Power Delivery*, 31:1242–1250, 2016.

[6] X. H. Chen, B. Wang, Z. J. Cao, and Y. L. Miao. Analysis of the switchgear configuration for the ring collection grids of offshore wind farms. In *IOP Conference Series: Earth and Environmental Science*, volume 237, page 062007. IOP Publishing, 2019.

[7] S. Cherukupalli, R. Adapa, and E. C. Bascom. Implementation of quasi-real-time rating software to monitor 525 kv cable systems. *IEEE Transactions on Power Delivery*, 34:1309–1316, 2019.

[8] R. Chippendale, J. A. Pilgrim, A. Kazerooni, and D. Ruthven. Cyclic rating of wind farm cable connections. *CIRED - Open Access Proceedings Journal*, 2017.

[9] R. D. Chippendale, J. A. Pilgrim, K. F. Goddard, and P Cangy. Analytical thermal rating method for cables installed in J-tubes. *IEEE Transactions on Power Delivery*, 32(4):1721–1729, 2017.

[10] M. A. H. Colin, J. Dix, and J. A. Pilgrim. Export cable rating optimisation by wind power ramp and thermal risk estimation. *IET Renewable Power Generation*, 15:1564–1581, 2021.

[11] M. A. H. Colin and J. A. Pilgrim. Cable thermal risk estimation for overplanted wind farms. *IEEE Transactions on Power Delivery*, 35(2):609–617, 2019.

[12] M. EL-Azab, W. A. Omran, S. F. Mekhamer, and H. E. A. Talaat. Congestion management of power systems by optimizing grid topology and using dynamic thermal rating. *Electric Power Systems Research*, 199:107433, 2021.

[13] D. Enescu, A. Russo, R. Porumb, and G. Seritan. Dynamic thermal rating of electric cables: A conceptual overview. In *2020 55th International Universities Power Engineering Conference (UPEC)*, pages 1–6. IEEE, 2020.

[14] V. A. Evangelopoulos, P.S. Georgilakis, and N. D. Hatziargyriou. Optimal operation of smart distribution networks: A review of models, methods and future research. *Electric Power Systems Research*, 140:95–106, 2016.

[15] L. Exizidis, F. Vallée, Z. De Grève, J. Lobry, and V. Chatziathanasiou. Thermal behavior of power cables in offshore wind sites considering wind speed uncertainty. *Applied Thermal Engineering*, 91:471–478, 2015.

[16] A. A. Ezzat. Turbine-specific short-term wind speed forecasting considering within-farm wind field dependencies and fluctuations. *Applied Energy*, 269:115034, 2020.

[17] M. Fischetti and D. Pisinger. Optimizing wind farm cable routing considering power losses. *European Journal of Operational Research*, 270(3):917–930, 2018.

[18] European Centre for Medium-Range Weather Forecasts. Era5, Aug 2022. https://www.ecmwf.int/en/forecasts/datasets/reanalysis-datasets/era5, accessed Februari 2023.

[19] G. Giebel and G. Kariniotakis. *Renewable Energy Forecasting*, chapter 3 - Wind power forecasting—a review of the state of the art, pages 59–109. Woodhead Publishing Series in Energy. Woodhead Publishing, 2017.

[20] E. Gulski, G. J. Anders, R. A. Jongen, J. Parciak, J. Siemiński, E. Piesowicz, S. Paszkiewicz, and I. Irska. Discussion of electrical and thermal aspects of offshore wind farms' power cables reliability. *Renewable and Sustainable Energy Reviews*, 151:111580, 2021.

[21] Gurobi Optimization, LLC. Gurobi Optimizer Reference Manual, 2023. https://www.gurobi.com.

[22] GWEC. Global offshore wind report 2022. Technical report, Global Wind Energy Council, 2022. https://gwec.net/gwecs-global-offshore-wind-report, accessed December 2022.

[23] P. Hou, W. Hu, M. Soltani, and Z. Chen. Optimized placement of wind turbines in large-scale offshore wind farm using particle swarm optimization algorithm. *IEEE Transactions on Sustainable Energy*, 6(4):1272–1282, 2015.

[24] IEC. IEC 60287-1: Electric cables – Calculation of the cyclic and emergency current rating of cables. Part 1: Cyclic rating factor for cables up to and including 18/30 (36) kV. International standard, International Electrotechnical Organization, 2008.

[25] IEC. IEC 60287-1: Electric cables – Calculation of the current rating, Part 1: Current rating equations (100% load factor) and calculation of losses. International standard, International Electrotechnical Organization, 2014.

[26] IEC. IEC 60287-2: Electric cables – Calculation of the current rating, Part 2: Thermal resistance. International standard, International Electrotechnical Organization, 2017.

[27] The MathWorks Inc. goodnessOfFit, 2023. https://nl.mathworks.com/help/ident/ref/goodnessoffit.html.

[28] A. R. Jordehi. How to deal with uncertainties in electric power systems? A review. *Renewable and sustainable energy reviews*, 96:145–155, 2018.

[29] B. R. Karthikeya and R. J. Schütt. Overview of wind park control strategies. *IEEE Transactions on Sustainable Energy*, 5(2):416–422, 2014.

[30] S. H. H. Kazmi. *Dynamic Rating based Design and Operation of Offshore Windfarm Export Systems*. PhD thesis, Technical University of Denmark, 2021.

[31] S. H. H. Kazmi, J. Holbøll, T. H. Olesen, and T. S. Sørensen. Thermoelectric modelling and optimization of offshore windfarm export systems-state of the art. In *2019 1st Global Power, Energy and Communication Conference (GPECOM)*, pages 331–336. IEEE, 2019.

[32] S. H. H. Kazmi, R. Østerø, R. Holbøll, T. H. Olesen, and T. S. Sørensen. Thermal analysis and debottlenecking of hvac export cables for offshore windfarms. In *CIRED 2021-The 26th International Conference and Exhibition on Electricity Distribution*, volume 2021, pages 614–618. IET, 2021.

[33] S. H. H. Kazmi, N. Viaforaz, T. S. Sorensen, T. H. Olesen, B. C. Pal, and J. Holboll. Offshore windfarm design optimization using dynamic rating for transmission components. *IEEE Transactions on Power Systems*, 37:1820–1830, 2022.

[34] J. Kiviluoma, H. Holttinen, D. Weir, R. Scharff, L. Söder, N. Menemenlis, N. A. Cutululis, I. Danti Lopez, E. Lannoye, A. Estanqueiro, et al. Variability in large-scale wind power generation. *Wind Energy*, 19(9):1649–1665, 2016.

[35] T. Kvarts, I. Arana, R. S. Olsen, and P. Mortensen. Systematic description of dynamic load for cables for offshore wind farms. method and experience. CIGRE, 2016.

[36] C. M. Lai and J. Teh. Comprehensive review of the dynamic thermal rating system for sustainable electrical power systems. *Energy Reports*, 8:3263–3288, 2022.

[37] Y. Li, B. Hu, K. Xie, L. Wang, Y. Xiang, R. Xiao, and D. Kong. Day-ahead scheduling of power system incorporating network topology optimization and dynamic thermal rating. *IEEE Access*, 7:35287–35301, 2019.

[38] S. Lumbreras and A. Ramos. Offshore wind farm electrical design: a review. *Wind Energy*, 16(3):459–473, 2013.

[39] S. Lumbreras, A. Ramos, and P. Sánchez-Martin. Offshore wind farm electrical design using a hybrid of ordinal optimization and mixed-integer programming. *Wind Energy*, 18(12):2241–2258, 2015.

[40] M. Mahdavi, H. H. Alhelou, N. D. Hatziargyriou, and F. Jurado. Reconfiguration of electric power distribution systems: Comprehensive review and classification. *IEEE Access*, 2021.

[41] M Mirzaei, T Göçmen, G Giebel, P. E. Sørensen, and N. K. Poulsen. Estimation of the possible power of a wind farm. *IFAC Proceedings Volumes*, 47(3):6782–6787, 2014.

[42] M. Numan, D. Feng, F. Abbas, S. Habib, and S. Hao. Coordinated operation of reconfigurable networks with dynamic line rating for optimal utilization of renewable generation. *International Journal of Electrical Power & Energy Systems*, 125:106473, 2021.

[43] R. S. Olsen. *Dynamic loadability of cable based transmission grids*. PhD thesis, Technical University of Denmark, Department of Electrical Engineering, 2013.

[44] R. S. Olsen, G. J. Anders, J. Holboell, and U. S. Gudmundsdóttir. Modelling of dynamic transmission cable temperature considering soil-specific heat, thermal resistivity, and precipitation. *IEEE Transactions on Power Delivery*, 28(3):1909–1917, 2013.

[45] R. S. Olsen, J. Holboll, and U. S. Gudmundsdottir. Dynamic temperature estimation and real time emergency rating of transmission cables. In *2012 IEEE power and energy society general meeting*, pages 1–8, 2012.

[46] K. R. Padiyar and A. M. Kulkarni. *Dynamics and control of electric transmission and microgrids*. John Wiley & Sons, 2019.

[47] V.T. Paschos. *Concepts of Combinatorial Optimization*. Wiley, 2014.

[48] J. A. Pérez-Rúa and N. A. Cutululis. Electrical cable optimization in offshore wind farms—a review. *IEEE Access*, 7:85796–85811, 2019.

[49] P. Pinson. *Estimation of the uncertainty in wind power forecasting*. PhD thesis, École Nationale Supérieure des Mines de Paris, 2006.

[50] K. Purchala, L. Meeus, D. Van Dommelen, and R. Belmans. Usefulness of DC power flow for active power flow analysis. In *IEEE Power Engineering Society General Meeting, 2005*, pages 454–459 Vol. 1, 2005.

[51] M. Rahmani-Andebili. Dynamic and adaptive reconfiguration of electrical distribution system including renewables applying stochastic model predictive control. *IET Generation, Transmission & Distribution*, 11(16):3912–3921, 2017.

[52] M. M. Rienecker, M. J. Suarez, R. Gelaro, and R. Todling. Merra: Nasa's modern-era retrospective analysis for research and applications. *Journal of Climate*, 24(14):3624 – 3648, 2011.

[53] P. Sanchez-Martin, A. Ramos, and J. F. Alonso. Probabilistic midterm transmission planning in a liberalized market. *IEEE Transactions on Power Systems*, 20(4):2135–2142, 2005.

[54] J. Scholz, E. Wiebe, V. Scheffer, and C. Becker. Economic power control for offshore wind farms with loop connection cables. *at-Automatisierungstechnik*, 68(9):765–780, 2020.

[55] J. Shin and J. Kim. Optimal design for offshore wind farm considering inner grid layout and offshore substation location. *IEEE Transactions on Power Systems*, 32(3):2041–2048, 2016.

[56] R. S. Singh, S. Cobben, and V. Ćuk. Pmu-based cable temperature monitoring and thermal assessment for dynamic line rating. *IEEE Transactions on Power Delivery*, 36(3):1859–1868, 2020.

[57] S. S. Soman, H. Zareipour, O. Malik, and P. Mandal. A review of wind power and wind speed forecasting methods with different time horizons. In *North American Power Symposium 2010*, pages 1–8, 2010.

[58] C. Strang-Moran. Subsea cable management: Failure trending for offshore wind. *Wind Energy Science Discussions*, pages 1–11, 2020.

[59] K. Suomalainen, C. A. Silva, P. Ferrão, and S. Connors. Synthetic wind speed scenarios including diurnal effects: Implications for wind power dimensioning. *Energy*, 37(1):41–50, 2012.

[60] Inc. The MathWorks. greyest. https://nl.mathworks.com/help/ident/ref/greyest.html, accessed May 2023.

[61] UNFCCC. The Paris Agreement, 2015. UNTC XXVII 7.d.

[62] R. A. M. Van Amerongen. A general-purpose version of the fast decoupled load flow. *IEEE Transactions on Power Systems*, 4(2):760–770, 1989.

[63] K. Van den Bergh, E. Delarue, and W. D'Haeseleer. DC power flow in unit commitment models. Working paper, KU Leuven Energy Institute, Leuven, 2014.

[64] M. Verhaegen and V. Verdult. *Filtering and system identification: a least squares approach*. Cambridge university press, 2007.

[65] B. Wang, X. Wang, Z. Song, L. Zhang, S. Wang, and C. Xin. Fault state operation analysis for offshore wind farm with ring-topology collector system: An OPF and topology optimization method. In *2021 IEEE 5th Conference on Energy Internet and Energy System Integration (EI2)*, pages 119–124, 2021.

[66] Y. Wang, Q. Hu, L. Li, A. M. Foley, and D. Srinivasan. Approaches to wind power curve modeling: A review and discussion. *Renewable and Sustainable Energy Reviews*, 116:109422, 2019.

[67] A. J. Wood, B. F. Wollenberg, and G. B. Sheblé. *Power Generation, Operation, and Control (3rd Edition)*. John Wiley & Sons, 2014.

[68] Y. K. Wu, S. M. Chang, and P. Mandal. Grid-connected wind power plants: A survey on the integration requirements in modern grid codes. *IEEE Transactions on Industry Applications*, 55(6):5584–5593, 2019.

Glossary

List of acronyms

AC	Alternating Current
CTR	Cyclic Thermal Rating
DC	Direct Current
DTS	Distributed Temperature Sensing
DTR	Dynamic Thermal Rating
ELS	Elongated String
FCC	Full Capacity Cable
IEC	International Electrotechnical Commission
MILP	Mixed-Integer Linear Programming
MINLP	Mixed-Integer Nonlinear Programming
MIQCP	Mixed-Integer Quadratically Constrained Programming
QCLP	Quadratically Constrained Linear Programming
OSS	Offshore Substation
OWF	Offshore Wind Farm
NRMSE	Normalized Root Mean Square Error
NMSE	Normalized Mean Square Error
STR	Static Thermal Rating

List of symbols

Sets

$\mathcal{A}$	Set of directed operable cables
$\mathcal{E}$	Set of undirected operable cables
$\mathcal{H}_t$	Set of hours on the prediction horizon
$\mathcal{L}_t$	Set of days on the prediction horizon
$\mathcal{S}$	Set of possible power scenarios
$\mathcal{T}$	Set of inoperative turbines
$\mathcal{V}$	Set of nodes

Parameters

$\mathbb{P}_s$	Probability of scenario s
b_{ij}	Admittance of cable (i, j) [p.u.]
c	Penalty coefficient for switching actions (open-loop)
c_1	Penalty coefficient for switching actions (receding horizon)
c_2	Penalty coefficient for differences in deviations from the power forecast
I^{rated}	Rated current [A]
N	Number of turbines
$N_{\text{p}}^{\text{long}}$	Prediction window of long-term model [day]
$N_{\text{p}}^{\text{short}}$	Prediction window of short-term model [h]
P_{f}	Power factor
P_i^{poss}	Possible power of turbine i [p.u.]
P_i^{r}	Rated power of turbine i [p.u.]
$P_{i,k\|t}^{\text{forecast}}$	Power forecast of turbine i made at hour t concerning time step k [p.u.]
$P_{i,s}^{\text{poss}}$	Possible power of turbine i at scenario s [p.u.]
p_{ij}^{CTR}	Power flow limit through cable (i, j) for CTR [p.u]
p_{ij}^{STR}	Power flow limit through cable (i, j) for STR [p.u.]
r_{ij}	Resistance of cable (i, j) [p.u.]
$T^{\max}$	Cable temperature limit [°C]
$T_{ij,t}^{\text{DTS}}$	DTS measurement of cable (i, j) made at hour t [°C]
$w_{i,k\|t}^{\text{forecast}}$	Wind speed forecast made at hour t concerning time step k and turbine i [m/s]
$w_{i,k}$	Nacelle wind speed measured by turbine i at time step k [m/s]
x_{ij}	Reactance of cable (i, j) [p.u.]
z_{ij}^{standard}	Standard configuration of cable (i, j)

Variables

$\psi_{i,j,k}$	Auxiliary variable to transform 1-norm objective function of stage 1 into linear objective function
θ_i	Voltage angle of node i [rad]
$\theta_{i,k}$	Voltage angle of node i at time step k [rad]
$\theta_{i,t}^{\text{sp}}$	Voltage angle of turbine i at hour t for production at setpoint [rad]
$\varrho_{i,j,t}$	Auxiliary variable to transform 1-norm objective function of stage 2 into linear objective function
Ξ	Vector of decision variables
$\zeta_{ij,k}$	Auxiliary variable to transform 1-norm objective function into linear objective function
ζ_{ij}	Auxiliary variable to transform 1-norm objective function into linear objective function
I	Current [A]
p	Active power flow [W]
P_i	Power production of turbine i [p.u.]
P_i^{sp}	Setpoint of turbine i [p.u.]
$P_{i,k}$	Power production of turbine i at time step k under the assumption of a perfect forecast [p.u.]
$P_{i,s}$	Power production of turbine i for scenario s [p.u.]
$P_{i,t}^{\text{sp}}$	Setpoint of turbine i at hour t [p.u.]
$p_{ij,t}$	Power flow through cable (i,j) at hour t [p.u.]
$p_{ij,t}^{\text{sp}}$	Power flow at hour t for production at setpoint [p.u.]
p_{ij}	Power flow through cable (i,j) [p.u.]
p_{ij}^{sp}	Power flow from i to j for production at setpoint [p.u.]
t	Time step [h]
$T_{ij,t}$	Temperature of cable (i,j) at hour t [°C]
V	Voltage [V]
$z_{ij,k}$	Binary variable for on/off status of cable (i,j) at time step k
z_{ij}	Binary variable for on/off status of cable (i,j)